Volume 66A
Number 6
Nov.–Dec. 1962

Physics and Chemistry

U.S. DEPARTMENT OF COMMERCE

SECTION A

JOURNAL OF RESEARCH

NATIONAL BUREAU OF STANDARDS

Journal of Research

of the

National Bureau of Standards

A. Physics and Chemistry

NOV.–DEC. • 1962

VOLUME • 66A

NUMBER • 6

Editor: C. W. Beckett

Associate Editors: D. D. Wagman
J. M. Richardson

Publication dates:
Feb. 1, Apr. 1, June 1, Aug. 1, Oct. 1, Dec. 1, 1962.

JOURNAL OF RESEARCH

The National Bureau of Standards Journal of Research reports research and development in the fields of activity shown at right. Also included from time to time are survey articles on topics closely related to the Bureau's scientific and technical program.

The Journal is published in four separate sections as follows:

A. Physics and Chemistry

Contains papers of interest primarily to scientists working in these fields. Issued six times a year. Annual subscription: domestic, $4.00; foreign, $4.75.

B. Mathematics and Mathematical Physics

Presents studies and compilations designed mainly for the mathematician and the theoretical physicist. Issued quarterly. Annual subscription: domestic, $2.25; foreign, $2.75.

C. Engineering and Instrumentation

Reports research and development results of interest chiefly to the engineer and the applied scientist. Issued quarterly. Annual subscription: domestic, $2.25; foreign, $2.75.

D. Radio Propagation

Reports work in radio propagation, upper atmospheric physics, and communications. Issued six times a year. Annual subscription: domestic, $4.00; foreign, $4.75.

U.S. DEPARTMENT OF COMMERCE
Luther H. Hodges, Secretary

NATIONAL BUREAU OF STANDARDS
A. V. Astin, Director

Functions and Activities

The functions of the National Bureau of Standards are set forth in the Act of Congress, March 3, 1901, as amended. These include the development and maintenance of the national standards of measurement and the provision of means and methods for making measurements consistent with these standards; the determination of physical constants and properties of materials; the development of methods and instruments for testing materials, devices, and structures; advisory services to government agencies on scientific and technical problems; invention and development of devices to serve special needs of the Government; and the development of standard practices, codes, and specifications. The work includes basic and applied research, development, engineering, instrumentation, testing, evaluation, calibration services, and various consultation and information services. The Bureau also serves as the Federal technical research center in a number of specialized fields. The scope of activities of the National Bureau of Standards is suggested in the following listing of the divisions and sections engaged in technical work.

Washington, D.C.

Electricity. Resistance and Reactance. Electrochemistry. Electrical Instruments. Magnetic Measurements. Dielectrics. High Voltage.

Metrology. Photometry and Colorimetry. Refractometry. Photographic Research. Length. Engineering Metrology. Mass and Scale. Volumetry and Densimetry.

Heat. Temperature Physics. Heat Measurements. Cryogenic Physics. Equation of State. Statistical Physics.

Radiation Physics. X-ray. Radioactivity. Radiation Theory. High Energy Radiation. Radiological Equipment. Nucleonic Instrumentation. Neutron Physics.

Analytical and Inorganic Chemistry. Pure Substances. Spectrochemistry. Solution Chemistry. Standard Reference Materials. Applied Analytical Research. Crystal Chemistry.

Mechanics. Sound. Pressure and Vacuum. Fluid Mechanics. Engineering Mechanics. Rheology. Combustion Controls.

Polymers. Macromolecules: Synthesis and Structure. Polymer Chemistry. Polymer Physics. Polymer Characterization. Polymer Evaluation and Testing. Applied Polymer Standards and Research. Dental Research.

Metallurgy. Engineering Metallurgy. Microscopy and Diffraction. Metal Reactions. Metal Physics. Electrolysis and Metal Deposition.

Inorganic Solids. Engineering Ceramics. Glass. Solid State Chemistry. Crystal Growth. Physical Properties. Crystallography.

Building Research. Structural Engineering. Fire Research. Mechanical Systems. Organic Building Materials. Heat Transfer. Inorganic Building Materials. Metallic Building Materials.

Applied Mathematics. Numerical Analysis. Computation. Statistical Engineering. Mathematical Physics. Operations Research.

Data Processing Systems. Components and Techniques. Computer Technology. Measurements Automation. Engineering Applications. Systems Analysis.

Atomic Physics. Spectroscopy. Infrared Spectroscopy. Solid State Physics. Electron Physics. Atomic Physics.

Instrumentation. Engineering Electronics. Electron Devices. Electronic Instrumentation. Mechanical Instruments. Basic Instrumentation.

Physical Chemistry. Thermochemistry. Surface Chemistry. Organic Chemistry. Molecular Spectroscopy. Molecular Kinetics. Mass Spectrometry.

Office of Weights and Measures

Boulder, Colo.

Cryogenic Engineering. Cryogenic Equipment. Cryogenic Processes. Properties of Materials. Cryogenic Technical Services.

Central Radio Propagation Laboratory

Ionosphere Research and Propagation. Low Frequency and Very Low Frequency Research. Ionosphere Research. Prediction Services. Sun-Earth Relationships. Field Engineering. Radio Warning Services. Vertical Soundings Research.

Radio Propagation Engineering. Data Reduction Instrumentation. Radio Noise. Tropospheric Measurements. Tropospheric Analysis. Propagation-Terrain Effects. Radio-Meteorology. Lower Atmosphere Physics.

Radio Systems. Applied Electromagnetic Theory. High Frequency and Very High Frequency Research. Modulation Research. Antenna Research. Navigation Systems.

Upper Atmosphere and Space Physics. Upper Atmosphere and Plasma Physics. Ionosphere and Exosphere Scatter. Airglow and Aurora. Ionospheric Radio Astronomy.

Radio Standards Laboratory

Radio Physics. Radio Broadcast Service. Radio and Microwave Materials. Atomic Frequency and Time-Interval Standards. Millimeter-Wave Research.

Circuit Standards. High Frequency Electrical Standards. Microwave Circuit Standards. Electronic Calibration Center.

Order all publications from the Superintendent of Documents U.S. Government Printing Office, Washington 25, D.C.

Use of funds for printing this publication approved by the Director of the Bureau of the Budget (June 19, 1961).

JOURNAL OF RESEARCH of the National Bureau of Standards—A. Physics and Chemistry
Vol. 66A, No. 6, November–December 1962

Heat of Formation of Nitronium Perchlorate

Alexis A. Gilliland

(July 25, 1962)

Calorimetric measurements of the heat of solution of nitronium perchlorate (NO_2ClO_4) and of a mixture of potassium nitrate and potassium perchlorate in aqueous potassium hydroxide have been made. These are combined to give:

$$NO_2ClO_4(c) + 4KOH(\text{in } 5300\ H_2O) \rightarrow KClO_4(c) + KNO_3(c) + 2KOH(\text{in } 5300\ H_2O) + H_2O(\text{liq})$$
$$\Delta H = -285.80 \pm 0.38 \text{ kj/mole}$$
$$= -68.31 \pm 0.09 \text{ kcal/mole}$$

from which the standard heat of formation of nitronium perchlorate is calculated as

$$\Delta Hf°(25\ °C)\ NO_2ClO_4(c) = 37.19 \pm 1.0 \text{ kj/mole}$$
$$= 8.89 \pm 0.25 \text{ kcal/mole},$$

in which the uncertainty represents twice the estimated overall standard deviation of the result.

1. Introduction

This investigation was carried out in the Thermochemistry Section of the National Bureau of Standards as part of a program, currently in progress, on the determination of the thermodynamic properties of the "light element" compounds. Nitronium perchlorate is a white crystalline material stable at temperatures up to 120 °C. It is extremely hygroscopic, reacting rapidly with water to form nitric and perchloric acids. The heat of formation of NO_2ClO_4 can be determined by measuring this heat of decomposition. In this investigation, aqueous solutions of potassium hydroxide were used, as the potassium salts of the acids provided more suitable reference substances.

2. Materials

The potassium nitrate and potassium perchlorate were reagent grade materials, dried at 120 °C and stored in a desiccator over anhydrous magnesium perchlorate. The potassium hydroxide was reagent grade material; the calorimetric solutions were prepared with CO_2-free distilled water, and standardized against potassium acid phthalate. The NO_2ClO_4 was obtained from the Callery Chemical Company as a white crystalline powder; an analysis furnished by them showed:

Nitrogen	6.75– 6.74	theoretical	6.874 milliatoms/g
Chlorine	6.90– 6.82	theoretical	6.874 milliatoms/g
Total acid	13.61–13.71	theoretical	13.75 milliequiv/g
NO^+	0.06– 0.1	theoretical	0.00 milliequiv/g

Analyses for total acid by titrations with standard base, and for NO^+ by oxidation with standard ceric sulfate solution and back titration with standard ferrous ammonium sulfate gave:

Total acid	13.74 ±0.01 milliequiv/g
NO^+	0.06 ±0.01 milliequiv/g

The addition of silver nitrate to the acid solution gave a negative test for chloride ion.

From the ratio of total acid measured to total acid theoretical, the purity of the sample was estimated to be 99.93 mole percent or 99.65 weight percent. Since NO_2ClO_4 is extremely hygroscopic the major impurity is presumed to be water.

3. Units of Energy, Molecular Weights, and Conversion Factors

The joule was taken as the unit of energy. All instruments were calibrated in terms of standards maintained at the National Bureau of Standards. For conversion to the conventional thermochemical calorie, one calorie is taken as 4.1840 joules. All weights are corrected to vacuum.

All atomic weights were taken from the 1957 International Table of Atomic Weights [1].[1] The heat capacities were taken, where possible, from the literature [2]. For NO_2ClO_4, an estimated value of 36 cal/deg mole was used.

4. Apparatus and Procedure

The glass calorimeter, thermometric system, apparatus for measurement of electrical energy, and general calorimetric procedure have been described [3, 4, 5]. The calorimeter contained 454.6

[1] Figures in brackets indicate the literature references at the end of this paper

g of a 0.04126 N KOH solution. The sealed glass ampoule contained about 0.005 mole NO_2ClO_4. The calorimeter assembly was placed in a thermostatically controlled water-bath maintained at 25.0 ±0.002 °C. After the run, the calorimeter solution was titrated with standard acid, using a Beckman pH meter, as a check on the mass of sample and completeness of reaction. No calculations were based on the titrated values of NO_2ClO_4, since the weighed mass of sample was more accurate.

The heat of solution of an equimolar mixture of crystalline KNO_3 and $KClO_4$ was measured in the same apparatus. The calorimeter contained 454.6 g of a 0.02077 N KOH solution. The sample size was adjusted to give the same final solution as in the NO_2ClO_4 hydrolysis experiment.

Two series of electrical energy calibrations were carried out, one with 454.6 g of 0.04126 N KOH solution and a bulb containing 0.005 mole NO_2ClO_4, the second with 454.6 g of 0.02077 N KOH solution and a bulb containing 0.005 moles each of KNO_3 and $KClO_4$.

5. Results and Calculations

The results of the calibration experiments on the calorimetric system used for the measurement of the heat of reaction of NO_2ClO_4 are given in table 1. ΔRc corresponds to the corrected temperature rise of the system [6]. The energy equivalent, Es, of the "standard" system was obtained as the ratio of the quantity of electrical energy, Ee, to ΔRc, the corresponding rise in temperature.

TABLE 1. *Electrical calibrations of the* NO_2ClO_4 *system*

Expt.	ΔRc	Ee	Es
	Ohm	*j*	*j/ohm*
1	0.094266	1,990.86	21,119.6
2	.097337	2,053.87	21,100.6
3	.096767	2,042.58	21,108.2
4	.096023	2,026.13	21,100.5
5	.095990	2,025.34	21,105.6
Mean			21,106.9
Standard deviation of the mean			±3.5

The results of the experiments on the hydrolysis and neutralization of NO_2ClO_4 in solution I are given in table 3. Here, Δe is the change in the energy equivalent from the "standard" system, due to deviations in the mass of the glass bulb and sample from that of the reference bulb and sample. The term q(dil) represents the correction for the dilution of the individual final solutions to a uniform concentration. This was calculated from the data in [2], assuming that only the KOH(aq) contributed any heat effect. The total energy, q, is shown by the equation $q=\Delta Rc(Es+\Delta e)+q(\text{dil})$.

The results of the electrical calibration experiments on the $KNO_3/KClO_4$ system, and heat of solution experiments with the equimolar mixture of KNO_3 and $KClO_4$, are given in tables 2 and 4, respectively.

The term $q(KNO_3)$ in table 4 is the product of the difference between moles of $KClO_4$ and moles of KNO_3 and the heat of solution of KNO_3. It is applied to make the molar quantities of KNO_3 and $KClO_4$ exactly equal.

TABLE 2. *Electrical calibration on* $KNO_3/KClO_4$ *system*

Expt.	ΔRc	Ee	Es
	Ohm	*j*	*j/ohm*
1	0.092808	1962.35	21,144.1
2	.085947	1817.33	21,144.8
3	.095268	2013.70	21,137.2
4	.093441	1975.56	21,142.3
Mean			21,142.1
Standard deviation of the mean			±1.7

For the reaction

$$NO_2ClO_4(c)+[4KOH+5300\ H_2O](\text{soln})\rightarrow [KNO_3+KClO_4+2KOH+5301\ H_2O](\text{soln})$$
$$\Delta H=-199.02\pm0.35\ \text{kj}/145.465\ \text{g sample}$$
$$=-47.57\pm0.08\ \text{kcal}/145.465\ \text{g sample} \quad (1)$$

based upon mass of sample.

This value must be corrected for the presence of 0.35 weight percent moisture. If it is present as the hydrolysis products HNO_3 and $HClO_4$, it corresponds to 0.0283 mole of each acid.

TABLE 3. *Results of the experiments on the hydrolysis of* NO_2ClO_4

Expt.	Δe	ΔRc	q(dil)	q	Weighed NO_2ClO_4	Titrated NO_2ClO_4	$\frac{NO_2ClO_4(t)}{NO_2ClO_4(w)}$	$-\Delta H$ (25 °C)
	j	*Ohm*	*j*	*j*	*Mole*	*Mole*	%	*kj/mole*
1[a]	−13.6	0.023575	0.84	498.11	0.0024629	0.00238[b]	96.7	202.24
2	−10.1	.042890	.15	904.99	.0045364	.004546	100.2	199.50
3[a]	−10.2	.041598	.15	877.73	.0044650	.004434	99.4	196.58
4	−9.7	.049401	.00	1042.22	.0052450	.005253	100.2	198.71
5	−7.0	.063000	−.53	1328.76	.0066728	.006603	99.0	199.13
6	−7.7	.059705	−.38	1259.35	.0063211	.006246	98.8	199.23
7	−9.9	.046153	.04	973.73	.0049043	.004901	100.0	198.55
Mean								199.02
Standard deviation of the mean								±0.17

[a] Not included in mean value.
[b] Methyl orange end point.

TABLE 4. *Results of the experiments on the solution of* KNO_3 *and* $KClO_4$

Expt.	Δe	$-\Delta Rc$	KNO_3	$KClO_4$	$qKNO_3$	q	ΔH (25 °C)
	j	*Ohm*	*Mole*	*Mole*	*j*	*j*	*kj/mole*
1	−0.47	0.020236	0.0048956	0.0049288	−1.16	428.98	87.03
2	−1.43	.020453	.0049324	.0049920	−2.09	434.48	87.04
3	−1.54	.020401	.0049127	.0049985	−3.00	434.29	86.88
4	−1.32	.020485	.0049677	.0049943	−0.93	434.00	86.90
5	−1.36	.020450	.0049381	.0049863	−1.69	434.02	87.04
Mean							86.98
Standard deviation of the mean							±0.04

Therefore eq (1) actually corresponds to

$$0.9682\ NO_2ClO_4(c)+0.0283\ HNO_3(liq)+0.0283\ HClO_4(liq)+[4\ KOH+5300\ H_2O](soln)\longrightarrow[0.9965\ KNO_3+0.9965\ KClO_4+2.0070\ KOH+5301\ H_2O](soln)$$

$$\Delta H=-199.02\pm0.35\ kj = -47.57\pm0.08\ kcal.$$

For 1 mole of NO_2ClO_4 this becomes

$$NO_2ClO_4(c)+0.0292\ HNO_3(liq)+0.0292\ HClO_4(liq)+1.0328\ [4\ KOH+5300\ H_2O]\longrightarrow[1.0292\ KNO_3+1.0292\ KClO_4+2.0728\ KOH+5475\ H_2O]+1.0584\ H_2O(liq)$$

$$\Delta H=-205.56\pm0.36\ kj/mole = -49.13\pm0.09\ kcal/mole. \quad (1a)$$

From data in the literature [2], eq (1b) may be evaluated:

$$HClO_4(liq)+HNO_3(liq)+[4\ KOH+5300\ H_2O]\longrightarrow[KClO_4+KNO_3+2\ KOH+5300\ H_2O]+2\ H_2O(liq)$$

$$\Delta H=-230.9\ kj/mole = -55.2\ kcal/mole. \quad (1b)$$

Appropriate combination of eqs (1a) and (1b) gives

$$NO_2ClO_4(c)+1.0036\ [4\ KOH+5300\ H_2O]\longrightarrow[KClO_4+KNO_3+2.0144\ KOH+5320\ H_2O]+H_2O(liq)$$

$$\Delta H=-198.82\ kj/mole = -47.52\ kcal/mole. \quad (2)$$

From table 4 we have

$$KNO_3(c)+KClO_4(c)+[2\ KOH+5300H_2O](soln)\longrightarrow[KNO_3+KClO_4+2\ KOH+5300\ H_2O](soln)$$

$$\Delta H=86.98\pm0.07\ kj/mole = 20.79\pm0.02\ kcal/mole. \quad (3)$$

Combining eqs (2) and (3) and neglecting small dilution effects, we obtain:

$$NO_2ClO_4(c)+4\ KOH(in\ 5300\ H_2O)\longrightarrow KClO_4(c)+KNO_3(c)+2\ KOH(in\ 5300\ H_2O)+H_2O(liq)$$

$$\Delta H=-285.80\ kj/mole = -68.31\ kcal/mole. \quad (4)$$

If we take the following values for the heats of formation of the other substances in the reaction [7]

Substance	$\Delta Hf°_{298.15}$ (kcal/mole)
$KClO_4(c)$	−103.45
$KNO_3(c)$	−118.12
$H_2O(liq)$	−68.314
$KOH(2650\ H_2O)$	−115.23

we compute for $NO_2ClO_4(c)$

$$\Delta Hf°_{298.15}=37.19\pm1.0\ kj/mole = 8.89\pm0.25\ kcal/mole.$$

The uncertainty interval for the measured heats has been taken as twice the overall standard deviation of the mean based on the sum of the variances from the calibration and reaction experiments and reasonable variances assigned to the auxiliary data and the analysis for total acid.

6. Discussion

Cordes and Fetter [8] measured the heat of reaction of NO_2ClO_4 with water, they report a value for the heat of formation of $NO_2ClO_4(c)$ of 8.0 ±0.4 kcal/mole. Recalculating their data with the more recent auxiliary heats of formation used for this work, their value becomes 8.7 ±0.4 kcal/mole, in excellent agreement with the results obtained here.

7. References

[1] E. Wichers, J. Am. Chem. Soc. **80,** 4121 (1958).
[2] F. D. Rossini, D. D. Wagman, W. H. Evans, S. Levine, and I. Jaffe, Selected values of chemical thermodynamic properties, NBS Circ. **500** (U.S. Government Printing Office, Washington 25, D.C., 1952).
[3] W. H. Johnson, A. A. Gilliland, and E. J. Prosen, J. Research NBS **63A** (Phys. and Chem.) 161 (1959).
[4] E. J. Prosen, W. H. Johnson, and F. Y. Pergiel, J. Research NBS **62,** 43 (1959) RP2927.
[5] E. J. Prosen, F. W. Maron, and F. D. Rossini, J. Research NBS **46,** 106 (1951) RP2181.
[6] E. J. Prosen, Ch. 6 in Experimental Thermochemistry, F. D. Rossini, ed. (Interscience Publishers, Inc., New York, N.Y., 1956).
[7] D. D. Wagman, NBS, private communication.
[8] H. F. Cordes and N. R. Fetter, J. Phys. Chem. **62,** 1340 (1958).

(Paper 66A6–179)

JOURNAL OF RESEARCH of the National Bureau of Standards—A. Physics and Chemistry
Vol. 66A, No. 6, November–December 1962

Phase Equilibrium Relations in the Binary System Bismuth Sesquioxide-Niobium Pentoxide

R. S. Roth and J. L. Waring

(August 2, 1962)

The phase equilibrium diagram for the binary system bismuth sesquioxide-niobium pentoxide has been constructed from observations of fusion characteristics and X-ray diffraction data. In the system five binary compounds were observed with Bi_2O_3:Nb_2O_5 ratios of 5:3, 1:1, 4:9, 1:5, and 1:6. The 1:1 compound was found to transform irreversibly (in laboratory time) from the orthorhombic bismutotantalite type structure to a triclinic form at about 1,020 °C and melt congruently at 1,245 °C. The 5:3 compound melts incongruently at 1,193 °C the 4:9 at 1,183 °C and the 1:6 at 1,242 °C. The 1:5 compound has a maximum temperature of stability at 1,095 °C and the 4:9 and 1:6 compounds have minimum temperatures of stability at 1,070 °C and 1,002 °C respectively. Nb_2O_5 was found to enter into solid solution in Bi_2O_3, up to about 23.5 mole percent Nb_2O_5. The melting point is increased and the monoclinic-cubic phase transformation temperature is decreased. A morphotropic phase change occurrs at about 19.5 mole percent Nb_2O_5 from the cubic to a pseudocubic structure.

1. Introduction

A study of phase relationships in the binary system Bi_2O_3—Nb_2O_5 has been conducted as part of a program of fundamental phase equilibria studies of ceramic materials. Attempts to synthesize an orthorhombic $BiNbO_4$ compound isostructural with the mineral bismutotantalite have been reported as failures by several workers [1, 2].[1] Aurivillius [2] has indicated that the resultant material was triclinic. No systematic attempt to study the phase equilibrium relations in the entire binary system has been previously published.

X-ray diffraction data, together with the melting points of the compounds and the solidus and liquidus temperatures at various compositions across the system have been obtained in order to construct an equilibrium diagram.

2. Sample Preparation and Test Methods

The following starting materials were employed for the preparation of specimens:

Nb_2O_5—high-purity grade niobium pentoxide. Spectrographic analysis indicated less than about 0.01 percent Si, 0.001 percent Ca and Mg, with As, Cu, and Ta only questionably present.

Bi_2O_3—Reagent grade bismuth sesquioxide. Spectrographic analysis indicated less than about 0.01 percent Fe and Si, 0.001 percent Al and Pb, and 0.0001 percent Ag, Ca, Cr, Cu, Mg, and Mn, with Co questionably present.

For the preparation of the specimens the weight percentages were calculated to within ±0.01 percent, with no corrections made for percentage purity of the raw materials except for loss on ignition. The starting materials were weighed to the nearest ±0.1 mg, in sufficient quantities to yield 3 g batches. For most compositions each batch was mixed in a mechanical shaker for about 15 min and pressed into a disk in a ⅝ in. diam mold at 10,000 lb/in.^{2} The disks were sandwiched between Pt foil disks, stacked in a MgO crucible and calcined in air to 700 °C for either 3 or 6 hr in an electrically heated furnace. Some compositions were prepared by grinding a slurry of the weighed mixture and alcohol with an agate mortar and pestle for a few minutes. The slurry was then allowed to dry in air or dried under an infrared lamp, or in a drying oven, then pressed into a pellet and fired in the usual manner.

Following the preliminary heat treatment the disks were ground in an agate mortar, remixed, and a portion of the specimen reformed in a ⅝ in. mold at 10,000 lb/in.^{2} and reheated to a desired temperature.

Subsolidus as well as melting point data were obtained by the quenching technique on samples sealed in platinum tubes. An electrically heated vertical tube furnace wound with 80 percent Pt–20 percent Rh wire was used for the quenching experiments. The furnace was controlled by an a-c Wheatstone bridge controller which was capable of holding the temperature to at least ±2 °C for an extended period of time. Temperatures were measured with a Pt versus Pt 10 percent Rh thermocouple which had been calibrated against the melting points of NaCl (800.4 °C [3]) and Au (1,063 °C [4]). The thermocouple was recalibrated several times during the course of the work. When the tubes were opened the specimens were examined for physical appearances of melting. Specimens were

[1] Figures in brackets indicate the literature references at the end of this paper.

suspended in the furnace by fine Pt wire. In order to quench, the wire was burned off, allowing the sealed tubes to drop out of the heating chamber into a beaker of water. The first sign of glazing of the surface of the specimen was interpreted as the first experimental evidence for the solidus temperature. Acceptance of this appearance as evidence of melting was found justified in many specimens by an abrupt difference in the X-ray diffraction patterns of the specimens. The formation of a concave meniscus, without the formation of relatively large crystals, indicated the liquidus temperature. The precision of the temperature measurements for the experimental data points is about ±2 °C and the overall accuracy of the reported temperatures is probably about ±5 °C.

Equilibrium was considered to have been obtained when the X-ray diffraction patterns of specimens successively heated for longer times and/or at higher temperatures showed no change. X-ray diffraction powder patterns were made using a high angle recording Geiger counter diffractometer and nickel-filtered copper radiation, with the Geiger counter traversing the specimen at ¼°2θ/min and the radiation being recorded on the chart at 1°2θ/in. The unit cell dimensions reported can be considered accurate to about ±2 in the last decimal place listed.

3. Compounds in the Bi_2O_3-Nb_2O_5 System

3.1. Bi_2O_3

Four polymorphs of Bi_2O_3 have been reported. The equilibrium and stability relations have been somewhat confused mainly because Bi_2O_3 reacts with almost any container, and also because the high-temperature forms are difficult or impossible to quench.

a. Low-Temperature Monoclinic Modification

It has been recognized by several workers [5, 6, 7, 8] that the monoclinic form is the true low-temperature stable modification. The structure of this phase has been described by Sillen [6,9] who has shown by single crystal studies that, although the powder pattern can be indexed on the basis of orthorhombic symmetry, the true symmetry is monoclinic. The indexed X-ray diffraction powder pattern has been given by Sillen [6] and by Swanson et al. [10].

b. High-Temperature Cubic Modification

The monoclinic form of Bi_2O_3 transforms reversibly to a high-temperature form above 700 °C. This transformation was first reported by Guertler [5] to be at 704 °C using DTA apparatus, but since the composition of the container was not stated the results of this work were questioned by Schumb and Rittner [7]. Apparently only Pt can be used as a container for Bi_2O_3 at any appreciable temperature without fear of considerable contamination. Schumb and Rittner [7], using Pt containers found a temperature of 710 °C as the transformation point. However, they postulated that the high-temperature form was tetragonal.

DTA and high-temperature X-ray data (to be reported in more detail in a future publication) have shown that the Bi_2O_3 used in this study transforms from monoclinic to cubic at 730 ±5 °C, this phase remaining stable to the melting point at 825 ±5 °C. However, on cooling the cubic form of Bi_2O_3, it was observed that the monoclinic phase did not reform at 730 °C. Instead, the cubic phase supercooled to about 650 °C, then transformed to a tetragonal phase before reverting again to the monoclinic form at about 450 °C.

The cubic form has an X-ray diffraction powder pattern resembling that of a face-centered cubic cell of about 5.5 A. However Sillen [6] has pointed out that it is probably simple cubic with ordered oxygen vacancy positions somewhat similar to the cubic forms of Sb_2O_3 and As_2O_3.

c. Metastable Tetragonal Modification

A tetragonal form, structurally related to the cubic modification, was first reported by Sillen [6] who prepared it by very fast cooling of Bi_2O_3 vapor. It was also prepared by Schumb and Rittner [7] by a different method of condensation of a vapor. Both workers used a graphite furnace. The tetragonal form could not be obtained in this laboratory by condensing Bi_2O_3 vapors from a Pt dish of molten Bi_2O_3 onto a glass slide. It is still not known whether the graphite is necessary for obtaining the tetragonal form at room temperature. DTA and high-temperature X-ray patterns made in this laboratory on pure Bi_2O_3 indicate that under the conditions of the experiments the tetragonal form only occurs on cooling of the cubic form. It is found only in the range of 650 to 450 °C where the monoclinic form is the stable phase.

Sillen [6] reported the unit cell dimension of the tetragonal phase to be a=10.93 A, c=5.62 A, and Schumb and Rittner [7] obtained a=10.93 A, c=5.63 A. In the present study the tetragonal form was obtained at room temperature by quenching, from 773 °C, a mixture of 99 mole percent Bi_2O_3 and 1 mole percent Nb_2O_5. The unit cell dimensions of this phase are a=10.938 A, c=5.632 A.

d. Metastable Body-Centered Cubic Phase(s)

Sillen [6] first reported the occurrence of a body-centered cubic phase (a=10.08 A), which he found by fusing Bi_2O_3 in a porcelain crucible. He recognized that this phase was probably impure, and considered it to be a compound of Bi_2O_3 and a second metal oxide in the proportion of about 12 Bi^{+3} ions to one other metal cation. Schumb and Rittner [7] were able to prepare a body-centered cubic phase (a=10.245 A) which they considered to be a metastable form of pure Bi_2O_3(z=13) different from Sillen's phase. However, this phase could only be made by moderately fast cooling of the previously formed tetragonal phase. It should be pointed out here that even this "pure bismuth oxide" body-centered cubic phase may well have had some carbon atoms present in the lattice, since the

original tetragonal material had been prepared in a graphite crucible. In this laboratory a body-centered cubic phase has been found to occur in a large number of binary systems containing Bi_2O_3. The thermal stability of the phases found in these systems will be discussed in a future publication.

3.2. Compound $5Bi_2O_3 \cdot 3Nb_2O_5$

A compound was found in the present study at a ratio of $5Bi_2O_3 \cdot 3Nb_2O_5$. The X-ray diffraction powder pattern listed in table 1 can be partially indexed on the basis of a tetragonally distorted pyrochlore type structure with a c/a ratio less than one. The pseudotetragonal parameters are $a=10.912$ A, $c=10.496$ A. If the c axis is doubled (20.992 A) then the relatively strong peak at 6.99 A can be indexed as (003). However, this larger value does not account for all the extra peaks and the true symmetry is probably less than tetragonal. It should be noted that the powder pattern is always of quite poor quality regardless of the temperature from which the specimen is quenched or the length of time at which the specimen is held at temperature. This phenomenon is often indicative of a nonquenchable phase transformation and may indicate that the compound is actually tetragonal somewhat above room temperature.

The X-ray diffraction powder pattern of the compound $5Bi_2O_3 \cdot 3Nb_2O_5$ is similar to that of the pseudotetragonally distorted pyrochlore previously found for $3PbO \cdot Nb_2O_5$ [11]. However, in the latter compound the c/a ratio is greater than one instead of less than one. Another example of a tetragonally distorted pyrochlore with c/a less than one was found by C. R. Robbins of this laboratory, in a specimen of $2Bi_2O_3:GeO_2$ quenched from the liquid.

TABLE 1. *X-Ray diffraction powder data for the compound* $5Bi_2O_3 \cdot 3Nb_2O_5$ *(CuKα radiation)*

d	I/I_0	hkl	d	I/I_0	hkl
10.54	1	----------	1.6393	20	622
6.99	9	----------	1.5943	11	226
5.91	1	----------	1.5551	7	444
3.800	4	202			
3.440	2	301	1.4918	2	604
			1.4731	1	406
3.214	3	113	1.3634	3	800
3.111	100	222	1.3117	1	008
3.013	4	----------	1.2800	2	822
2.786	3	----------			
2.728	37	400	1.2483	3	662
			1.2293	4	626
2.624	22	004	1.2206	4	840
2.372	5	204	1.2110	2	804
2.292	5	323	1.1819	2	408
1.9297	19	440			
1.8915	23	404	1.1072	2	844
			1.0844	1	448
1.8645	3	----------	1.0484	2	10, 2, 2
1.7098	3	----------			

3.3. Compound $Bi_2O_3 \cdot Nb_2O_5$

Although this composition has not been found in nature, the analogous composition $Bi_2O_3 \cdot Ta_2O_5$ has been found and is called bismutotantalite. Both Dihlstrom [1] and Aurivillius [2] attempted to synthesize $BiNbO_4$ and $BiTaO_4$ but found that the synthetic compounds were different from the naturally occurring bismutotantalite, which is orthorhombic [12] and apparently isostructural with stibiotantalite ($SbTaO_4$) and antimony tetroxide (Sb_2O_4) [Dihlstrom, 1].

a. Low-Temperature Orthorhombic Modification

The low-temperature orthorhombic modification, was found in all solid-state preparations of the 1:1 composition heated below about 1,020 °C. However, once the high-temperature modification was formed the transformation could not be reversed by heating at lower temperatures. The X-ray diffraction powder pattern of the low-temperature modification is given in table 2, indexed on the basis of an orthorhombic unit cell with $a=4.980$ A, $b=11.70$ A, and $c=5.675$ A.

TABLE 2. *X-Ray diffraction powder data for the low temperature orthorhombic form of* $Bi_2O_3 \cdot Nb_2O_5$ *(CuKα radiation)*

d	I/I_0	hkl	d	I/I_0	hkl
5.84	12	020	1.6969	3	152
4.576	8	110	1.6934	16	123
3.740	20	101	1.6879	9	232
3.564	15	111			
3.153	100	121	1.6439	3	310
			1.6337	4	251
3.071	8	130	1.6106	5	133
2.924	40	040	1.6080	7	062
2.838	26	002	1.5933	2	301
2.758	7	012			
2.700	3	131	1.5772	14	242
			1.5377	20	321
2.553	21	022	1.5278	3	330
2.490	22	200	1.5140	11	143
2.412	2	112	1.4942	2	213
2.305	20	141			
2.294	8	032	1.4635	6	080
			1.4621	4	252
2.292	10	220	1.4411	2	072
2.272	3	122	1.4228	3	312
2.238	6	211	1.4190	2	004
2.123	1	221			
2.085	3	132	1.4120	2	153
			1.4089	2	014
2.037	24	042	1.4063	2	233
1.9852	3	151	1.4003	2	341
1.9689	6	231	1.3799	8	024
1.9485	2	060			
1.8967	27	240	1.3636	3	104/181
			1.3564	1	114
1.8721	17	202	1.3547	2	350
1.8486	8	212	1.3513	5	262
1.8070	3	052	1.3479	3	271
1.7800	13	222			
1.7694	14	103	1.3333	2	034
			1.3126	4	163
1.7492	4	113	1.3011	4	082
1.7302	34	161			

b. High-Temperature Triclinic Modification

From about 1,020 °C to the melting point, about 1,245 °C, the stable modification of $Bi_2O_3 \cdot Nb_2O_5$ is the triclinic form reported by Aurivillius [2]. The X-ray diffraction powder pattern, listed in table 3, was indexed on the basis of a triclinic unit cell with $a=7.61_1$A, $b=5.53_6$A, $c=7.91_9$A, $\alpha=89.88°$, $\beta=77.43°$, $\gamma=87.15°$ as compared with the rather inaccurate values calculated by Aurivillius [2] from Weissenburg photographs of $a=7.7_1$A, $b=5.5_5$A, $c=7.9_7$A, $\alpha=89°$, $\beta=77°$, $\gamma=87°$.

TABLE 3. *X-ray diffraction power data for the high temperature triclinic form of* $Bi_2O_3 \cdot Nb_2O_5$ *(CuKα radiation)*

d	I/I_o	hkl[a]	d	I/I_o	hkl[a]
7.41	21	100	2.219	7	
6.09	2	$10\bar{1}$	2.177	4	
4.544	8	$\bar{1}10$			
4.324	3	110	2.166	6	
3.867	14	002	2.115	15	
			2.073	11	
3.779	4	$10\bar{2}$	2.048	4	
3.710	15	200	2.011	12	
3.666	2	$20\bar{1}$			
3.187	68	$01\bar{2}$	1.9803	23	
3.154	100	$102/\bar{2}10$	1.9348	15	
			1.9019	3	
3.149	97	012	1.8919	6	
3.102	24	$11\bar{2}$	1.8635	21	
3.025	44	$20\bar{2}$			
3.013	56	210	1.8567	15	
2.763	33	020	1.8363	6	
			1.8164	4	
2.706	3	112	1.7974	6	
2.690	7	$\bar{2}12$	1.7878	23	
2.620	8	$21\bar{2}/10\bar{3}$			
2.590	2	021	1.7775	5	
2.549	6	$120/\bar{1}21$	1.7666	6	
			1.7471	6	
2.474	8	300	1.7345	8	
2.428	25	202	1.7208	4	
2.370	4	$20\bar{3}/\bar{1}13$			
2.326	4	$30\bar{2}$	1.7160	5	
2.301	2		1.7074	7	
			1.6857	9	
2.274	4		1.6822	7	
2.255	4		1.6732	9	
2.246	5		1.6690	7	

[a] Due to the complexity of the pattern only those *hkl* values have been given which can be assigned with reasonable certainty.

3.4. Compound $4Bi_2O_3 \cdot 9Nb_2O_5$

This compound was found to be stable from about 1,070 °C to the incongruent melting point of 1,183 °C. The X-ray diffraction powder pattern, listed in table 4, can be indexed on the basis of a hexagonal unit cell with $a=6.447$A, $c=19.778$ A. There is no indication on the powder pattern that the true symmetry might have $a=\sqrt{3}$ 6.447 A=11.166 A.

A compound with a similar X-ray diffraction powder pattern $Ba(Nb_{.75}Li_{.25})O_3$ has $a=\sqrt{3}$ 5.797 A=10.040 A, $c=19.072$A; the increase in a is represented by only one small peak in the powder diffraction pattern. These X-ray diffraction powder patterns are similar to those of the hexagonal compounds $5BaO \cdot 2Nb_2O_5$ [13], $5BaO \cdot 2Ta_2O_5$ [14], Hex-$BaTiO_3$ [15] and Rhomb $PbO \cdot Nb_2O_5$ [11]. It can be assumed that all of these compounds are structurally related, the major difference being in the stacking sequence of layers of the large cations plus O^{-2} ions.

TABLE 4. *X-ray diffraction power data for the compound* $4Bi_2O_3 \cdot 9Nb_2O_5$ *(CuKα radiation)*

d	I/I_o	hkl	d	I/I_o	hkl
9.86	13	002	1.5703	18	1, 1, 11
4.946	4	004	1.5324	14	224
3.294	93	006	1.4931	9	225
3.179	83	111	1.4869	5	308
3.063	100	112	1.4133	2	0, 0, 14
2.895	10	113	1.4000	4	227
2.699	73	114	1.3554	3	3, 0, 10
2.499	28	115	1.3503	4	228
2.471	6	008	1.2496	5	2, 2, 10
2.308	4	116	1.2340	10	2, 1, 13
2.125	11	117	1.2203	5	1, 1, 15
1.9778	7	0, 0, 10	1.2162	5	411
1.9616	29	118	1.2096	4	412
1.8610	57	300	1.2003	3	2, 2, 11
1.8158	11	119	1.1833	5	414
1.6857	27	1, 1, 10	1.1646	4	415
1.6483	8	0, 0, 12	1.1539	3	1, 1, 16
1.6210	39	306	1.0749	2	330
1.6070	11	221	1.0376	3	4, 1, 10
1.5913	11	222	1.0215	2	336
			1.0088	4	4, 1, 11

3.5. Compounds $Bi_2O_3 \cdot 5Nb_2O_5$ and $Bi_2O_3 \cdot 6Nb_2O_5$

The compound $Bi_2O_3 \cdot 5Nb_2O_5$ was found to be stable from room temperature to a dissociation temperature of about 1,095 °C. The unindexed X-ray diffraction powder pattern of this compound is listed in table 5. The compound $Bi_2O_3 \cdot 6Nb_2O_5$ was found to be stable from about 1,002 °C to the incongruent melting point of 1,242 °C. The unindexed X-ray diffraction powder pattern of this compound is given in table 6. The X-ray patterns of these two compounds are very complex and obviously of low symmetry. From the general appearance of the two patterns it can be concluded that these two compounds are structurally related and probably also structurally related to pure Nb_2O_5.

TABLE 5. *X-ray diffraction powder data for the compound* $Bi_2O_3 \cdot 5Nb_2O_5$ *(CuKα radiation)*

d	I/I_0	d	I/I_0	d	I/I_0
12.4	15	3.319	15	2.843	45
12.2	15	3.276	15	2.781	60
8.55	15	3.196	50	2.763	15
3.945	100	3.073	20	2.722	15
3.921	45	3.062	30	2.601	20
3.854	30	3.001	90	2.566	5
3.599	30	2.964	35	2.487	5
3.523	20	2.940	65	2.424	5
3.453	20	2.900	5	2.373	45
3.367	80	2.859	30		

TABLE 6. *X-ray diffraction powder data for the compound* $Bi_2O_3 \cdot 6Nb_2O_5$ *(CuKα radiation)*

d	I/I_0	d	I/I_0	d	I/I_0
7.49	5	3.206	40	2.736	10
6.15	5	3.129	25	2.596	40
5.92	10	3.089	20	2.592	35
3.929	100	3.032	40	2.439	5
3.673	25	3.000	60	2.402	10
3.619	15	2.964	15	2.386	10
3.455	30	2.930	40	2.352	10
3.442	35	2.854	10	2.294	5
3.310	10	2.788	30	2.275	10
3.274	20	2.773	55		

3.6. Nb_2O_5

The stability relations of the various reported polymorphs of Nb_2O_5 have been summarized by several workers [16, 17, 18, 19]. Bi_2O_3, unlike PbO [11], has no catalytic action on the thermal stability of the various modifications of Nb_2O_5. Since it has been concluded [11, 16, 19] that the high-temperature monoclinic form of Nb_2O_5 (H-Nb_2O_5) is the only stable form, no phase transformation temperature has been indicated. The X-ray powder pattern and unit cell dimensions of the stable form were previously reported [11].

4. Discussion of Phase Equilibria

The phase equilibrium diagram of the binary system Bi_2O_3—Nb_2O_5 is shown in figure 1. The experimental data from which this diagram was constructed are given in table 7. The designation Per. in table 7 stands for the perovskite structure type and signifies that the material which crystallizes in this structure type must have been in the liquid state when quenched (see discussion of metastable compounds in section 5). The system contains one compound which melts congruently, $Bi_2O_3 \cdot Nb_2O_5$; three compounds which melt incongruently, $5Bi_2O_3 \cdot 3Nb_2O_5$, $4Bi_2O_3 \cdot 9Nb_2O_5$, and $Bi_2O_3 \cdot 6Nb_2O_5$; and one compound which dissociates before melting, $Bi_2O_3 \cdot 5Nb_2O_5$. In addition $Bi_2O_3 \cdot Nb_2O_5$ has two polymorphs and $4Bi_2O_3 \cdot 9Nb_2O_5$ and $Bi_2O_3 \cdot 6Nb_2O_5$ both apparently have minimum temperatures of stability.

The high-temperature cubic polymorph of Bi_2O_3 is stabilized by the addition of Nb_2O_5 in solid solution. When specimens containing 1, 2, 3, and 4 mole percent Nb_2O_5 are quenched from the region between the monoclinic-cubic phase transformation and the solidus temperature the resultant material is tetragonal with the unit cell dimensions shown in table 8. However, high-temperature X-ray patterns show the compositions to be really cubic at these temperatures. The unit cell dimensions of the cubic and pseudocubic solid solutions from 5 mole percent Nb_2O_5 to 25 mole percent Nb_2O_5 are also given in table 8.

TABLE 7. *Experimental data for compositions in the binary system* Bi_2O_3–Nb_2O_5

Composition		Heat treatment				Results	
		Calcine [a]		Quench [b]			
Bi_2O_3	Nb_2O_5	Temp	Time	Temp	Time	Physical observation	X-ray diffraction analyses [c]
Mole %	*Mole %*	*°C*	*hr*	*°C*	*hr*		
100	0			826	0.083	just begun to melt	Mon-Bi_2O_3
				924	.083	melted	Do.
90	1	700	3				Mon-Bi_2O_3
				721	16.0	no melting	Tet-Bi_2O_{3ss}+Mon-Bi_2O_3
				725	16.0	do	Tet-Bi_2O_{3ss}+Mon-Bi_2O_3 (tr)
				773	2.0	do	Tet-Bi_2O_{3ss}
				827	0.083	just begun to melt	
				833	.017	partially melted	Tet-Bi_2O_{3ss}+Mon-Bi_2O_3
				840	.017	considerably melted	
				850	.017	almost completely melted	Tet-Bi_2O_{3ss}+Mon-Bi_2O_3
				861	.017	completely melted (?)	
				880	.017	completely melted	
98	2	700	3				Mon-Bi_2O_3
				721	16.0	no melting	Tet-Bi_2O_{3ss}+Mon-Bi_2O_3
				725	16.0	do	Tet-Bi_2O_{3ss}
				773	2.0	do	Do.
				834	0.017	do	Do.
				840	.017	just begun to melt	
				850	.017	partially melted	
				861	.067	do	Tet-Bi_2O_{3ss}+Mon-Bi_2O_3
				880	.017	almost completely melted	
				901	.017	completely melted	
97	3	700	3				Mon-Bi_2O_3+b.c.c.-Bi_2O_{3ss}
				700	16.5	no melting	Mon-Bi_2O_3+C-Bi_2O_{3ss}
				712	17.0	do	Tet-Bi_2O_{3ss}+Mon-Bi_2O_3
				775	64.0	do	Tet-Bi_2O_{3ss}
				834	0.083	do	
				840	.017	do	
				850	.017	just begun to melt	Tet-Bi_2O_{3ss}+Mon-Bi_2O_3 (tr)
				861	.017	partially melted	
				880	.017	do	
				900	.017	completely melted (?)	
96	4	700	3				b.c.c. Bi_2O_{3ss}(a=10.263A)+C-Bi_2O_{3ss} (tr)
				700	16.5	no melting	C-Bi_2O_{3ss}+Mon-Bi_2O_3
				712	17.0	do	Tet-Bi_2O_{3ss}
				775	64.0	do	Do.
				840	0.017	do	
				861	.033	partially melted	
				880	.017	do	
				899	.017	almost completely melted	
				920	.017	completely melted (?)	
95	5	700	3				b.c.c. Bi_2O_{3ss}+C-Bi_2O_{3ss}
(19.1)				615/485	1/16	no melting	Mon-Bi_2O_3+C-Bi_2O_{3ss}+b.c.c. Bi_2O_{3ss} (tr)
				500	2.0	do	b.c.c. Bi_2O_{3ss}+C-Bi_2O_{3ss}
				567	15.5	do	Mon-Bi_2O_3+C-Bi_2O_{3ss}+b.c.c. Bi_2O_{3ss} (tr)
				596	0.5	do	Do.
				632	1.0	do	Mon-Bi_2O_3+C-Bi_2O_{3ss}
				693	1.0	do	C-Bi_2O_{3ss}+Mon-Bi_2O_3
				700	3.0	do	C-Bi_2O_{3ss}+Mon-Bi_2O_3 (tr)
				782	16.0	do	C-Bi_2O_{3ss} (poorly crystalline)
				850	0.167	do	Do.
				860	.167	do	Do.
				869	.167	partially melted	C-Bi_2O_{3ss}+Tet-Bi_2O_{3ss} (tr)
				885	.017	considerably melted	C-Bi_2O_{3ss}+Tet-Bi_2O_{3ss}
				885	.167	tube leaked	(from outside of tube only) Tet-Bi_2O_{3ss}
				903	.033	considerably melted	C-Bi_2O_{3ss}+Tet-Bi_2O_{3ss}+Mon-Bi_2O_3
				920	.033	do	
				941	.067	completely melted	
				1,008	.017	do	C-Bi_2O_{3ss}+Tet-Bi_2O_{3ss}

See footnotes at end of table.

TABLE 7. *Experimental data for compositions in the binary system* Bi_2O_3–Nb_2O_5—Continued

Composition		Heat treatment				Results	
		Calcine [a]		Quench [b]		Physical observation	X-ray diffraction analyses [c]
Bi_2O_3	Nb_2O_5	Temp	Time	Temp	Time		
Mole %	*Mole %*	*°C*	*hr*	*°C*	*hr*		
92.31 (12:1)	7.69	700	3	603	65.0	no melting	C-Bi_2O_{3ss}+b.c.c. Bi_2O_{3ss}
				650	44.0	do	Mon-Bi_2O_3+C-Bi_2O_{3ss}
				681	17.0	do	C-Bi_2O_{3ss}+Mon-Bi_2O_3
				783	1.0	do	C-Bi_2O_{3ss}+Mon-Bi_2O_3 (tr)
				889	0.5	do	C-Bi_2O_{3ss}
				904	.25	just begun to melt	Do.
				912	.25	partially melted	C-Bi_2O_{3ss}+Tet-Bi_2O_{3ss} (tr)
				941	.167	do	C-Bi_2O_{3ss}+Tet-Bi_2O_{3ss}
				956	.083	do	C-Bi_2O_{3ss}+Tet-Bi_2O_{3ss}+Mon-Bi_2O_3
				975	.017	completely melted (?)	
90.91 (10:1)	9.09	700	3				C-Bi_2O_{3ss}+b.c.c. Bi_2O_{3ss}+b.c.c.'-Bi_2O_{3ss} (tr)
				603	65.0	no melting	C-Bi_2O_{3ss}+Mon-Bi_2O_3+b.c.c. Bi_2O_{3ss} (tr)+b.c.c.'-Bi_2O_{3ss}(tr)
				650	44.0	do	C-Bi_2O_{3ss}+Mon-Bi_2O_3+b.c.c.'-Bi_2O_{3ss} (tr)
				681	17.0	do	C-Bi_2O_{3ss}+b.c.c.'-Bi_2O_{3ss} (tr)
				869	17.0	do	C-Bi_2O_{3ss}
				904	0.133	do	Do.
				937	.32	partially melted	C-Bi_2O_{3ss}+Tet-Bi_2O_{3ss}
				965	.017	do	Do.
				976	.033	do	
				996	.033	almost completely melted	
				1,012	.033	completely melted	
88	12	700	3				C-Bi_2O_{3ss}+b.c.c.'-Bi_2O_{3ss} (tr)
				622	18	no melting	C-Bi_2O_{3ss}+Mon-Bi_2O_3
				928	16	do	C-Bi_2O_{3ss}
				944	0.417	do	Do.
				960	.417	do	Do.
				988	.083	partially melted	C-Bi_2O_{3ss}+Tet-Bi_2O_{3ss}
				1,012	.067	do	
				1,041	.067	completely melted	
85	15	700	3				C-Bi_2O_{3ss}
				622	18	no melting	C-Bi_2O_{3ss}+Mon-Bi_2O_3
				928	16	do	C-Bi_2O_{3ss}
				1,026	0.017	do	Do.
				1,033	.033	just begun to melt	C-Bi_2O_{3ss}+Tet-Bi_2O_{3ss} (tr)
				1,038	.033	partially melted	Do.
				1,054	.067	do	
				1,073	.067	completely melted	
84	16	700	6				C-Bi_2O_{3ss}
				600	16	no melting	C-Bi_2O_{3ss}+b.c.c. Bi_2O_{3ss}
				619	22	do	C-Bi_2O_{3ss}+Mon-Bi_2O_3 (tr)
				1,004	1.0	do	C-Bi_2O_{3ss}
				1,050	0.083	partially melted	
				1,060	.083	do	
				1,069	.083	considerably melted	
				1,080	.083	completely melted	
83	17	700	6				
				600	16	no melting	C-Bi_2O_{3ss}+b.c.c. Bi_2O_{3ss}
				619	22	do	C-Bi_2O_{3ss}+Mon-Bi_2O_3 (tr)
				1,004	1.0	do	C-Bi_2O_{3ss}
				1,050	0.083	do	
				1,060	.083	partially melted	
				1,070	.083	do	
				1,090	.083	completely melted	
82	18	700	6				
				599	16	no melting	C-Bi_2O_{3ss}+b.c.c.-Bi_2O_{3ss}
				615	18	do	C-Bi_2O_{3ss}+Mon-Bi_2O_3 (tr)
				1,004	2	do	C-Bi_2O_{3ss}
				1,060	0.083	do	
				1,070	.083	partially melted	
				1,090	.083	almost completely melted	
81	19	700	6				
				599	16	no melting	C-Bi_2O_{3ss}+bcc Bi_2O_{3ss}(tr)
				615	18	do	C-Bi_2O_{3ss}+Mon−Bi_2O_3(tr)
				1,004	2	do	C-Bi_2O_{3ss}
				1,070	0.083	do	C′-Bi_2O_{3ss}
				1,080	0.083	partially melted	
80	20	700	3				C′-Bi_2O_{3ss}+bcc′Bi_2O_{3ss}
				503	70.5	no melting	Do.
				599	23	do	Do.
				869	17	do	C′-Bi_2O_{3ss}
				1,010	16	do	Do.
				1,056	0.5	do	Do.
				1,080	1.0	just begun to melt	
				1,101	0.167	completely melted	C′-Bi_2O_{3ss}
79	21	700	6				
				1,050	2	no melting	C′-Bi_2O_{3ss}
				1,080	0.083	do	
				1,090	.083	do	
				1,095	.083	just begun to melt	
				1,106	.083	almost completely melted	
				1,115	.083	completely melted	
78	22	700	6				
				1,050	2	no melting	C′-Bi_2O_{3ss}
				1,090	0.083	do	
				1,115	.083	almost completely melted	

See footnotes at end of table.

TABLE 7. *Experimental data for compositions in the binary system* Bi_2O_3–Nb_2O_5—Continued

Composition		Heat treatment				Results	
		Calcine [a]		Quench [b]			
Bi_2O_3	Nb_2O_5	Temp	Time	Temp	Time	Physical observation	X-ray diffraction analyses [c]
Mole %	*Mole %*	*° C*	*hr*	*° C*	*hr*		
77	23	700	6				
				1,050	21.5	no melting	C′-Bi_2O_{3ss}
				1,115	0.083	almost completely melted	
				1,124	.083	completely melted(?)	
76	24	700	6				
				1,050	21.5	no melting	C′-Bi_2O_{3ss}+5Bi_2O_3·3Nb_2O_5(tr)
				1,096	0.083	do	
				1,124	.083	considerably melted	
				1,135	.167	completely melted	
75	25	700	3				C′-Bi_2O_{3ss}+5Bi_2O_3·3Nb_2O_5
				503	70.5	no melting	Do.
				1,080	0.5	do	Do.
				1,081	16.0	do	Do.
				1,090	0.5	do	
				1,101	.5	partially melted	
				1,110	.75	considerably melted	
				1,135	.25	almost completely melted	
70	30	700	3				
				1,095	0.133	no melting	
				1,101	.083	just begun to melt	
				1,153	.083	partially melted	
				1,166	.083	considerably melted	
				1,174	.083	completely melted	
66.67 (2:1)	33.33	700	3				C′-Bi_2O_{3ss}+5Bi_2O_3·3Nb_2O_5
				1,095	.083	no melting	
				1,106	.083	partially melted	
				1,149	2.5	do	C′-Bi_2O_{3ss}+5Bi_2O_3·3Nb_2O_5
				1,160	0.33	do	Do.
				1,170	.167	considerably melted	
				1,180	.083	almost completely melted	
				1,191	.033	completely melted	
62.5 (5:3)	37.5	700	3				C′-Bi_2O_{3ss}+5Bi_2O_3·3Nb_2O_5+L-Bi_2O_3·Nb_2O_5
				1,008	16.0	no melting	5Bi_2O_3·3Nb_2O_5
				1,146	1.0	do	5Bi_2O_3·3Nb_2O_5+C′Bi_2O_{3ss}(tr)+H-Bi_2O_3·Nb_2O_5(tr)
				1,150	64.0	do	5Bi_2O_3·3Nb_2O_5
				1,170	0.167	do	
				1,180	.083	do	
				1,191	.033	do	
				1,196	.083	partially melted	5Bi_2O_3·3Nb_2O_5+H-Bi_2O_3·Nb_2O_5(tr)+C′-Bi_2O_{3ss}(tr)
				1,200	1.0	completely melted (?)	5Bi_2O_3·3Nb_2O_5+C′−Bi_2O_{3ss}+H−Bi_2O_3·Nb_2O_5
60	40	700	3				5Bi_2O_3·3Nb_2O_5+L−Bi_2O_3·Nb_2O_5
				945	16.0	no melting	Do.
				1,057	0.667	do	5Bi_2O_3·3Nb_2O_5+H−Bi_2O_3·Nb_2O_5
				1,127	.5	do	Do.
				1,151	.5	do	Do.
				1,175	.333	do	Do.
				1,191	.033	do	Do.
				1,195	.5	partially melted	5Bi_2O_3·3Nb_2O_5+H−Bi_2O_3·Nb_2O_5
				1,200	.167	considerably melted	
				1,210	.083	almost completely melted	
				1,220	.167	completely melted	
55	45	700	3				
				1,189	0.083	no melting	
				1,195	.083	partially melted	
				1,230	.083	considerably melted	
				1,240	.083	completely melted	
50 (1:1)	50	700	3				L−Bi_2O_3·Nb_2O_5+5Bi_2O_3·3Nb_2O_5+L−Nb_2O_5
				945	16.5	no melting	L−Bi_2O_3·Nb_2O_5
				1,001	16.0	do	Do.
				1,008	184.0	do	Do.
				1,024	2.833	do	Do.
				1,024	114.0	do	L−Bi_2O_3·Nb_2O_5+H−Bi_2O_3·Nb_2O_5(tr)
				1,036	15.5	do	H−Bi_2O_3·Nb_2O_5
				1,051	1.75	do	Do.
				1,156	20.0	do	Do.
				1,225	0.5	do	Do.
				1,241	.33	do	Do.
				1,252	.33	completely melted	Do.
		1,150	33				
				1,008	184.0	no melting	H−Bi_2O_3·Nb_2O_5
				1,240	0.167	do	
		1,200	3	1,246	.167	completely melted	
							H−Bi_2O_3·Nb_2O5
				1,001	16.0	no melting	Do.
				1,024	114.0	do	Do.
45	55	700	3				
				1,169	0.167	no melting	
				1,179	.167	do	
				1,182	.167	just begun to melt	
				1,230	.083	considerably melted	
				1,240	.083	almost completely melted	
				1,246	.167	completely melted	
40	60	700	3				
				1,145	17.0	no melting	H−Bi_2O_3·Nb_2O_5+4Bi_2O_3·9Nb_2O_5
				1,169	0.167	do	Do.
				1,179	.167	do	

See footnotes at end of table.

TABLE 7. *Experimental data for compositions in the binary system* Bi_2O_3–Nb_2O_5—Continued

Composition		Heat treatment				Results	
		Calcine [a]		Quench [b]			
Bi_2O_3	Nb_2O_5	Temp	Time	Temp	Time	Physical observation	X-ray diffraction analyses [c]
Mole %	*Mole %*	*°C*	*hr*	*°C*	*hr*		
40	60			1,181	.083	partially melted	H−Bi_2O_3·Nb_2O_5+4Bi_2O_3·9Nb_2O_5+Per
				1,194	.083	considerably melted	H−Bi_2O_3·Nb_2O_5+Per
				1,201	.167	do	Do.
				1,212	.083	almost completely melted	
				1,223	.083	completely melted	
36	64	700	3				
				1,173	.083	no melting	
				1,177	.083	do	
				1,179	.083	do	H−Bi_2O_3·Nb_2O_5+4Bi_2O_3·9Nb_2O_5
				1,182	.167	partially melted	
				1,185	.083	completely melted	
33.33 (1:2)	66.67	700	3				
				1,145	17.0	no melting	4Bi_2O_3·9Nb_2O_5+H−Bi_2O_3·Nb_2O_5
				1,180	0.083	considerably melted	4Bi_2O_3·9Nb_2O_5+H−Bi_2O_3·Nb_2O_5+Per
				1,194	.083	completely melted	Per+H−Bi_2O_3·Nb_2O_5
32	68	700	3				
				1,149	2.0	no melting	4Bi_2O_3·9Nb_2O_5+H−Bi_2O_3·Nb_2O_5+Bi_2O_3·6Nb_2O_5
				1,149	17.0	do	4Bi_2O_3·9Nb_2O_5+H−Bi_2O_3·Nb_2O_5(tr)
		1,150	33				Do.
				1,170	0.167	no melting	
				1,175	.167	do	
				1,181	.167	just begun to melt	
				1,186	.083	completely melted	
31.25 (5:11)	68.75	700	3				
				1,149	2.0	no melting	4Bi_2O_3·9Nb_2O_5+H−Bi_2O_3·Nb_2O_5+Bi_2O_3·6Nb_2O_5
				1,149	17.0	do	4Bi_2O_3·9Nb_2O_5+H-Bi_2O_3·Nb_2O_5(tr)
30.77 (4:9)	69.23	700	3				
				1,001	23.0	no melting	L-Bi_2O_3·Nb_2O_5+Bi_2O_3·5Nb_2O_5
				1,040	1.0	do	H-Bi_2O_3·Nb_2O_5+Bi_2O_3·6Nb_2O_5+Bi_2O_3·5Nb_2O_5
				1,061	40.0	do	H-Bi_2O_3·Nb_2O_5+Bi_2O_3·5Nb_2O_5
				1,075	64.0	do	H-Bi_2O_3·Nb_2O_5+Bi_2O_3·5Nb_2O_5+4Bi_2O_3·9Nb_2O_5
				1,149	2.0	do	4Bi_2O_3·9Nb_2O_5+H-Bi_2O_3·Nb_2O_5+Bi_2O_3·6Nb_2O_5
				1,151	16.0	do	4Bi_2O_3·9Nb_2O_5
				1,151	70.0	do	Do.
				1,170	0.167	do	4Bi_2O_3·9Nb_2O_5+Bi_2O_3·6Nb_2O_5+H-Bi_2O_3·Nb_2O_5
				1,180	.083	partially melted (metastable melting of non-reacted components)	4Bi_2O_3·9Nb_2O_5+Bi_2O_3·6Nb_2O_5+H-Bi_2O_3·Nb_2O_5+Per
		1,150	77				4Bi_2O_3·9Nb_2O_5
				1,001	23	no melting	4Bi_2O_3·9Nb_2O_5+Bi_2O_3·5Nb_2O_5+Bi_2O_3·Nb_2O_5(?)
				1,061	40	do	4Bi_2O_3·9Nb_2O_5+Bi_2O_3·5Nb_2O_5(tr)
				1,075	64	do	4Bi_2O_3·9Nb_2O_5
				1,180	0.033	do	
				1,185	.033	partially melted	4Bi_2O_3·9Nb_2O_5+H-Bi_2O_3·Nb_2O_5+Bi_2O_3·6Nb_2O_5+Per
				1,185	1.0	considerably melted	Per+4Bi_2O_3·9Nb_2O_5+H-Bi_2O_3·Nb_2O_5+Bi_2O_3·6Nb_2O_5
				1,190	0.083	do	Per+H-Bi_2O_3·Nb_2O_5+Bi_2O_3·6Nb_2O_5
				1,190	1.0	do	
				1,194	0.167	completely melted	Per+H-Bi_2O_3·Nb_2O_5
				1,210		do	Do.
30	70	700	3				
				1,149	2.0	no melting	4Bi_2O_3·9Nb_2O_5+H-Bi_2O_3·Nb_2O_5+Bi_2O_3·6Nb_2O_5
				1,152	18.0	do	4Bi_2O_3·9Nb_2O_5+Bi_2O_3·6Nb_2O_5
		1,150	33				
				1,180	0.167	no melting	
				1,185	.167	partially melted	
				1,200	.25	completely melted	
28.57 (2:5)	71.43	700	3				
				1,083	16.0	no melting	H-Bi_2O_3·Nb_2O_5+4Bi_2O_3·9Nb_2O_5+Bi_2O_3·5Nb_2O_5+Bi_2O_3·6Nb_2O_5(?)
				1,102	1.0	do	4Bi_2O_3·9Nb_2O_5+H−$Bi_2O_3Nb_2O_5$+Bi_2O_3·6Nb_2O_5
				1,149	17.0	do	4Bi_2O_3·9Nb_2O_5+Bi_2O_3·6Nb_2O_5
				1,150	2.0	do	Do.
				1,150	18.0	do	Do.
		1,142	16				Do.
				1,180	0.167	no melting	
				1,187	.167	partially melted	Per+H-Bi_2O_3·Nb_2O_5+Bi_2O_3·6Nb_2O_5
				1,200	.167	almost completely melted	
				1,210	.167	completely melted	
25 (1:3)	75	700	3				L-Bi_2O_3·Nb_2O_5+5Bi_2O_3·3Nb_2O_5+L-Nb_2O_5
				1,001	18.0	no melting	L-Bi_2O_3·Nb_2O_5+Bi_2O_3·5Nb_2O_5
				1,083	16.0	do	4$Bi_2O_3$9Nb_2O_5+Bi_2O_3·5Nb_2O_5+H-Bi_2O_3·Nb_2O_5+Bi_2O_3·6Nb_2O_5(?)
				1,085	1.0	do	H-Bi_2O_3·Nb_2O_5+Bi_2O_3·6Nb_2O_5+4Bi_2O_3·9Nb_2O_5(tr)
				1,092	65.0	do	4Bi_2O_3·9Nb_2O_5+Bi_2O_3·5Nb_2O_5+H-Bi_2O_3·Nb_2O_5+Bi_2O_3·6Nb_2O_5(?)
				1,105	1.0	no melting	4Bi_2O_3·9Nb_2O_5+Bi_2O_3·6Nb_2O_5+H-Bi_2O_3·Nb_2O_5
				1,173	0.33	do	4Bi_2O_3·9Nb_2O_5+Bi_2O_3·6Nb_2O_5
				1,200	.5	partially melted	Bi_2O_3·6Nb_2O_5+H-Bi_2O_3·Nb_2O_5
				1,219	.667	considerably melted	Per+Bi_2O_3·6Nb_2O_5+H-Bi_2O_3·Nb_2O_5
				1,231	.583	almost completely melted	Do.
				1,388	.167	completely melted	H-Bi_2O_3·Nb_2O_5+Unknown
		1,150	33				4Bi_2O_3·9Nb_2O_5+Bi_2O_3·6Nb_2O_5
				1,001	18.0	no melting	4Bi_2O_3·9Nb_2O_5+Bi_2O_3·5Nb_2O_5+Bi_2O_3·Nb_2O_5(tr)
				1,092	65.0	do	4Bi_2O_3·9Nb_2O_5+Bi_2O_3·6Nb_2O_5+Bi_2O_3·5Nb_2O_5
				1,180	0.167	do	
				1,185	.25	partially melted	
				1,230	.167	almost completely melted	
				1,240	.167	completely melted	

See footnotes at end of table.

TABLE 7. *Experimental data for compositions in the binary system* Bi_2O_3–Nb_2O_5—Continued

Composition		Heat treatment				Results	
		Calcine [a]		Quench [b]			
Bi_2O_3	Nb_2O_5	Temp	Time	Temp	Time	Physical observation	X-ray diffraction analyses [c]
Mole %	*Mole %*	*°C*	*hr*	*°C*	*hr*		
20	80	700	3				
(1:4)		910	9				
				999	19.0	no melting	
				1,050	4.0	do	
		1,060	18				
				1,075	88.5	no melting	
		1,150	24				
				1,246	0.167	partially melted	H-Nb_2O_5+Per+H-Bi_2O_3·Nb_2O_5
				1,299	0.167	considerably melted	
				1,310	.167	do	
				1,319	.083	do	
				1,325	.167	almost completely melted	
				1,334	.167	completely melted(?)	Per+H-Bi_2O_3·Nb_2O_5+H-Nb_2O_5+unknown
				1,359	.167	completely melted	Do.
18.18	81.82	700	3				
(2:9)		910	9				L-Bi_2O_3·Nb_2O_5+Bi_2O_3·5Nb_2O_5+H-Nb_2O_5
				999	19.0	no melting	
				1,050	4.0	do	Bi_2O_3·5Nb_2O_5+H-Bi_2O_3·Nb_2O_5
		1,060	18				Do.
				1,075	88.5	no melting	
		1,150	24				
				1,319	0.167	partially melted	
				1,334	.25	do	H-Nb_2O_5+Per+H-Bi_2O_3·Nb_2O_5
				1,339	.083	considerably melted	
				1,350	.167	almost completely melted	Per+H-Bi_2O_3·Nb_2O_5+H-Nb_2O_5
				1,359	.25	completely melted(?)	Per+H-Nb_2O_5+H-Bi_2O_3·Nb_2O_5+unknown
				1,378	.083	completely melted	Do.
16.67	83.33	700	3				
(1:5)				1,088	21.0	no melting	Bi_2O_3·5Nb_2O_5+H-Nb_2O_5+Bi_2O_3·6Nb_2O_5+H-Bi_2O_3·Nb_2O_5
				1,096	16.0	do	Bi_2O_3·6Nb_2O_5+Bi_2O_3·5Nb_2O_5+4Bi_2O_3·9Nb_2O_5
				1,105	16.0	do	Bi_2O_3·6Nb_2O_5+4Bi_2O_3·9Nb_2O_5
				1,153	90.0	do	Do.
		910	9				
				999	19.0	no melting	Bi_2O_3·5Nb_2O_5+H-Bi_2O_3·Nb_2O_5(tr)+H-Nb_2O_5(tr)
				1,050	4.0	do	
		1,060	18				Bi_2O_3·5Nb_2O_5
				1,075	88.5	no melting	Do.
				1,088	21.0	do	Do.
				1,096	16.0	do	Bi_2O_3·5Nb_2O_5+Bi_2O_3·6Nb_2O_5(tr)
				1,105	16.0	do	Do.
				1,153	90.0	do	Bi_2O_3·6Nb_2O_5+4Bi_2O_3·9Nb_2O_5
		1,150	24				
				1,180	0.167	no melting	
				1,185	.167	just begun to melt	Bi_2O_3·6Nb_2O_5+Per
				1,230	.167	partially melted	
				1,240	.083	partially melted	Bi_2O_3·6Nb_2O_5+Per
				1,245	.167	do	Per+H-Nb_2O_5+H-Bi_2O_3·Nb_2O_5+Bi_2O_3·6Nb_2O
				1,339	.167	considerably melted	
				1,351	.083	do	
				1,378	.05	almost completely melted	
				1,401	.167	completely melted	Per+H-Nb_2O_5+H-Bi_2O_3·Nb_2O_5+unknown
15.39	84.61	700	6				
(2:11)		1060	23				Bi_2O_3·5Nb_2O_5+Bi_2O_3·6Nb_2O_5
		1150	24				
				1,339	0.167	partially melted	
				1,251	.033	considerably melted	
				1,400	.167	completely melted	
14.29	85.71	700	3				L-Nb_2O_5+L-Bi_2O_3·Nb_2O_5+5Bi_2O_3·3Nb_2O_5(tr)
(1:6)							
				1,000	21.0	no melting	Bi_2O_3·5Nb_2O_5+H-Nb_2O_5
				1,005	1.0	do	Bi_2O_3·6Nb_2O_5+H-Nb_2O_5(tr)+Bi_2O_3·5Nb_2O_5(tr)
				1,014	1.5	do	Do.
				1,019	1.0	do	Do.
				1,040	1.0	do	Do.
				1,075	16.0	do	Bi_2O_3·6Nb_2O_5
				1,174	16.5	do	Do.
				1,201	1.0	do	Bi_2O_3·6Nb_2O_5
				1,220	1.0	do	Do.
				1,248	1.0	partially melted	H-Nb_2O_5+Per+H-Bi_2O_3·Nb_2O_5
				1,277	1.0	do	Do.
				1,282	68.0	do	Do.
				1,305	0.33	do	Do.
				1,311	.33	partially melted	
				1,322	.5	do	
				1,351	1.0	considerably melted	H-Nb_2O_5+Per+H-Bi_2O_3·Nb_2O_5
	1150	33					
				1,000	21	no melting	Bi_2O_3·6Nb_2O_5+Bi_2O_3·5Nb_2O_5+H-Nb_2O_5(tr)
				1,075	16.0	do	Bi_2O_3·6Nb_2O_5
				1,240	2.0	do	Do.
				1,244	0.167	partially melted	
				1,350	.167	considerably melted	
				1,359	.167	do	
				1,378	.05	do	
				1,400	.167	almost completely melted	
				1,425	.083	completely melted	

See footnotes at end of table.

TABLE 7. *Experimental data for compositions in the binary system* Bi_2O_3–Nb_2O_5—Continued

Composition		Heat treatment				Results	
		Calcine [a]		Quench [b]			
Bi_2O_3	Nb_2O_5	Temp	Time	Temp	Time	Physical observation	X-ray diffraction analyses [c]
Mole %	*Mole %*	*°C*	*hr*	*°C*	*hr*		
9.09 (1:10)	90.91	700	3				L-Nb_2O_5+L-Bi_2O_3·Nb_2O_5+5Bi_2O_3·3Nb_2O_5(tr)
				898	16.0	no melting	Bi_2O_3·5Nb_2O_5+H-Nb_2O_5
				1,005	1.0	do	Bi_2O_3·6Nb_2O_5+H-Nb_2O_5
				1,014	1.5	do	Do.
				1,019	1.0	do	Do.
				1,284	0.5	partially melted	
				1,295	.5	do	
				1,301	.33	do	
				1,310	.33	do	
		1,150	24				
				1,240	0.167	no melting	Bi_2O_3·6Nb_2O_5+H-Nb_2O_5
				1,245	.167	partially melted	
				1,401	.083	considerably melted	
				1,426	.083	do	
				1,451	.083	completely melted	
5	95	700	3				
		1,150	24				
				1,240	0.167	no melting	H-Nb_2O_5+Bi_2O_3·6Nb_2O_5
				1,245	.167	just begun to melt	
				1,425	.083	partially melted	
				1,451	.083	considerably melted	
				1,480	.083	completely melted	
0	100			1,480	.083	no melting	
				1,484	.083	do	
				1,486	.083	completely melted	
				1,489	.083	do	
				1,491	.083	do	

[a] All calcined specimens were heated and cooled at the rate of approximately 4°/min. All specimens were first calcined at 700 °C and then small portions of this calcine were recalcined at one or more desired higher temperatures.

[b] All specimens were quenched in sealed Pt tubes.

[c] The phases identified are given in the order of the amount present at room temperature. The phases are not necessarily those present at the temperature to which the specimen was heated. C—cubic, C′—pseudocubic, b.c.c.—body-centered cubic (a=10.263 A), b.c.c.′—body-centered cubic (a = 10.15–10.19 A), Tet—tetragonal, Mon—monoclinic, L—low-temperature polymorph, H—high-temperature polymorph, Per—perovskite (a = 3.94A), a composition of approximately Bi_2O_3:3Nb_2O_5, always metastable in this system and occurs only upon quenching the liquid, ss—solid solution, tr—trace, just barely discernable in X-ray pattern.

TABLE 8. *Unit cell dimensions of tetragonal and cubic* Bi_2O_3 *solid solutions*

Composition		Heat treatment, quench		Unit cell dimensions	
Bi_2O_3	Nb_2O_5	Temp	Time	a	c
Mole %	*Mole %*	*°C*	*hr*	*A*	*A*
99	1	773	2	10.938	5.632
98	2	773	2	10.921	5.638
97	3	775	64	5.461	5.646
96	4	775	64	5.464	5.647
95	5	782	16	[a] 5.525	
92.31	7.69	783	1	5.540	
90.91	9.09	869	17	5.533	
88	12	928	16	5.521	
85	15	928	16	5.510	
84	16	1,004	1	5.504	
83	17	1,004	1	5.499	
82	18	1,004	2	5.494	
81	19	1,004	2	5.490	
80	20	1,010	16	[b] 5.483	
79	21	1,050	2	5.480	
78	22	1,050	2	5.477	
77	23	1,050	21.5	5.471	
76	24	1,050	21.5	5.469	
75	25	1,081	16	5.469	

[a] This material was poorly crystalline and the value given is an average-value for the cubic and tetragonal phases.

[b] From 20 to 25 mole percent Nb_2O_5 the parameters represent the values measured for the pseudocubic cell.

The melting points of the solid solutions increase from the melting point of pure Bi_2O_3, 825 °C [20], to about 1,055 °C at 17 mole percent Nb_2O_5. A morphotropic transformation occurs in the solid solution at this point curving to a eutectoid at about 610 °C and 19.5 mole percent Nb_2O_5. The cubic-monoclinic transformation temperature is lowered from about 730 °C to the above-mentioned eutectoid although there is very little solid solution in the monoclinic phase.

The solid solution higher in Nb_2O_5 content is designated C′ss in table 7. It is apparently only pseudocubic with several very small superstructure peaks in the X-ray diffraction pattern corresponding to d spacings of about 8.4 A, 2.69 A, and 2.35 A. The two phase region between the two solid solution fields is too narrow to be found by experimentation and is shown as dashed lines in figure 1. The C′ss is apparently stable from room temperature to the solidus which extends to about 1,096 °C at 23 mole percent Nb_2O_5. The peritectic for this solidus occurs at about 20 mole percent Nb_2O_5.

The liquidus rises smoothly from the 1,096 °C peritectic to another peritectic at 36.5 mole percent Nb_2O_5 and 1,193 °C corresponding to the incongruent melting temperature of the compound 5Bi_2O_3·3Nb_2O_5. There is little or no solid solution on either side of this compound, or any other of the compounds in the binary system, as shown by the similarity of the unit cell dimensions of the pure compound to those of the same compound in a two phase region.

The liquidus again rises smoothly from the 1,193 °C peritectic to the congruent melting point of Bi_2O_3·Nb_2O_5 at 1,245 °C. This compound was observed to crystallize in two polymorphic forms.

The low-temperature orthorhombic form was found to transform to the triclinic form at-about 1,020 °C. However this phase transformation could not be reversed. Neither polymorph appeared changed after 184 hr at 1,008 °C, but a small amount of the high-temperature form was present in the original low form after 114 hr at 1,024 °C (see table 7). Because of the inability to reverse the phase transformation the polymorphic change is shown as a dashed line in figure 1.

The liquidus curve falls smoothly from 1,245 °C to a eutectic at 1,180 °C and about 64 mole percent Nb_2O_5. The liquidus then rises very shallowly to a peritectic point at about 68 mole percent Nb_2O_5 and 1,183 °C, the incongruent melting temperature of the $4Bi_2O_3 \cdot 9Nb_2O_5$ compound. This compound needs a long period of heating time at relatively high temperatures in order to form a single phase. It also takes a relatively long time to be completely transformed to liquid plus the $Bi_2O_3 \cdot 6Nb_2O_5$ com-

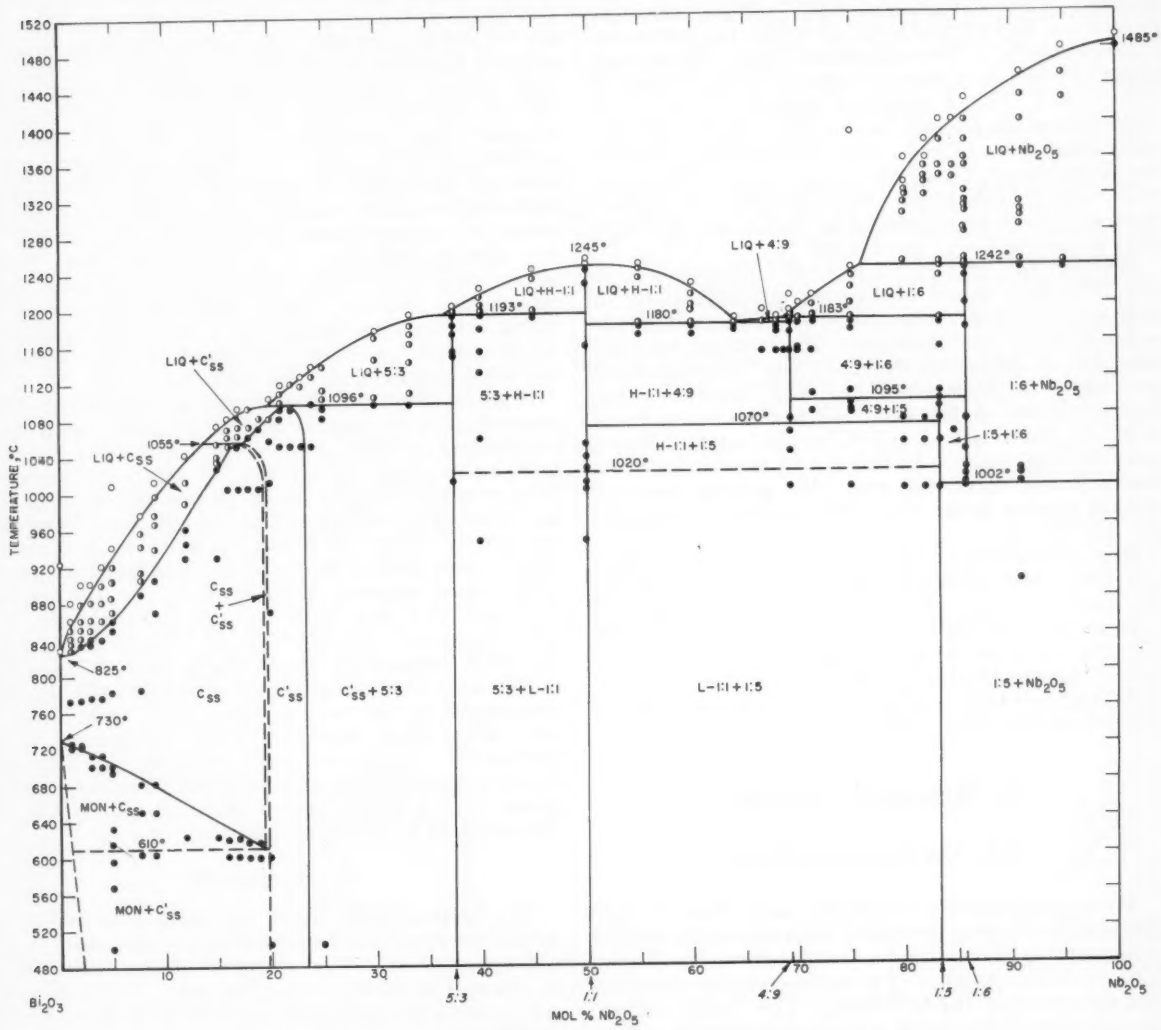

FIGURE 1. *Phase equilibrium diagram for the system* Bi_2O_3-Nb_2O_5

●—no melting
◑—partially melted
○—completely melted
L—low temperature modification
H—high temperature modification
C—cubic
C'—pseudocubic
Mon—monoclinic
LIQ—liquid

pound (see table 7). The hexagonal $4Bi_2O_3 \cdot 9Nb_2O_5$ compound is not formed at all-below about 1,070 °C. Specimens preheated to form a single phase are slowly decomposed to triclinic $Bi_2O_3 \cdot Nb_2O_5$ and the $Bi_2O_5 \cdot 5Nb_2O_5$ compound, when heated below about 1,070 °C. The $4Bi_2O_3 \cdot 9Nb_2O_5$ compound can therefore be concluded to have a minimum temperature of stability at about 1,070 °C.

The compound $Bi_2O_3 \cdot 5Nb_2O_5$ was found to have a maximum temperature of stability of about 1,095 °C. The preformed compound slowly decomposed to $4Bi_2O_3 \cdot 9Nb_2O_5$ and $Bi_2O_3 \cdot 6Nb_2O_5$ above this temperature, while the original 700° calcined material showed no $Bi_2O_3 \cdot 5Nb_2O_5$ at all when heated much above 1,095 °C. The compound $Bi_2O_3 \cdot 6Nb_2O_5$ was found to have a minimum temperature of stability at about 1,002 °C. A specimen heated for 21 hr at 1,000 °C contained only $Bi_2O_3 \cdot 5Nb_2O_5$ and H-Nb_2O_5, while heating for 1 hr at 1,005 °C was enough to form the $Bi_2O_3 \cdot 6Nb_2O_5$ phase with only traces of the other two. The preformed $Bi_2O_3 \cdot 6Nb_2O_5$ compound showed definite traces of $Bi_2O_3 \cdot 5Nb_2O_5$ and H-Nb_2O_5 after reheating for 21 hr at 1,000 °C.

$Bi_2O_3 \cdot 6Nb_2O_5$ was found to melt incongruently at 1,242 °C to a liquid containing approximately 76 mole percent Nb_2O_5 plus crystalline Nb_2O_5 with little or no Bi_2O_3 in solid solution. The liquidus between the 1,183 °C peritectic and the 1,242 °C peritectic is essentially a straight line. The liquidus rises smoothly from the last peritectic to the melting point of Nb_2O_5, found to be 1,485 °C for the batch of Nb_2O_5 used for this study. As this Nb_2O_5 is essentially Ta free it is not surprising that this melting point is several degrees lower than that previously reported [11, 13, 16, 19].

It is interesting to note that although both BaO and PbO enter into solid solution in Nb_2O_5 [11, 13] the Bi_2O_3 does not. Considering that the radius and polarizability of Pb^{+2} and Bi^{+3} are very similar [20] this fact must be dependent on the difference in valence. It should also be noted that unlike PbO [11] Bi_2O_3 has no catalytic effect upon the temperature of the metastable phase transformations in Nb_2O_5.

5. Metastable Phases

5.1. The Perovskite Phase

When compositions containing more than 50 mole percent Nb_2O_5 were quenched from above the solidus a metastable phase always formed from the liquid. The maximum amount of this phase occurred around the composition $Bi_2O_3 \cdot 3Nb_2O_5$. The X-ray diffraction pattern of this phase could be interpreted as that of a poorly crystalline cubic perovskite with $a \cong 3.94$A. Specimens quenched from above about 1,380 °C (well above the liquidus) contained another metastable phase which had an X-ray diffraction pattern similar to the cubic perovskite, but with extra lines. The metastable perovskite in this system can be compared with the distorted perovskite compound $La_2O_3 \cdot 3Nb_2O_5$, previously reported [21].

5.2. The System Bi_2O_3–Nb_2O_5–Alcohol

A large number of metastable phases were found to occur in the Bi_2O_3-Nb_2O_5 system if either methyl or ethyl alcohol was used for wet mixing of the end members, and the resultant material was pressed into a pellet and fired without first thoroughly drying the mixture. Two separate body centered cubic phases were observed in mixtures containing 3 to 25 mole percent Nb_2O_5 which had been wet mixed with methyl alcohol. The first phase, labeled b.c.c. in table 7, had a unit cell dimension of $a=10.263$ A. This phase decomposed quickly in quench runs above 750 °C and did not affect the melting point measurements. However specimens containing 16 to 24 mole percent Nb_2O_5 originally mixed with methyl alcohol contained large amounts of a second body centered cubic phase (labeled b.c.c.′ in table 7) with a about 10.15 to 10.19 A. These specimens were found to dissociate to unknown phases which had metastable melting points several hundred degrees below the melting values of specimens prepared without alcohol, and had to be discarded. For these latter compositions only the dry-mixed specimens are reported in table 7. Other unknown phases were found in mixtures containing 1 to 4 mole percent Nb_2O_5 which had been wet-mixed in ethyl alcohol and were also discarded for table 7.

It seems likely that Bi_2O_3 forms a series of complex compounds with methyl and ethyl alcohol and can incorporate Nb_2O_5 into these compounds. The first b.c.c. phase ($a=10.263$ A) seems to contain little or no Nb_2O_5 and probably contains only Bi_2O_3 and alcohol or carbon. The second (b.c.c.′) phase apparently contained about 12 to 15 mole percent Nb_2O_5 (plus alcohol or carbon). The body-centered cubic phase appears to be built up by spheres of Bi^{+3} and O^{-2} ions with a large tetrahedrally coordinated hole in the center [6, 8]. This host lattice, by itself apparently thermodynamically unstable, is stabilized in some cases by the addition of a second component in the central hole. It is possible that this phase may therefore be a clathrate type compound. A more complete study by high-temperature X-ray diffraction, of the body-centered cubic phase with a large number of other oxides will be discussed in a future publication.

6. Summary

The system Bi_2O_3–Nb_2O_5 was studied by means of solid state reactions, fusion characteristics, and X-ray diffraction data. The existence of five compounds in this system was shown. They are: $5Bi_2O_3 \cdot 3Nb_2O_5$, which melts incongruently at 1,193 °C to $Bi_2O_3 \cdot Nb_2O_5$ and liquid containing about 36.5 mole percent Nb_2O_5; $Bi_2O_3 \cdot Nb_2O_5$ which melts congruently at 1,245 °C, and has a phase transition (irreversible in laboratory time) at about 1,020 °C from a low-temperature orthorhombic structure to a high temperature triclinic form; $4Bi_2O_3 \cdot 9Nb_2O_5$ which has a minimum temperature of stability at 1,070 °C and melts incongruently to $Bi_2O_3 \cdot 6Nb_2O_5$ and liquid containing about 68 mole percent Nb_2O_5; $Bi_2O_3 \cdot 5Nb_2O_5$ which

has a maximum temperature of stability, decomposing at 1095 °C to $4Bi_2O_3 \cdot 9Nb_2O_5$ plus $Bi_2O_3 \cdot 6Nb_2O_5$; and $Bi_2O_3 \cdot 6Nb_2O_5$ which has a minimum temperature of stability at 1,002 °C and melts incongruently at 1,242 °C to Nb_2O_5 and a liquid containing about 76 mole percent Nb_2O_5. The only eutectic in the system occurs at 1,180 °C and about 64 mole percent Nb_2O_5.

Nb_2O_5 enters into solid solution in the high-temperature cubic form of Bi_2O_3, raising the melting point to about 1,055 °C and lowering the monoclinic to cubic phase transition from about 730 °C to about 610 °C. A morphotropic transition occurs in the solid solution at about 19.5 mole percent to a pseudocubic form, and further solid solution occurs from 19.5 mole percent to about 23.5 mole percent Nb_2O_5. The pseudocubic form of Bi_2O_3 solid solution is stable from room temperature to a maximum solidus temperature of 1,096 °C. No solid solution was observed in Nb_2O_5 or in any of the five binary compounds in the system.

(Paper 66A6–180)

7. References

[1] K. Dihlström, Z. Anorg. Allgem. Chem. **239,** 57–64 (1938).
[2] B. Aurivillius, Arkiv Kemi **3** [20] 153–161 (1951).
[3] H. S. Roberts, Phys. Rev. **23,** 386–95 (1924).
[4] H. F. Stimson, J. Research NBS **65A** (Phys. and Chem.) 139–145 (1961).
[5] W. Guertler, Z. Anorg. Chem. **37,** 222 (1903).
[6] L. G. Sillén, Arkiv Kemi **12A** [18] 1–15 (1937).
[7] W. C. Schumb and E. S. Rittner, J. Am. Chem. Soc. **65,** 1055–1060 (1943).
[8] B. Aurivillius and L. G. Sillén, Nature **155** [3932] 305–306 (1945).
[9] L. G. Sillén, Z. Krist. **103** [4] 274–290 (1941).
[10] H. E. Swanson, M. C. Morris, and E. H. Evans, NBS Mono. 25, Sec. 2 (to be published).
[11] R. S. Roth, J. Research NBS **62** [27] (1959) RP2925.
[12] C. S. Hurlbut, Jr., Am. Min. **42** [3, 4] 178–183 (1957).
[13] R. S. Roth and J. L. Waring, J. Research NBS **65A** (Phys. and Chem.) No. 4, 337–344 (1961).
[14] F. Galasso and L. Katz, Acta Cryst. **14** [6] 647–650 (1961).
[15] R. O. Burbank and H. T. Evans, Acta Cryst. **1** 330 (1948).
[16] F. Holtzberg, A. Reisman, M. Berry, and M. Berkenblit, J. Am. Chem. Soc. **79** 2039–2043 (1957).
[17] M. W. Shafer and R. Roy, Z. Krist. **110** [3] 241–248 (1958).
[18] H. J. Goldschmidt, J. Inst. Metals **87,** 235–239 (1958–59).
[19] A. Reisman and F. Holzberg, J. Am. Chem. Soc. **81,** 3182–3184 (1959).
[20] E. M. Levin and C. L. McDaniel, J. Am. Ceram. Soc. **45,** No. 8, 355–360 (Aug. 1962).
[21] R. S. Roth, in "Rare Earth Research," Ed., E. V. Kleber, The Macmillan Co. (1961), pp. 88–95.

JOURNAL OF RESEARCH of the National Bureau of Standards—A. Physics and Chemistry
Vol. 66A, No. 6, November–December 1962

Elastic Constants of Rutile (TiO_2)

J. B. Wachtman, Jr., W. E. Tefft, and D. G. Lam, Jr.

(August 9, 1962)

The six elastic constants (and six elastic compliances) of rutile were determined in the kilocycle per second frequency range by a resonance method. The standard deviations range from 0.2 percent for s_{11} to 4.3 percent for s_{13}.

1. Introduction

The electrical properties of rutile make it a promising material for solid state electronic devices and a large literature on such properties exists and has been surveyed [*1*, *2*, *3*].[1] Comparatively little information on the mechanical properties of rutile was available until recently. The linear compressibilities had been measured by Bridgman [*4*], and a set of elastic constants was calculated from spectroscopic data by Dayal and Appalanarasimham [*5*]. No further work on elastic properties was apparently done until the recent independent and nearly simultaneous measurements of three groups. Vick, Hollander, and Brown [*6*], determined four of the six elastic constants of rutile directly from pulse velocity measurements and calculated the other two by combining Bridgman's linear compressibilities with their own data. Verma [*7*] published a set of the elastic constants calculated from his pulse velocity measurements. The present writers reported [*8*] a set of values determined by least squares fitting of the theoretical equations for the orientation dependence for elastic moduli to a set of experimental values determined on 10 single-crystal rutile rods by resonance in the audiofrequency range. Appreciable discrepancies existed for some of the constants, especially between those of Verma and those of the other investigators. Vick and Hollander [*9*] checked their measurements and published a refined set of values which are little different from their first set. The most serious discrepancies were removed when it was discovered that the direction which Verma took to be [100] was in fact [110]. It is an interesting property of the 4/mmm crystalographic point group, to which rutile belongs, that the x axis may be taken as either [100] or [110] and a self consistent matrix of elastic constants results which has the same form (but three of the six constants will have different numerical values). There is thus no internal inconsistency in Verma's work but his results should be expressed in terms of [100] as the x axis to agree with the usual convention and to permit direct comparison with other values. This calculation has been done by Birch [*10*] and the resulting values agree fairly well with the results of other investigators but not as well as would be expected from the accuracy of methods of measurement which were used. The present writers wished to refine their data; their initial results were based upon measurements on 10 rods whose rod axes were all near the [001] axis. A comparatively large uncertainty in c_{11} and c_{66} resulted. This situation was improved when six additional rods were eventually obtained and the present results agree well with the values calculated by Birch in the sense that there is now no statistically significant difference for any of the c_{ij}. The standard deviations are, however, appreciably larger than those obtained by the authors on corundum [*11*] using the same resonance method. The most important source of this variability is believed to be caused by the presence of a profusion of small angle boundaries whose existence is shown by back-reflection Laue patterns.

The present paper gives the method of applying the resonance technique to tetragonal crystals because it apparently has not been previously described for this crystal system. The general method has been described previously and reference [*11*] may be consulted for general background.

2. Description of Specimens

All specimens were synthetic "single crystals" grown by the Verneuil flame-fusion technique using an oxygen-hydrogen flame. Such specimens in the as grown state characteristically contain two types of defect: (1) they are oxygen deficient and (2) they have many small angle boundaries (as much as 2° misorientation across a single boundary). The first type of defect is easily removed by heating in oxygen at temperatures around 1,000 °C. Parenthetically we note that the difficult problems of obtaining exact stoichiometry and of measuring small deviations from stoichiometry do not concern us here. The elastic constants do undoubtedly depend to some extent on the degree of reduction but the effect is very small as noted by Vick and Hollander [*9*]. We have not carried out a systematic study of the effect of reduction on all of the c_{ij} but observations of the very small changes produced in several heavily reduced (jet black) rods indicate that the effect which the possible small remaining oxygen deficiency in our nominally stoichiometric rods may have on the c_{ij}

[1] Italicized figures in brackets indicate the literature references at the end of this paper.

at room temperature is too small to be of any concern. Heavy reduction did show a measurable effect on the temperature dependence of Young's modulus at high temperature [12] but this is outside the scope of our present considerations. Our specimens were heated for about 24 hr in flowing O_2 at about 800 °C and we consider them to be effectively stoichiometric.

The second type of defect appears in all rutile single crystals examined by the authors and no method of removing it is known. Back-reflection Laue patterns were taken at random on many specimens; perhaps one fourth of the patterns show double spots indicating a change of orientation of 1 or 2 deg. If this were a systematic, progressive change of orientation along a rod, one end would differ greatly in orientation from the other and the crystals would be useless for our work. Fortunately, as table 1 shows, this is not so. Laue patterns were taken at the center and at both ends of each rod. Duplicate patterns were taken on specimens 21 and 22 to indicate the precision of the method. The resulting standard deviations were 0.12° for θ and 0.16° for ϕ where θ and ϕ are the usual spherical polar angles. The colatitude, θ, is the angle between the rod axis and [001]; the angle ϕ is the angle between [100] and the projection of the rod axis on the (001) plane. The orientation apparently shifts back and forth in a random manner from one small angle boundary to another. The average values of θ and ϕ were used for each rod in the calculations. It is hoped that better temperature, atmosphere, and powder feed control during crystal growth would reduce the number of the boundaries and this is being attempted at the National Bureau of Standards and elsewhere.

Both the Linde Co.[2] and the National Lead Co. were asked for high-purity single crystal specimens and both graciously gave us some of their production. The National Lead specimens were in the form of boules intended for gem stones, and rods cut from these proved to be too short for our use. Some of the Linde rods were long enough to permit cylinders of useful length to be ground from them. These rods are listed as numbers 21 through 30 in table 1 and our first set of elastic constants [8] was calculated from results on these rods.

The manufacturer's analysis for a typical Linde rutile single crystal indicates the following oxides at each stated percentage: 0.01–B_2O_3, ZnO, ZrO_2, Sb_2O_3; 0.005–Al_2O_3, U_2O_5, Fe_2O_3, SrO, MoO, PbO, SnO_2; 0.003–SiO_2, CaO, Cr_2O_3, Co_2O_3, BaO; 0.002–MnO, NiO; 0.0005–MgO, Ag_2O, CuO. The lack of any rods with high θ values in this set is apparent from table 1. The Linde Co. then made a special series of growth runs and produced rod number 44 with a very useful orientation. Additional rods were also needed and a successful effort was made by W. S. Brower and S. F. Holley of the National Bureau of Standards to grow rods parallel to the [100] axis. The purest available TiO_2 powder from National Lead Co. was used. The manufacturer's analysis of the impurities in percent is: 0.02–SiO_2; 0.01–Nb; less than 0.005–W; 0.001–Fe_2O_3; less than 0.001–Al_2O_3, Sb_2O_3, Pb, V, Cr; less than 0.0005–Hg, less than 0.0003–Cu; less than 0.00005–Mn. Spectroscopic analysis of single crystals after growth showed no significant change in the major impurities.

[2] A division of Union Carbide and Carbon Co.

TABLE 1. *Properties of "single crystal" rutile specimens*

Specimen number	Mass	Length	End		Center		Other end	
			θ	ϕ	θ	ϕ	θ	ϕ
			All angles in degrees					
Linde rods								
	g	cm						
21	2.6317	13.236	12.5 12.3	2.6 2.2	12.7	2.1	14.3 14.2	1.8 1.5
22	2.2113	13.178	37.9 38.0	12.5 12.5	38.9	10.2	40.1 40.2	8.0 8.1
23	2.8205	12.168	14.0	7.3	16.1	7.0	14.8	6.3
24	2.3654	11.714	43.3	34.1	45.6	37.9	44.7	33.6
25	2.3770	11.178	11.2	37.9	11.4	29.0	11.9	36.3
26	1.2718	7.534	8.0	26.6	7.8	22.8	8.4	26.1
27	1.2769	6.986	14.6	18.8	14.2	19.0	15.0	20.9
28	1.2561	6.080	39.0	40.0	42.4	40.0	43.0	45.0
29	0.8562	6.004	12.9	7.8	14.0	5.6	13.7	6.0
30	1.1523	5.816	58.7	24.0	58.5	24.2	59.3	23.7
44	15.0251	9.848	88.8	44.1	88.4	43.4	90.0	44.5
NBS rods								
41	8.0767	8.508	12.9	9.2	12.9	8.0	13.5	9.3
42	5.8920	6.256	7.0	20.0	6.9	21.0	6.2	19.0
49	7.1208	11.128	87.8	0.0	87.8	0.0	88.0	1.5
50	21.5907	17.107	88.8	5.4	89.5	5.4	90.0	5.0
51	16.0263	17.634	86.2	0.4	86.2	1.0	86.8	0.9

3. Relation of Young's Modulus and Shear Modulus to Elastic Compliances and to Orientation

In this section the elastic moduli measured in resonance experiments are expressed in terms of the elastic compliances and the orientation. The method of solving these equations for the compliances is then described. The theory and experiment closely parallel work on corundum [11] and therefore only a brief description will be given.

In relating the elastic compliances to Young's modulus, it is necessary to distinguish between the "free" Young's modulus, Y_f, and the "pure" Young's modulus, Y_p, when analyzing flexural or torsional tests. The free Young's modulus is the value obtained when the specimen is completely free to deform elastically under the applied tensile stress. The pure Young's modulus is the value obtained when the specimen is tested in flexure and is prevented from twisting. In an isotropic medium the free and pure moduli are identical. Calculation of Young's modulus from flexural vibrations of slender, cylindrical rods of nonisotropic material corresponds to measurements of Y_f. For such rods the modulus determined from torsional resonance is the pure shear modulus, G_p. The validity of these results is discussed by Brown [13].

The following treatment develops the relation between the measured quantities, Y_f and G_p, and the elastic compliances, s_{ij}, expressed in the standard rectangular coordinate system for tetragonal crystals, $x_1x_2x_3$, described by Nye [14]. It is convenient

to introduce a rotated coordinate system, $x_1'x_2'x_3'$, with the x_3' axis along the rod axis. The free elastic moduli for measurements along the rod axis are related to the compliances expressed in the primed coordinate system by

$$s_{33}'=\frac{1}{Y_f}, \tag{1}$$

and

$$\frac{s_{44}'+s_{55}'}{2}=\frac{1}{G_f}. \tag{2}$$

Brown [13] and Hearmon [15] give the following equation relating the pure shear modulus, G_p, to the free shear modulus, G_f:

$$G_f=G_p(1-\epsilon'), \tag{3}$$

where

$$\epsilon'=\frac{s_{34}'^2+s_{35}'^2}{s_{33}'(s_{44}'+s_{55}')}. \tag{4}$$

Equations (2), (3), and (4) can be combined to give

$$\frac{1}{G_f}=\frac{1}{G_p}+\frac{(s_{34}'^2+s_{35}'^2)\,Y_f}{2}. \tag{5}$$

It is now necessary to express the primed quantities in eqs (1), (2), and (5) in terms of the unprimed compliances and the orientation. This is done for eqs (2) and (3) by writing out the tensor transformations and expressing the direction cosines in terms of the colatitude, θ, and the azimuth, ϕ. In other words, θ is the angle between x_3 and x_3' and ϕ is the angle between x_1 and the projection of x_3' on the x_1x_2 plane. The tensor transformation gives

$$s_{33}'=s_{11}\sin^4\theta+s_{33}\cos^4\theta+(2s_{13}+s_{44})\sin^2\theta\cos^2\theta+\frac{1}{2}\left(s_{12}-s_{11}+\frac{s_{66}}{2}\right)\sin^4\theta\sin^2 2\phi, \tag{6}$$

and

$$\frac{s_{44}'+s_{55}'}{2}=\frac{1}{2}s_{66}\sin^2\theta+\frac{1}{2}s_{44}(1+\cos^2\theta)+2(s_{11}+s_{33}-s_{44}-2s_{13})\sin^2\theta\cos^2\theta+\left(s_{11}-s_{12}-\frac{s_{66}}{2}\right)\sin^4\theta\sin^2 2\phi. \tag{7}$$

The directions of the x_1' and x_2' axes have not been specified except for the requirement that $x_1'x_2'x_3'$ form a right handed rectangular system because eqs (1) and (2) are independent of their directions. This independence also holds for (5) because $s_{34}'^2+s_{35}'^2$ depends only on the direction of x_3' as Hearmon [15] states. It is convenient to write s_{34}' and s_{35}' separately, however, and these quantities are not specified by the direction of x_3' alone. For simplicity x_2' was chosen to lie in the x_1x_2 plane and x_1' is then uniquely specified. The tensor transformations give

$$s_{34}'=\frac{1}{2}\left(\frac{s_{66}}{2}+s_{12}-s_{11}\right)\sin^3\theta\sin 4\phi, \tag{8}$$

and

$$s_{35}'=2(s_{11}+s_{33}-s_{44}-2s_{13})\sin^3\theta\cos\theta+(2s_{13}+s_{44}-2s_{33})\sin\theta\cos\theta+\left(s_{12}+\frac{s_{66}}{2}-s_{11}\right)\times\sin^3\theta\cos\theta\sin^2 2\phi. \tag{9}$$

A set of elastic compliances can be determined from the preceding equations in the following manner: Assume that values of Y_f and G_p have been determined on at least four rods. Equation (6) is written for each value of Y_f and the resulting system of simultaneous equations is solved for s_{11}, s_{33}, $2s_{13}+s_{44}$, and $s_{12}-s_{11}+s_{44}/2$. These results are used in eqs (8), (9), and (7) to calculate values of G_f from the measured values of G_p. Equation (7) is written for each value of G_f and the resulting system of simultaneous equations is solved for s_{44}, s_{66}, $s_{11}+s_{33}-s_{44}-2s_{13}$, and $s_{11}-s_{12}-s_{66}/2$. In this way two independent values of s_{12} and s_{13} are obtained which may be compared for consistency. If more than four specimens are used, a good check on the consistency of the whole set of s_{ij} values is then available.

4. Relation of Elastic Moduli to Resonance Frequencies

The values of Y_f and G_p needed for the calculation of the elastic compliances were obtained by resonance frequency measurements on slender, cylindrical rods. Young's modulus was calculated from the longitudinal resonance frequency for the five longest rods and from the flexural resonance frequency for all of the 16 rods used in this investigation. The shear modulus was calculated from the torsional resonance frequency of all 16 rods. For both of the Young's modulus calculations, the equation relating the resonance frequency to the appropriate modulus is approximate but the approximations are very good.

For longitudinal vibrations, Young's modulus of an isotropic medium can be calculated from Rayleigh's equation [16] which can be written

$$Y=4\rho l^2f^2\left(1+\pi^2\frac{\sigma^2r^2}{4l^2}\right)^2 \tag{10}$$

where ρ is the density in g/cm^3, l is the length in cm, f is the fundemental longitudinal resonance frequency in cycles per second, σ is Poisson's ratio, r is the radius in cm and Y is Young's modulus in dynes/cm^2. The term in parentheses is the Rayleigh correction term for the finite thickness of the rod and neglects higher powers of r/l. For the values of r/l used in the present work the difference between values given by Rayleigh's equation and a more accurate treatment by Bancroft [17] is much less than the experimental accuracy. The correction term should be modified for nonisotropic material, but a good estimate of the correction can be obtained by using an average value of Poisson's ratio in the

present equation. Taking $\sigma=0.30$ and $r/l=0.0113$ for the shortest of the five rods used in longitudinal resonance gives a Rayleigh correction factor of only 1.000006. The values of Y calculated from (10) should be very accurate despite the fact that rutile is nonisotropic.

For flexural vibrations of a cylindrical rod of isotropic material the best existing theory seems to be Pickett's [18] differential equation.[3] The result obtained can be expressed as the result for a rod of infinitesimal thickness multiplied by a dimensionless correction factor, T. This result is

$$Y=0.31547\rho\frac{l^4f^2}{r^2}T \tag{11}$$

where the symbols have the same meaning as in eq (10) except that here f is the flexural resonance frequency. Tefft [22] has calculated a table of T from Pickett's differential equation as a function of r/l and Poisson's ratio. Fortunately the T values are nearly equal to one and depend very little on the Poisson's ratio value for small r/l. The values of T for $\sigma=0.30$ were used for all calculations. The whole subject of the determination of elastic moduli of isotropic materials has been summarized [23] recently.

For torsional vibrations of an isotropic cylindrical rod, the equation

$$G=4\rho l^2f^2 \tag{12}$$

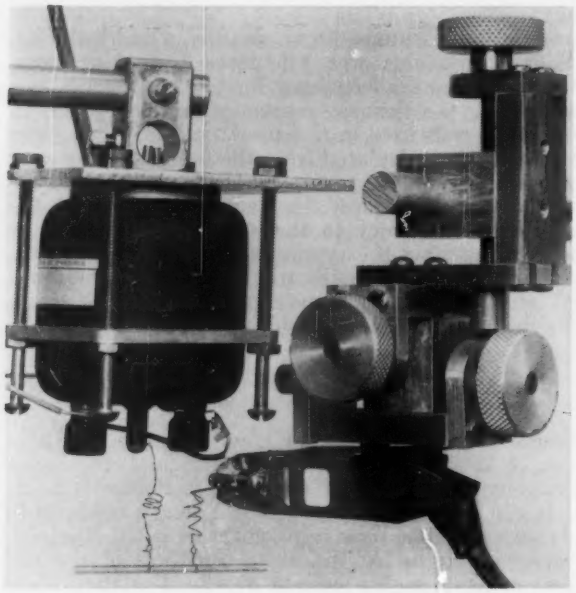

FIGURE 1. *Method used to measure torsional resonance frequency of short rods (about 6 cm long).*

The fine phosphor bronze springs have sufficient flexibility to permit relatively free specimen vibration and have sufficiently low damping not to cause excessive power loss.

[3] This equation should not be confused with an approximate differential equation derived by Timoshenko [19] and studied by Goens [20] and by Pickett [21].

is rigorously true. Here f is the torsional resonance frequency and the other symbols have their previous meanings. The significance of this equation for crystalline cylinders has been considered by Brown [13] and by Hearmon [15]. The details are complicated, but the result is, as previously stated, that for sufficiently slender rods eq (12) gives G_p and eqs (10) and (11) give Y_f.

The density value of 4.250 g/cm^3 reported by Swanson and Tatge [24] was used.

5. Method of Determining Resonance Frequencies

The general procedure for measuring resonance frequencies of slender cylinders has been described previously [*11*, *23*]. The specimen is suspended by fine threads tied in such a manner that free vibration is unimpeded; i.e., the threads are tied near the nodes of the vibrational mode being investigated. Vibration is excited either by air drive with a loudspeaker or by driving one of the suspending threads with a transducer. The resonance is detected by a pickup attached to another thread. The resonance frequency is measured with a crystal controlled counter having an accuracy of ± 0.1 c/s.

This method was successfully used in the present work for all resonance frequencies except the torsional frequencies on rods 26 through 30. In the case of torsional vibration the resonance frequencies are so large and the amplitude of motion so small that the resonances could not be detected using cotton or silk thread. A special procedure, shown in figure 1, was used. Fine springs, made from phosphor bronze wire, were used to couple the driver and pickup to the specimen. These springs were flexible enough to permit free vibration of the specimen, but had sufficiently low damping to permit adequate power transfer from the driver to the specimen and from the specimen to the pickup to allow resonance to be excited and detected. In this way the torsional resonance frequencies of specimens 26 through 30 were measured.

The value of Young's modulus calculated from the longitudinal resonance frequency was considered to be slightly more accurate than the value calculated from the flexural resonance frequency and was used in subsequent calculations when it was available (i.e., for those rods for which the longitudinal resonance frequency could be determined).

6. Results and Discussion

The flexural and longitudinal resonance frequencies are given in table 2 together with the reciprocal Young's modulus values calculated from these frequencies. Table 3 gives the corresponding torsional resonance frequencies and reciprocal shear modulus values. The values of $1/Y_f$, θ, and φ were used to write eq (6) for each rod. The resulting set of 16 simultaneous equations in four unknowns was then solved for the four linear combinations of s_{ij}

TABLE 2. *Young's modulus calculations*

Specimen number	Resonance flexural	Frequency longitudinal	$1/Y_f$ Flexural	$1/Y_f$ Longitudinal	W_y
			10^{-12} cm²/dyne		
Linde rods					
	c/s	*c/s*			
21	1166.5	35544	2.655	2.658	−0.008
22	943.0	31271	3.490	3.464	−.014
23	1485.2	38514	2.671	2.678	−.012
24	1393.0	37325	3.080	3.077	+.030
25	1703.8	42399	2.614	2.619	−.023
26	3338.2	----------	2.614	----------	−.003
27	3980.8	----------	2.689	----------	+.011
28	5317.5	----------	2.961	----------	+.024
29	4748.3	----------	2.702	----------	+.032
30	5001.8	----------	3.831	----------	−.050
44	5693.0	----------	2.7295	2.699	+.005
NBS rods					
41	6107.6	----------	2.655	----------	−0.018
42	11246	----------	2.617	----------	−.007
49	1840.6	26402	6.824	6.814	+.037
50	1111.6	17408	6.617	6.632	−.018
51	882.3	16740	6.714	6.750	−.007

$W_y = (1/Y_f)_{\text{observed}} - (1/Y_f)_{\text{calculated}}$ where Y_f computed from longitudinal resonance was used when available.

TABLE 3. *Shear modulus calculations*

Specimen number	Torsional resonance frequency	$1/G_p$	$1/G_f$	W_g
		10^{-12} cm²/dyne		
Linde rods				
	c/s			
21	20206	8.213	8.236	−0.046
22	19496	8.885	9.301	+.245
23	21936	8.250	8.281	−.059
24	20370	10.304	10.447	−.117
25	24070	8.099	8.110	−.138
26	35737	8.115	8.121	−.037
27	37942	8.372	8.396	+.057
28	39340	10.282	10.298	−.117
29	43920	8.459	8.483	+.188
30	42640	9.580	10.560	−.014
44	20260	14.778	14.796	+.047
NBS rods				
41	31319	8.285	8.307	+0.023
42	43016	8.123	8.127	−.004
49	26604	6.712	6.718	+.019
50	17215	6.782	6.947	−.011
51	16844	6.668	6.686	−.035

$W_g = (1/G_f)_{\text{observed}} - (1/G_f)_{\text{calculated}}$.

appearing as coefficients in eq (6). The process of solving an overdetermined set of simultaneous linear equations for the least squares best estimates of the coefficients and their standard deviations is a straightforward calculation and is described, for example, by Scheffe [*25*]. This calculation was done on an automatic computer and the resulting values of the coefficients are given in the first half of table 4. These coefficients were then used in eq (6) to calculate a value of $1/Y_f$ for each rod. The deviations of the calculated from the observed values of $1/Y_f$, labeled W_y, are listed in table 2 and provide an indication of how well eq (6) fits the data. These results were then used in eqs (8), (9), and (5) to obtain $1/G_f$ from $1/G_p$ for each rod. The values of $1/G_f$ were then used in eq (7) and a least squares solution for the coefficients was carried out as was done for eq (6). The resulting values of the coefficients are given in the second half of table 4. Deviations, W_G, between calculated and observed values of $1/G_f$ are listed in table 3.

TABLE 4. *Least squares best estimates of parameters in elastic moduli equations*

From equation for $1/Y_f$	
s_{11}	$6.788 \pm 0.015 \times 10^{-12}$ cm²/dyne
s_{33}	$2.592 \pm .011$
$2s_{13}+s_{44}$	$6.466 \pm .062$
$s_{11}-s_{12}-\frac{s_{66}}{2}$	$8.200 \pm .059$
From equation for $1/Gf$	
s_{44}	8.072 ± 0.048
s_{66}	$5.302 \pm .140$
$s_{11}+s_{33}-s_{44}-2s_{13}$	$2.880 \pm .157$
$s_{11}-s_{12}-s_{66}/2$	$8.077 \pm .132$

The deviations are standard deviations of the coefficients obtained from least squares calculations.

The results presented in table 4 give s_{11}, s_{33}, s_{44}, and s_{66} directly. A value of s_{12} and s_{13} can be calculated from their appearance in the $1/Y_f$ coefficients. A second value of each can be calculated using the $1/G_f$ coefficient in which they appear. For s_{12} the two values are -4.063 ± 0.088 and -3.940 ± 0.113; for s_{13} the result is -0.803 ± 0.039 and -0.786 ± 0.069 The results are thus self consistent. These values were weighted according to the reciprocals of their variances and the values of $s_{12} = -4.017 \pm 0.069$ and $s_{13} = -0.799 \pm 0.034$ were obtained.

The c_{ij} values can be calculated by inversion of the matrix of s_{ij} values. The equations for passing from c_{ij} to s_{ij} are given by Nye [*14*] and it is easy to show that the equations for obtaining c_{ij} from s_{ij} in this case are obtained by interchanging c's and s's. The result is

$$c_{11} = \frac{1}{2}\left[\frac{s_{33}}{s} + \frac{1}{s_{11}-s_{12}}\right]$$

$$c_{33} = \frac{s_{11}+s_{12}}{s}$$

$$c_{44} = \frac{1}{s_{44}}$$

$$c_{66} = \frac{1}{s_{66}}$$

$$c_{12} = \frac{1}{2}\left[\frac{s_{33}}{s} - \frac{1}{s_{11}-s_{12}}\right]$$

$$c_{13} = -\frac{s_{13}}{s}$$

where

$$s = s_{33}(s_{11}+s_{12}) - 2s_{13}^2.$$

The calculations were made by substituting for the s_{ij} the directly computed quantities of table 4. For each of the constants c_{11}, c_{33}, c_{12}, and c_{13} the two values were obtained and a weighted mean computed as in the case of s_{12} and s_{13}.

The s_{ij} and c_{ij} values are listed in table 5 for comparison with the work of other investigators. The present c_{ij} show no statistically significant differences from the values calculated by Birch. Using the simple test of twice the standard deviation we find, however, that the s_{11} and s_{12} values of Birch are significantly different from our results. This is probably caused by the fact that the equations for s_{11} and s_{12} (which have the same form as the above eqs for c_{11} and c_{12}) both involve the difference $c_{11}-c_{12}$. There is thus some reason to prefer the present s_{11} and s_{12} values as they are more directly determined; the same argument favors the c_{11} and c_{12} values of Verma-Birch. Our linear and volume compressibility values are also given in table 5 and are consistent with Bridgman and Verma-Birch.

It is interesting to compare the elastic properties of rutile single crystals with those of polycrystalline rutile. Huntington [*26*] discusses the problem of calculating elastic moduli of a pore-free polycrystalline solid from the single crystal elastic constants. Results calculated from theories of Reuss (which gives a lower bound) and of Voigt (which gives an upper bound) are given in table 6. The bulk modulus is determined within narrow limits but the Young's modulus and shear modulus values are not so well determined. This is a reflection of the fact that, as shown by figures 2 and 3, these two moduli depend strongly on orientation.

TABLE 5. *Elastic parameters of rutile*

c_{ij} in 10^{12} dyne/cm^2			s_{ij} in 10^{-12} cm^2/dyne		
	Bridgman [a]	Dayal and Appalanarasimham [b]	Vick and Hollander [c]	Verma recalculated by Birch [d]	Present work [e]
c_{11}	.....	3.005	2.48±.08	2.73	2.660±.066
c_{33}	.....	1.9	4.52±.08	4.84	4.699±.081
c_{44}	.....	1.324	1.20±.03	1.25	1.239±.007
c_{66}	.....	1.761	1.6 ±.1	1.94	1.886±.050
c_{12}	.....	1.76	2.0 ±.1	1.76	1.733±.071
c_{13}	.....	1.36	1.4 ±.1	1.49	1.362±.081
s_{11}	.....	5.8	11.8	6.55	6.788±.015
s_{33}	.....	8.9	2.7	2.59	2.592±.011
s_{44}	.....	7.6	8.3	8.00	8.072±.048
s_{66}	.....	5.7	6.2	5.16	5.302±.140
s_{12}	.....	−2.2	−9.0	−3.76	−4.017±.069
s_{13}	.....	−2.5	−0.86	−0.86	−0.799±.034
$s_{11}+s_{12}+s_{13}$	1.89	.....	.....	1.93	1.965±.069
$s_{33}+2s_{13}$	1.04	.....	.....	0.87	0.994±.067
$2s_{11}+s_{33}+2s_{12}+4s_{13}$	4.82	.....	.....	4.73	4.911±.166

[a] Measured statically. Present adiabatic values calculated from Bridgmen's isothermal values.
[b] c_{ij} computed from spectroscopic observations. s_{ij} computed by matrix inversion.
[c] Diagonal c_{ij} computed from pulse velocity measurements. c_{12} and c_{13} computed using Bridgman's linear compressibilities, s_{ij} by matrix inversion.
[d] c_{ij} computed from pulse velocity measurements, s_{ij} by matrix inversion.
[e] s_{ij} computed from resonance frequency measurements, c_{ij} by matrix inversion as explained in the text. The values for the linear and volume compressibilities given in the last three rows are not exactly the same as would be obtained by direct computation from the s_{ij} above, because the weighting is different for a combination of constants than for a single constant. The deviations shown for the present values are standard deviations for the compliances and constants obtained from least squares calculations.

TABLE 6. *Elastic moduli for polycrystalline rutile computed from Reuss and Voight theories* [a]

	Polycrystalline		Single crystal
	Reuss theory	Voight theory	
	All units 10^{12} dyne/cm^2		
Young's modulus	2.555	3.116	Orientation dependent see figure 2.
Shear modulus	0.990	1.244	Orientation dependent see figure 3.
Bulk modulus	2.025	2.103	2.025.

[a] Using values of the s_{ij} and c_{ij} given in the last column of table 5.

The writers have previously used the resonance method to determine the six elastic compliances, s_{ij}, of corundum [*11*] with standard deviations of about 0.1 percent for the diagonal compliances and about 1.0 percent for the off-diagonal compliances. The present uncertainties in the diagonal constants range from 0.2 percent for s_{11} to 2.6 percent in s_{66}. For the off-diagonal constants the values are 1.7 percent for s_{12} and 4.3 percent for s_{13}. These results are somewhat disappointing when compared with the precision achieved with corundum. Rutile differs from corundum in being more anisotropic but this should not cause such an increase in standard deviation if the orientation were constant throughout the specimen. The principal difficulty probably

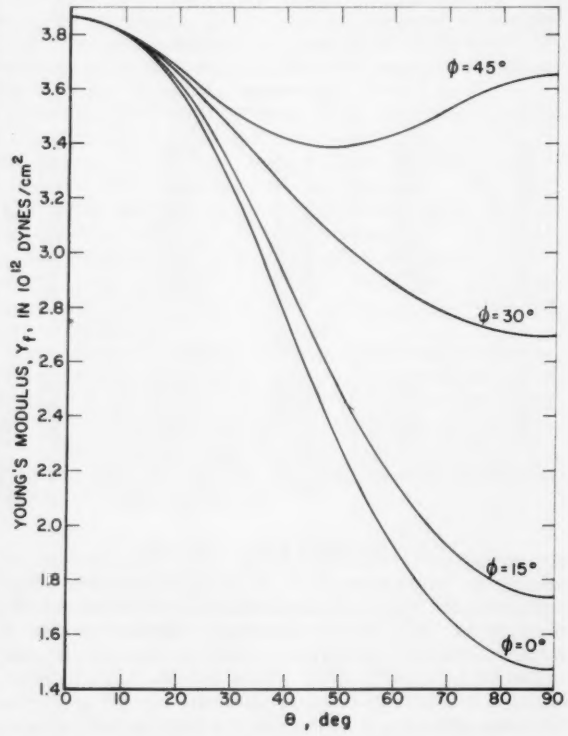

FIGURE 2. *Young's modulus, Y_θ, as a function of orientation, calculated from eqs (1) and (6), using the least squares best estimates of the coefficients given in table 4.*

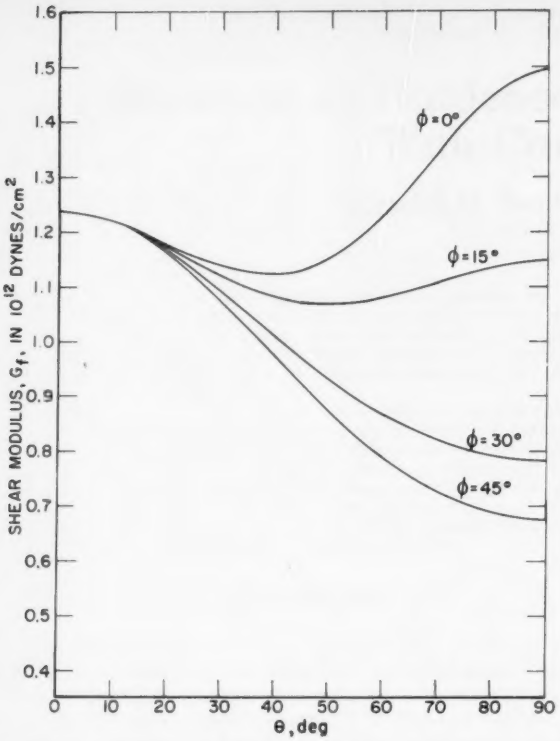

FIGURE 3. *Shear modulus, G_f, as a function of orientation, calculated from eqs (2) and (7), using the least squares best estimates of the coefficients given in table 4.*

is associated with the small angle boundaries. If specimens free of these boundaries are ever produced it would be interesting to repeat both the pulse velocity and resonance measurements and attempt to obtain agreement to 0.1 percent in the diagonal constants. It is probably not worthwhile to attempt to improve the agreement using existing specimens. The present results are accurate enough for most purposes and the general agreement of different observers leaves no question of serious error. The value of c_{33} calculated by Dayal and Appalanarasimham from spectroscopic data is in serious error, as previously noted [*9, 10*], and an extension of their calculation to correct this value might be worthwhile.

NOTE.—The writers were recently informed by Gilman [*27*] of unpublished work by himself and B. Chick on the elastic constants of rutile. They obtained $c_{33}=4.75\times10^{12}$ dynes/cm^2 and $c_{44}=1.23\times10^{12}$ dynes/cm^2. Both values are in good agreement with the results of the present work.

The writers gratefully acknowledge the help provided by the suppliers of the rutile powder and single crystals. In particular we thank W. S. Brower and S. F. Holley of the National Bureau of Standards, R. G. Rudness of the Linde Co., and M. D. Beals of the National Lead Co.

(Paper 66A6–181)

7. References

[1] F. A. Grant, Properties of rutile (titanium dioxide), Revs. Modern Phys. **31,** 646–764 (1959).
[2] H. P. R. Frederikse, Recent studies on rutile (TiO_2), J. Appl. Phys. Suppl. to **32,** 2211–2215 (1961).
[3] L. E. Hollander, Jr., and P. L. Castro, Bibliography and technical review of rutile, Lockheed Technical Report LMSD–894803 (1961), Astia number 257867.
[4] P. W. Bridgman, The linear compressibility of thirteen natural crystals, Am. J. Sci. **15,** 287 (1928).
[5] B. Dayal and N. Appalanarasimham, The evaluation of the elastic constants of rutile from spectroscopic data, J. Sci. Res. of Benares Hindu Univ. **1,** 26–30 (1950).
[6] G. L. Vick, L. E. Hollander, and A. E. Brown, Elastic moduli of single-crystal rutile (TiO_2), Bull. Am. Phys. Soc. Ser. II **4,** 463 (1959).
[7] R. K. Verma, Elasticity of some high density crystals, J. Geophys. Res. **65,** 757–766 (1960).
[8] J. B. Wachtman, Jr., W. E. Tefft, and D. G. Lam, Jr., Elastic constants of rutile (TiO_2), Bull. Am. Phys. Soc. Ser. II **5,** 278 (1960).
[9] G. L. Vick and L. E. Hollander, Ultrasonic measurement of the elastic moduli of rutile, J. Acoust. Soc. Am. **32,** 947 (1960).
[10] Francis Birch, Elastic Constants of Rutile—A correction to a paper by R. K. Verma, "Elasticity of Some High-Density Crystals," J. Geophys. Res. **65,** 3855–3856 (1960).
[11] J. B. Wachtman, Jr., W. E. Tefft, D. G. Lam, Jr., and R. P. Stinchfield, Elastic constants of synthetic single crystals corundum at room temperature, J. Research NBS **64A,** 213–228 (1960).
[12] J. B. Wachtman, Jr., and L. R. Doyle, Related effects of point defects on electrical and mechanical properties of nonmetallic crystalline solids, submitted to J. Am. Ceram. Soc.
[13] W. F. Brown, Jr., Interpretation of torsional frequencies of crystal specimens, Phys. Rev. **58,** 998–1001 (1940).
[14] J. F. Nye, Physical properties of crystals, (Oxford Univ. Press, London, England, 1957).
[15] R. F. S. Hearmon, The elastic constants of anisotropic materials, Rev. Mod. Phys. **18,** 409–440 (1946); The elastic constants of anisotropic materials II, Adv. in Phys. **5,** 323–382 (1956).
[16] Lord Rayleigh, The theory of sound, **1,** 251 (Dover Publications, New York, N.Y., 1945).
[17] Dennison Bancroft, The velocity of longitudinal waves in cylindrical bars, Phys. Rev. **59,** 588–293 (1941).
[18] Gerald Pickett, Flexural vibration of unrestrained cylinders and discs, J. App. Phys. **16,** 821 (1945).
[19] S. P. Timoshenko, On the correction for shear of the differential equation for transverse vibrations of prismatic bars, Phil. Mag. **41,** 744–746 (1921); On the transverse vibrations of bars of uniform cross-section, Phil. Mag. **43,** 125–131 (1922).
[20] E. Goens, Über die Bestimmung des Elastizitats moduls von Staben mit Hilfe von Biegungsschwingungen, Ann. Physik **11,** 649–768 (1931).
[21] Gerald Pickett, Equations for computing elastic constants from flexural and torsional resonant frequencies of vibration of prisms and cylinders, Proc. ASTM **45,** 846–865 (1945). (Also available as Bull. **7** of the Research Lab. of Portland Cement Assoc.).
[22] W. E. Tefft, Numerical solution of the frequency equations for the flexural vibration of cylindrical rods, J. Research NBS **64B,** 237–242 (1960).
[23] S. Spinner and W. E. Tefft, A Method for determining mechanical resonance frequencies and for calculating elastic moduli from these frequencies, Proc. ASTM **61,** 1221–1237 (1961).
[24] H. E. Swanson and Eleanor Tatge, Standard X-ray diffraction powder patterns, NBS Circ. 539, Vol. I (1953).
[25] H. Scheffe, The analysis of variance, (John Wiley & Sons, New York, N.Y., 1959).
[26] H. B. Huntington, The elastic constants of crystals, Solid State Phys. **7,** 213–351 (Academic Press, New York, N.Y., 1958).
[27] J. J. Gilman, Brown University, Private communication.

JOURNAL OF RESEARCH of the National Bureau of Standards—A. Physics and Chemistry
Vol. 66A, No. 6, November–December 1962

Reaction of Hardened Portland Cement Paste With Carbon Dioxide

Charles M. Hunt and Lewis A. Tomes [1]

(July 23, 1962)

The effect of age, water-cement ratio, and evaporable-water content on the reaction of hardened cement paste with carbon dioxide was investigated, using small cylinders of cement paste. The rate and extent of the reaction are subject to manipulation by varying the evaporable water content of the paste. Pastes of different age and water-cement ratio tend to dry at different rates, and this difference exerts an important indirect effect on carbonation.

Analysis of the specimens showed that less than one molecule of nonevaporable water was released for every molecule of carbon dioxide gained, except in paste of low water-cement ratio or at low levels of carbonation in other pastes. If calcium hydroxide were the only phase attacked, equimolecular CO_2–H_2O stoichiometry would be expected. The observed behavior does not rule out the possibility of some preferential attack on calcium hydroxide, but other phases can react while calcium hydroxide is still present. Water-cement ratio, particularly in very dense paste, may exert some effect on the comparative accessibility of different phases.

1. Introduction

Practical interest in the carbonation of hydrated portland cement stems from the fact that it modifies the properties of cement products. It usually improves the compressive strength [1–6],[2] but carbonation under some circumstances has been reported to be deleterious [7]. Jones [4] found the impact strength of cement-asbestos sheet to be adversely affected by carbonation. Also, water containing carbon dioxide may attack gel constituents and weaken concrete under prolonged exposure [8a]. When concrete, mortar, or hardened cement paste is allowed to react with carbon dioxide, shrinkage is observed [3, 9, 10, 11], but the carbonated product may exhibit somewhat greater volume stability than the original material [10, 11]. Carbonation has also been discussed as a possible cause of the crazing observed on some concrete surfaces [1, 8b].

The reaction of cement products with carbon dioxide is influenced by the colloidal structure of cement paste. It is partly a diffusion-controlled process in which water functions primarily as a barrier to the rapid movement of gas, and it is partly a moisture-controlled process in which a small amount of water is necessary before reaction will take place. Bessey [2] observed that the carbonation of mortar and sand-lime specimens proceeded more readily as the relative humidity of exposure was lowered. Lea and Desch [6] in discussing this behavior suggested that the rate of carbonation probably falls off again at some still lower relative humidity. There is now ample published experimental evidence to support this view [10, 12, 13]. The present paper describes some experiments with small specimens of paste, which examine in some detail the effect of age, water-cement ratio, and evaporable water content on the reaction of hydrated portland cement with carbon dioxide. Carbonation is considered primarily from the point of view of the water and carbon dioxide involved in the overall process.

2. Methods and Materials

2.1. Cements

Two cements were used for these experiments. Both met the requirements of Federal Specification SS–C–192 for type I cement. The chemical analysis of the cements is given in table 1. Cement No. 1 was used in the depth-of-penetration study. Cement No. 6 was used in all other experiments.

TABLE 1. *Chemical composition of cements*

Constituent	Cement	
	1	6
	Wt %	*Wt %*
CaO	64.0	63.2
SiO_2	22.0	21.8
Al_2O_3	5.2	5.1
Fe_2O_3	4.6	2.6
MgO	1.6	3.0
SO_3	1.5	2.4
Na_2O		0.3
K_2O		1.2
Ignition loss	0.2	0.6
CO_2		.2
Insoluble residue	.1	.1

2.2. Preparation of Specimens

Thirty to forty grams of cement were mixed with water and cast in cylindrical polystyrene molds, ½ in. in diameter and ½ in. deep. Nominal water-cement ratios of 0.3, 0.4, and 0.5 were selected, and an addi-

[1] Research associate representing the Calcium Chloride Institute at the National Bureau of Standards.
[2] Figures in brackets indicate the literature references at the end of this paper.

tional series of specimens of water-cement ratio 0.5 were prepared in which 1.56 percent of the cement was replaced with $CaCl_2$.

Curing for the first 24 hr took place in sealed molds. Curing beyond 24 hr took place in paraffin sealed glass jars containing a small amount of water in the bottom to maintain high relative humidity. The specimens were exposed to the vapor only.

Specimens for the measurement of depth of carbonation were cast in glass tubes 1 in. in diameter and 2½ in. deep. A nominal water-cement ratio of 0.5 was used. They were cured and allowed to remain in the tubes, so that the subsequent loss of water and gain of carbon dioxide were essentially unidirectional through the top surface. Samples for analysis were taken with a masonry drill, and sampling depths were measured with a depth gauge.

2.3. Carbonation of Specimens

Ten specimens were taken to represent each age and water-cement ratio. The specimens in each series are designated here by numbers 1 through 10, and the precarbonation treatment of each specimen is summarized as follows:

1. Placed in water 10 min and surface blotted.
2. No treatment.
3. Vacuum dried ½ hr.
4. Vacuum dried 2 hr.
5. Vacuum dried 5 hr.
6. Vacuum dried 24 hr.
7. Vacuum dried 72 hr.
8. Vacuum dried 7 days.
9. Vacuum dried 7 days after which the specimen was crushed and vacuum dried an additional 7 days.
10. No treatment and not exposed to carbon dioxide.

After pretreatment, specimens 1 through 9 were exposed to dried carbon dioxide at one atmosphere for a week in closed individual cells similar to the one illustrated in figure 1. The ambient temperature during exposure was 25°C. Specimen 10 was not dried or exposed to carbon dioxide and served as a check on the normal rate of hydration of the paste during the 1-week exposure period.

The depth-of-carbonation specimens, arbitrarily designated A, B, C, and D, were vacuum dried for periods of 30 min, 6 hr, 48 hr, and 7 days respectively. They were then exposed to carbon dioxide at 1 atm for a week in a glass jar equipped with a gas inlet trap containing *n*-butyl phthalate, similar to the one in figure 1.

2.4. Determination of Nonevaporable Water, Evaporable Water, and Carbon Dioxide

Nonevaporable water, W_n, was determined by a slight modification of the Copeland and Hayes procedure [14]. After exposure to carbon dioxide, the specimens were dried in a vacuum system containing a trap cooled with dry ice. The period of drying was selected so as to give each specimen a week of drying, including any drying received before carbonation.

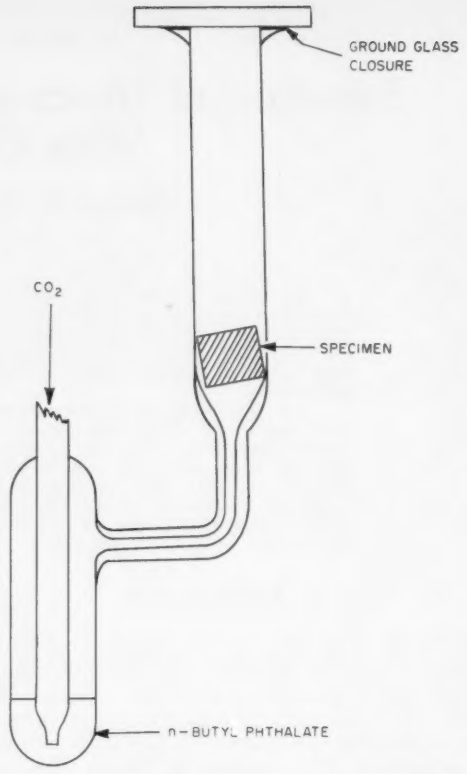

FIGURE 1. *Cell for exposing cylinders of hardened cement paste to carbon dioxide.*

The specimens were then crushed and dried for an additional week. The number 9 specimen of each series, which received this complete drying treatment before exposure to carbon dioxide, was given an additional 24 hr of drying after carbonation to compensate for the extra handling. Nonevaporable water was then determined by measuring the loss of weight at 1,050 °C and subtracting the carbon dioxide content of the specimen.

Evaporable water, W_e, was determined by measuring the loss in weight of each specimen during precarbonation drying and subtracting this loss from the total evaporable water content of the original hardened paste. The water lost by the number 9 specimen of each series was assumed to represent the total evaporable water content of the original paste.

Carbon dioxide was determined by digesting the paste in 4-normal hydrochloric acid and absorbing the evolved gas in Ascarite. The apparatus and procedure were similar to those described by Kolthoff and Sandell [15] with minor modifications which have been previously described [16].

2.5. Estimation of Pore Volume

Total pore volume, P_T, and gel pore volume, P_G, of the original hardened paste were calculated from the equations of Copeland and Hayes [17],

$$P_T = 0.99\ (W_o - 0.746\ W_n) \quad (1)$$

$$P_G = 2.36\ kW_n \quad (2)$$

where W_o is the original mixing water and represents the total pore volume at the start of hydration, k is a constant for any given cement, and W_n is the nonevaporable water content of the original paste. In the present experiments W_o was based on the total water in the paste immediately after removal from the mold after 24 hr, k was assumed to be 0.3, and W_n was based on the nonevaporable water content of the number 9 specimen of each series after carbonation. Such values of W_n are estimated to be 0.2 to 0.5 percent less than the true nonevaporable water content of the original paste. An uncertainty of 0.5 percent in W_n corresponds to an uncertainty in total pore volume of about 0.4 ml per hundred grams of ignited cement. Also, the equations of Copeland and Hayes are based upon vacuum-mixed pastes and would not include any entrained air in the specimens.

3. Results and Discussion

3.1. Effect of Predrying on Carbonation

The results obtained when ½-in. specimens of hardened cement paste of different age and water-cement ratio were partially dried and allowed to react with carbon dioxide are summarized in table 2. The data include evaporable water content before exposure to carbon dioxide and carbon dioxide and nonevaporable water content after exposure. Wide variations in the amount of carbon dioxide reacting with the pastes are evident in the table. Individual specimens contain as little as 0.82 or as much as 40.65 percent carbon dioxide after a week in an atmosphere of the gas. It is clear that the reaction is extremely responsive to the drying treatment received by the paste before exposure.

The effect of predrying is shown more clearly in figure 2 where carbon dioxide content is plotted as a function of drying time. Each age and water-

TABLE 2. *Evaporable water content of cement pastes before exposure to carbon dioxide and the nonevaporable water and carbon dioxide content after exposure*

Nominal w/c ratio	Specimen number	Original mixing water W_o	1-day hydration			7-day hydration			28-day hydration		
			W_e evap. H_2O before exposure	W_n nonevap. H_2O after exposure	CO_2 after exposure	W_e evap. H_2O before exposure	W_n nonevap. H_2O after exposure	CO_2 after exposure	W_e evap. H_2O before exposure	W_n nonevap. H_2O after exposure	CO_2 after exposure
		Percent of ignited cement									
0.3	1	30.6	23.39	10.00	4.28	20.60	10.96	2.33	19.07	12.94	1.08
	2		22.85	9.29	5.35	20.62	11.10	2.32	19.11	12.67	1.21
	3		20.44	8.90	6.49	18.80	10.40	4.13	17.82	12.61	2.34
	4		17.67	8.28	9.36	17.11	10.27	6.16	16.21	12.06	3.64
	5		14.84	7.15	13.39	15.10	9.12	8.56	13.62	10.46	6.57
	6		7.99	5.28	22.76	8.75	7.44	15.78	9.42	10.02	10.80
	7		4.39	7.53	2.59	4.08	6.21	21.85	5.66	10.95	8.23
	8		2.92	7.77	1.49	2.17	10.57	1.81	3.61	13.32	3.27
	9		0	7.99	0.82	0	10.60	0.98	0	12.99	1.10
	10			10.68	.41		11.65	.45		13.15	0.44
0.4	1	40.3	32.89	9.76	8.02	29.36	12.42	3.38	28.43	14.37	1.80
	2		32.41	9.76	9.15	29.42	12.28	3.77	28.52	14.53	1.79
	3		25.81	7.77	16.63	27.14	12.23	5.15	26.17	13.36	4.68
	4		18.61	6.46	24.90	24.01	10.89	8.84	23.16	12.61	8.07
	5		13.52	5.43	33.85	20.28	9.94	13.98	19.44	11.05	13.62
	6		5.18	7.42	30.04	11.29	7.37	26.50	9.69	8.16	26.79
	7		2.73	7.54	14.77	5.56	11.52	7.75	4.90	13.63	5.14
	8		1.79	7.55	1.34	3.68	11.95	1.86	3.08	14.01	1.94
	9		0	7.77	0.91	0	12.41	1.15	0	14.62	1.35
	10			12.36	.40		13.64	0.43		14.73	0.45
0.5	1	47.8	39.64	9.50	10.40	36.02	13.64	5.40	33.76	14.70	3.76
	2		39.59	9.45	10.87	36.11	13.46	5.46	33.82	14.70	4.15
	3		29.86	6.35	23.11	31.89	12.68	9.11	30.45	13.88	6.92
	4		18.61	4.95	37.32	26.90	10.43	16.07	26.13	12.69	13.00
	5		8.01	4.37	38.13	21.21	9.04	25.63	20.72	10.56	22.35
	6		1.94	7.13	1.59	9.36	6.92	40.65	8.95	8.15	35.84
	7		2.06	7.12	1.07	4.57	13.02	2.64	4.77	14.80	3.01
	8		0.43	7.17	0.98	3.28	13.02	1.80	2.94	14.72	2.07
	9		0	7.18	1.06	0	12.80	1.23	0	14.98	1.52
	10			13.31	0.47		14.88	0.49		15.62	0.50
0.5 $CaCl_2$ added	1	49.3	39.86	12.34	8.83	36.51	13.85	4.61	35.61	15.40	3.31
	2		39.84	12.22	9.14	36.59	14.30	4.82	35.77	15.49	3.37
	3		30.76	10.67	17.12	32.15	12.92	9.80	32.13	14.56	7.20
	4		19.64	7.19	32.05	26.16	11.59	18.20	25.51	12.35	15.88
	5		11.93	6.23	36.87	18.79	9.19	30.05	20.28	10.91	25.95
	6		3.79	9.45	3.14	9.82	6.88	39.08	9.55	7.94	40.33
	7		2.36	9.43	2.12	5.50	13.61	3.22	6.19	15.84	3.17
	8		1.94	9.34	1.83	4.12		2.43	3.76	15.84	2.63
	9		0	9.21	1.42	0	13.63	1.61	0	15.95	1.90
	10			15.63	0.65		15.31	0.50		16.42	0.60

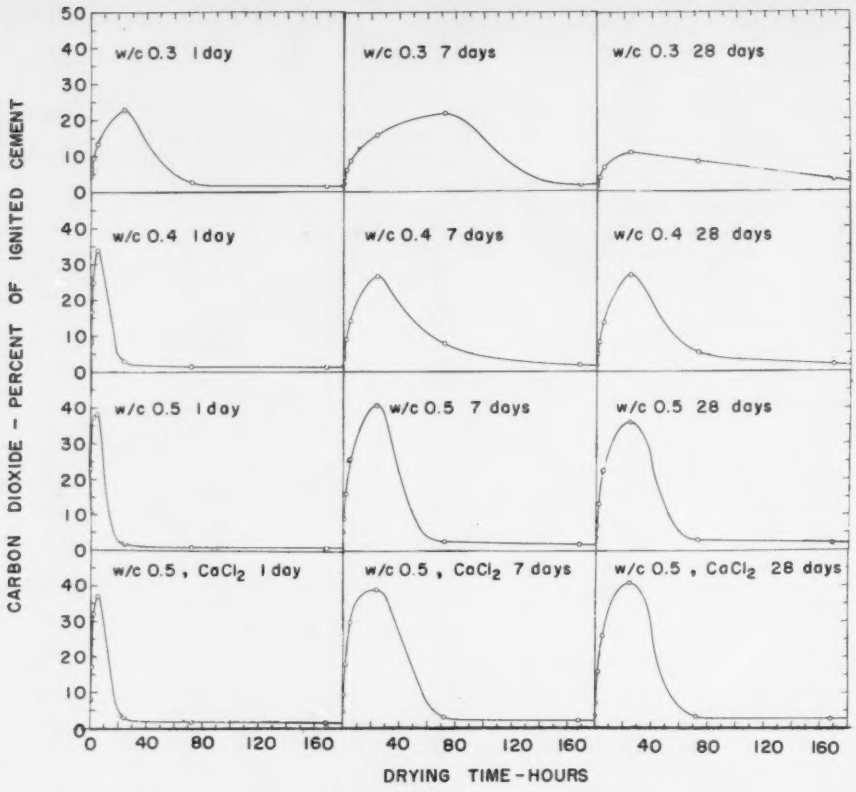

FIGURE 2. *Carbon dioxide content of cement pastes as a function of drying time before exposure to carbon dioxide.*

cement ratio is represented by a separate curve. For each paste there is an optimum condition for maximum reaction with carbon dioxide. Seven-day-old pastes are denser in structure and dry more slowly than 1-day-old pastes. Therefore they reach and pass through this optimum condition more slowly. This difference is evident from the shift of the maxima of the curves in figure 2. This shift would be expected to be greater in older specimens. However, the 28-day-old specimens do not appear to reach the optimum condition more slowly than 7-day specimens. The amount of additional hydration of these particular specimens between 7 and 28 days is apparently insufficient to make a significant change in their drying and carbonation characteristics, except in the very dense paste of water-cement ratio 0.3. At this water-cement ratio, reduced accessibility to carbon dioxide at 28 days is the predominant effect.

In general, young pastes of high water-cement ratio tend to carbonate more readily than older and denser pastes. For example, a 28-day-old specimen of water-cement ratio 0.3 would react with less carbon dioxide than a 1-day-old specimen of water-cement ratio 0.5, but if the comparison is arbitrarily made after 72 hr of drying, rather than at the time of maximum reaction, the opposite is true. Behavior such as this is probably one of the reasons why Leber and Blakey [9] were induced to comment that, "There is ample evidence that slight changes in carbon dioxide treatment, such as age at which treatment starts, will produce completely contradictory results."

The effect of calcium chloride was examined at one water-cement ratio, because it is a commonly used agent for accelerating the hydration of portland cement. It might be expected that a 1-day-old paste containing calcium chloride might behave as a slightly older specimen without calcium chloride. However, the two sets of curves in figure 2, representing water-cement ratio 0.5 with and without calcium choloride, show only slight differences. Apparently the reduction in bleeding produced by the accelerator has compensated for any increased hydration. In other words more hydration products are formed in the presence of calcium chloride, but there is also more space to fill. Therefore the net affect on the drying and carbonation characteristics of the paste is small.

3.2. Carbonation as a Function of Pore Space

Powers and Brownyard [18] have designated the pores remaining in the voids between the original particles, which become partially or completely filled with gel during hydration, as capillary pores. The

much smaller pores characteristic of the gel they have designated as gel pores. The sum of the capillary and gel pore space is the total pore space.

The pore volume of a saturated paste is equal to the volume of water required to fill the pores. For purposes of approximation, pore volume, in appropriate units, may be considered numerically equal to the weight or percentage of water required to fill the pores, since water in a saturated paste has a specific volume of 0.99 [19]. In order to examine carbonation from the standpoint of pore space, carbon dioxide content at the end of one week exposure is plotted in figure 3 as a function of the amount of evaporable water in the specimen at the start of exposure. For each hardened paste before carbonation the amount of the original mixing water, W_o, the total pore volume, P_T, and the volume of the gel pores, P_G, are marked on the abscissa of the graph. The difference between P_T and P_G on the abscissa is approximately numerically equal to the capillary pore volume in $cm^3/100$ g of cement, and the difference between W_o and P_T, to the net increase in the volume of solid phases during hydration. Figure 3 affords a visual comparison of the amount of evaporable water in each specimen at the beginning of each carbonation experiment and the amount of

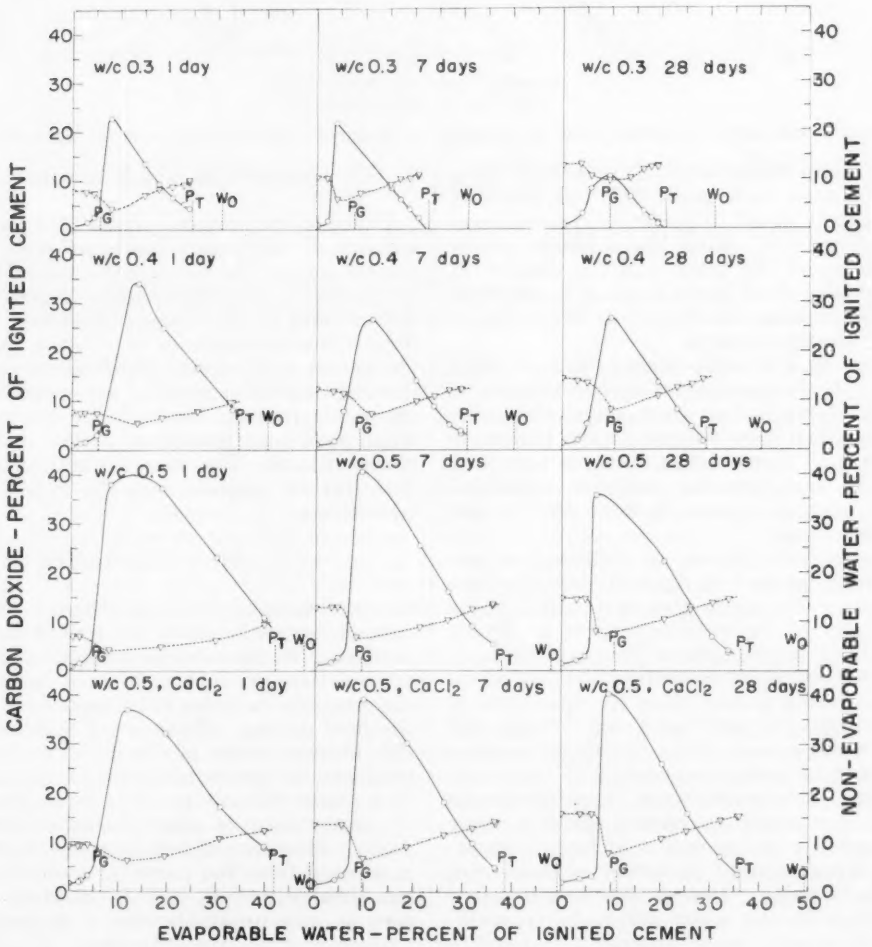
w/c 0.3 1 day
w/c 0.3 7 days
w/c 0.3 28 days
w/c 0.4 1 day
w/c 0.4 7 days
w/c 0.4 28 days
w/c 0.5 1 day
w/c 0.5 7 days
w/c 0.5 28 days
w/c 0.5, CaCl2 1 day
w/c 0.5, CaCl2 7 days
w/c 0.5, CaCl2 28 days
PG
PT
WO
CARBON DIOXIDE - PERCENT OF IGNITED CEMENT
NON-EVAPORABLE WATER - PERCENT OF IGNITED CEMENT
EVAPORABLE WATER - PERCENT OF IGNITED CEMENT

FIGURE 3. *Carbon dioxide and nonevaporable water content of cement pastes as a function of the evaporable water content of the pastes as determined before exposure to carbon dioxide.*

—○— Carbon dioxide content after a week of exposure to carbon dioxide
--▽-- Nonevaporable water content after a week of exposure to carbon dioxide
P_G Volume of gel pores
P_T Total pore volume
W_o Original water content of the fresh paste.

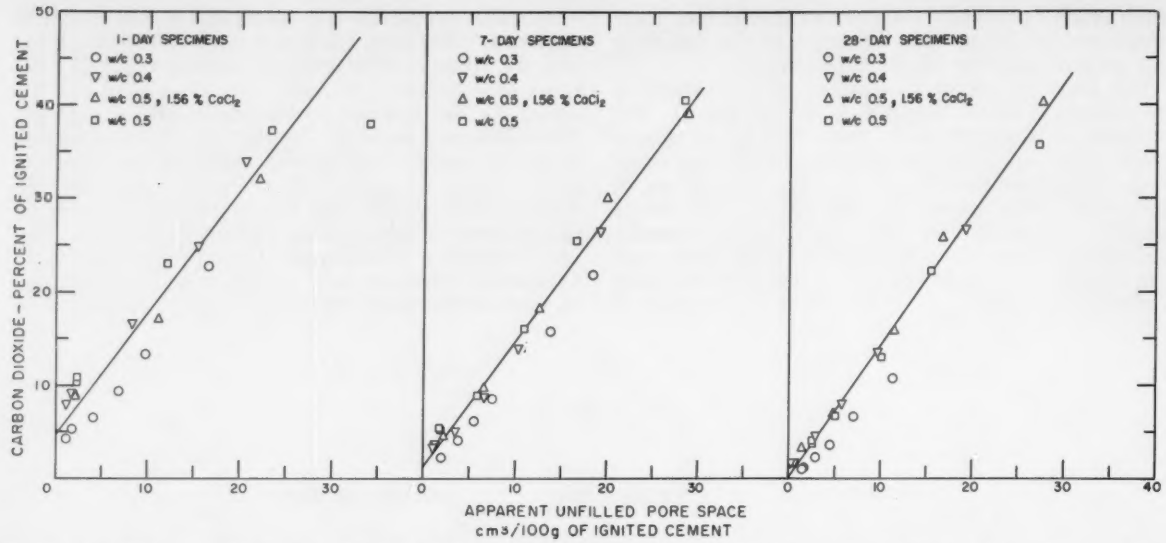

FIGURE 4. *Carbon dioxide content of cement paste as a function of apparent unfilled pore space at the beginning of carbo nation.*

water required to fill the pores. The difference along the abscissa between each point and the value of P_T is approximately equal to the unfilled pore space in $cm^3/100$ g of cement. Since less is known about the actual volume of the pores and the density of water in a partially dried paste than in a saturated paste, the value obtained is referred to in this paper as apparent unfilled pore space.

Considering only the right branch of each solid curve in figure 3, the amount of carbon dioxide in each specimen shows rather good correlation with the apparent unfilled pore volume at the beginning of carbonation. In figure 4 the data for 1-day-old specimens of all water-cement ratios is assembled in one graph, and the same is done for 7- and 28-day-old specimens.

Differences between pastes of different water-cement ratio may be seen in figure 4, but they are small considering the much greater possibility for loss of continuity of the capillary pores in denser pastes. According to estimates of Powers, Copeland, and Mann [20], based upon water-permeability measurements of saturated pastes, all of the specimens of water-cement ratio 0.3 and the 7- and 28-day-old specimens of water-cement ratio 0.4 might reasonably be expected to have completely lost their capillary continuity. However, when these specimens were dried and exposed to carbon dioxide, they behaved comparably to specimens of higher water-cement ratio which should definitely contain continuous capillary pores. Powers [21] has reported a 70-fold increase in the water permeability coefficient of a mature paste after bringing it to equilibrium with 79 percent relative humidity and carefully resaturating it. Therefore it is not surprising that partially dried pastes of low water-cement ratio should have considerable accessibility to carbon dioxide. Even if capillary continuity is lost in the hydration process, drying apparently creates passages.

3.3. Carbonation and Nonevaporable Water

Carbonation brings about a reduction in the amount of chemically combined water in hardened cement paste. In figure 3 this reduction is reflected by decreases in nonevaporable water shown by the dotted lines in the figure. It should be possible to draw some inferences as to whether calcium hydroxide is the only phase involved in carbonation by determining the amount of nonevaporable water lost during the process. Verbeck [10] has applied a somewhat analogous procedure to the analysis of autoclaved pastes. The reaction of calcium hydroxide with carbon dioxide may be represented by the equation,

$$Ca(OH)_2+CO_2 \rightarrow CaCO_3+H_2O. \qquad (3)$$

One molecule of water is released for every molecule of carbon dioxide accounted for in the final product. While calcium bicarbonate as a possible intermediate product should not be overlooked [8a], the analysis includes only carbonate stable during the final drying. Equation 3 is therefore a reasonable representation of the initial reactants and final products in the carbonation of calcium hydroxide. It is more difficult to write equations representing the carbonation of other phases in hardened cement paste. However, if less than one molecule of water is released from the paste for every molecule of carbon dioxide gained, and if hydration of the cement goes on at a negligible rate, it is clear that calcium hydroxide is not the only phase attacked in the carbonation process. If, on the other hand, equimolecular stoichiometry is observed, it is possible that calcium hydroxide is the only phase attacked, but the point is not unequivocally proven until more information is known about the behavior of other phases during carbonation and drying.

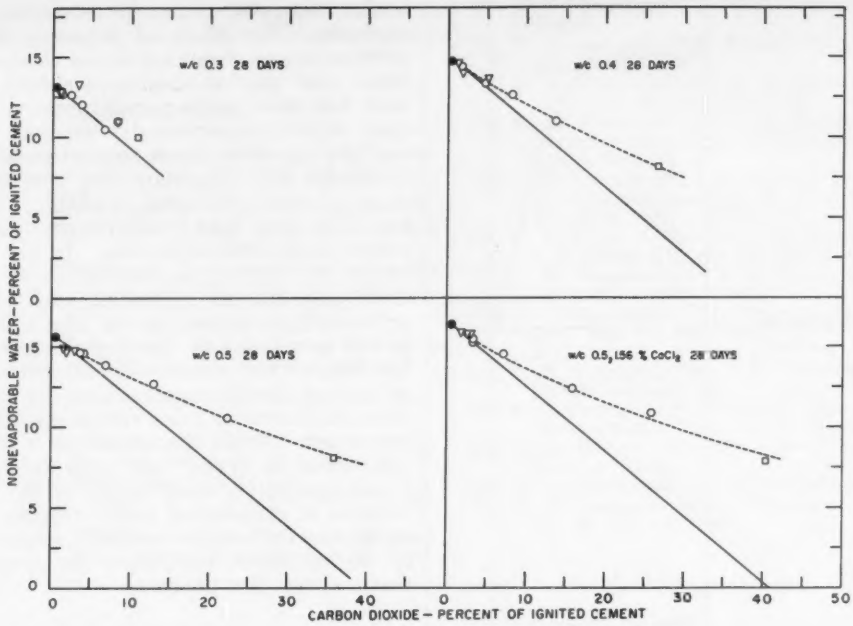

FIGURE 5. *Nonevaporable water content of cement paste as a function of carbon dioxide content.*

● Unexposed control specimen
□ Most highly carbonated specimen
○ Specimens containing more than the optimum evaporable water content for carbonation
▽ Specimens containing less than the optimum evaporable water content for carbonation
—— Theoretical slope if one molecule of water lost for each molecule of carbon dioxide gained.

In figure 5 the nonevaporable water contents of 28-day-old specimens are plotted as a function of carbon dioxide content. By limiting the analysis to 28-day-old pastes, hydration during the carbonation period is limited to less than 0.5 percent nonevaporable water. The solid straight lines in figure 5 correspond to the required theoretical slope if one molecule of water is lost for every molecule of carbon dioxide gained. Comparison of the experimental points with the theoretical slope shows that less water was released than required by the stoichiometry of eq 3, except in the paste of water-cement ratio 0.3 or at low levels of carbonation in the other pastes.

Verbeck [10] has estimated that it would be stoichiometrically possible to account for carbon dioxide contents equivalent to about 20 percent or more of ultimate carbonation by reaction with calcium and alkali hydroxides without attack on the main gel phases. Of course any such estimate depends upon the degree of hydration, since calcium hydroxide is one of the hydration products. For the cement represented in figure 5, 20 percent of ultimate carbonation corresponds to about 10 percent carbon dioxide based on the ignited weight of the cement. The form of the experimental curves for the pastes of water-cement ratios 0.4 and 0.5 suggests that there is some possibility of preferential attack on calcium hydroxide, particularly in the early stages of carbonation, but that other phases react while calcium hydroxide is still present. The data for paste of water-cement ratio 0.3 more nearly approximate the theoretical slope than the data for other pastes. From the point of view of CO_2–H_2O stoichiometry, this paste resembles autoclaved neat pastes [10]. A 28-day-old paste of water-cement ratio 0.3 would have a much lower surface area, as measured by nitrogen adsorption, than pastes of higher water-cement ratio. Autoclaved pastes have even lower surface areas. This factor seems to make a difference in the relative accessibility of the different phases to carbon dioxide.

3.4. Depth of Carbonation

In figure 6 the carbon dioxide content of four unidirectionally dried and exposed cylinders of paste is plotted as a function of average sampling depth. The A specimen, which was dried 30 min before exposure, showed only superficial carbonation after a week of exposure. The carbon dioxide content was already rather low at an average sampling depth of 5 mm. Longer drying resulted in deeper penetration into the paste. Specimen C, which was dried 48 hr, is of particular interest because it contained more carbon dioxide at a depth of 30 mm than near the surface. The specimen which was dried a week before exposure was too dry for optimum reaction. If any high-carbonation zone existed further inside the specimen, it was beyond the maximum sampling depth of about 38 mm.

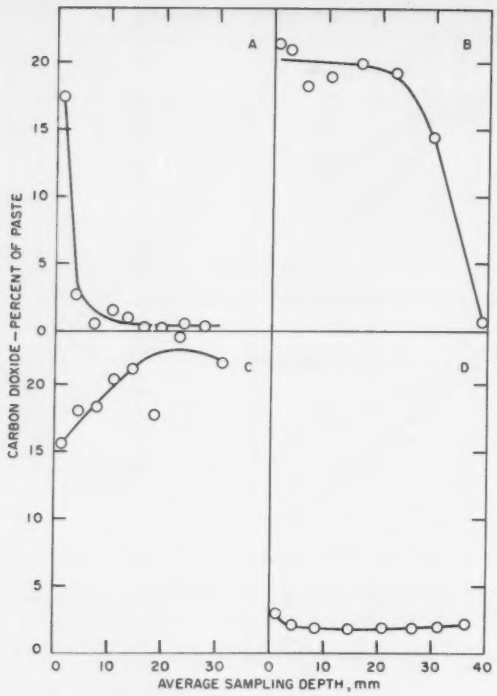

FIGURE 6. *Depth of carbonation.*

Drying time before exposure, A—30 min., B—6 hr., C—48 hr., D—1 week. A, B, and C exposed simultaneously in same chamber, D exposed separately.

Since reaction with carbon dioxide is influenced by the moisture content of the paste, a moisture gradient in a reacting specimen leads to different rates of carbonation in different parts of the specimen. Figure 6 is an experimental demonstration of this fact for a particular set of conditions. Gradients in moisture and carbon dioxide content probably existed also in the ½-in. specimens represented in figures 2, 3, 4, and 5. However, except for the wetter specimens, such gradients were probably small in comparison with those attained with larger specimens.

3.5 Carbonation and the Physical Characteristics of Hydrated Cement

In the results shown in figures 2 to 5, the water and carbon dioxide involved in the carbonation process have been accounted for, but no direct information has been obtained regarding the effect of carbonation on the compressive strength, shrinkage, or other physical properties or behavior of hardened paste. The physical characteristics of the product may depend not only on the amount of carbonate formed but also on the conditions under which it is formed. For example, Zalmanoff [22] found that the strengths of carbonated lime putties were greater if carbonation and drying took place simultaneously than if the specimens were first dried and then exposed to carbon dioxide. Possibly similar behavior might be observed with cement products. The effect of sequence of drying and carbonation on shrinkage is less clear. Verbeck [10] found that mortar specimens shrank more if they were first dried at 50 percent relative humidity and then exposed to carbon dioxide than if carbonation and drying took place simultaneously. However, Alexander and Wardlaw [23] concluded from the study of small specimens of paste, ⅛ in. in diameter and 2 in. long, that the sequence of drying and exposure made little difference. In the present experiments the drying characteristics of the specimens after carbonation indicated small differences in permeability, depending on the amount of water in the specimens at the beginning of carbonation. Specimens which were nearly saturated when exposed to carbon dioxide appeared to dry more slowly in vacuum thereafter than specimens which contained less water. When the specimens were crushed, the differences in drying rate were largely eliminated. These qualitative observations of the drying characteristics of carbonated pastes suggest that optimum conditions for reaction with CO_2 might not necessarily be optimum conditions for producing dense-textured reaction products.

4. Summary

Partially dried ½-in. cylinders of paste of nominal water-cement ratio 0.3, 0.4, and 0.5 reacted with increasing amounts of carbon dioxide as the water-cement ratio increased. The differences in the amounts of carbon dioxide reacting were greater at 28 days than at one day. However, pastes of different age and water-cement ratio tend to dry at different rates and reach, or go beyond, optimum conditions for carbonation at different rates. Under some circumstances this behavior can overshadow any inherent differences in reactivity or accessibility to carbon dioxide.

In pastes containing more than the optimum amount of evaporable water for carbonation the amount of carbon dioxide found after a week of exposure showed a linear relationship with the apparent unfilled pore volume at the beginning of carbonation.

Analysis of 28-day-old specimens showed that less than one molecule of water was released for every molecule of carbon dioxide gained, except in a paste of w/c ratio 0.3 and at low levels of carbonation in other pastes. This behavior does not rule out the possibility of some preferential attack on calcium hydroxide, but shows that other phases can react while calcium hydroxide is still present. Apparently in a very dense paste of low water-cement ratio the comparative accessibility of the various phases to carbon dioxide is different than in a paste of high ratio.

The effect of moisture gradients on the depth of carbonation was examined with unidirectionably dried cylinders, 1 in. in diameter and 2½ in. long. One of the predried specimens was found to have more carbonate formed at a depth of 2 to 3 cm than nearer the exposed surface.

The authors gratefully acknowledge the assistance of Vernon Dantzler in some of the measurements reported here.

5. References

[1] Annual Report Building Research Board, (1932), p. 34, Dept. of Scientific and Ind. Research, His Majesty's Stationery Office, London, (1933).
[2] G. E. Bessey, Soc. Chem. Ind. J. **52,** 287–293T (1933).
[3] F. L. Brady, Cement and Cement Mfgr. **4,** 1105–1109 (1931).
[4] F. E. Jones, Weathering Tests on Asbestos-Cement Roofing Materials, Dept. Scientific and Ind. Research, RP29, His Majesty's Stationery Office (1947).
[5] S. L. Meyers, Rock Products **52,** 96–98 (1949).
[6] F. M. Lea and C. H. Desch, The Chemistry of Cement and Concrete, p. 328, London, Edward Arnold Co., (1935).
[7] J. A. Kauer and R. L. Freeman, Proc. Am. Concrete Inst. **52,** 447–454 (1955).
[8] F. M. Lea, The Chemistry of Cement and Concrete, revised ed. of Lea and Desch, pp. (a.) 287–294; (b) 473–475, St. Martin's Press, (1956).
[9] I. Leber and F. A. Blakey, Proc. Am. Concrete Inst. **53,** 295–308 (1950).
[10] George Verbeck, Carbonation of Hydrated Portland Cement, Am. Soc. Testing Materials Special Tech. Publ. No. 205.
[11] H. T. Toennies, Proc. Am. Concrete Inst. **56,** 737–755 (1960).
[12] B. Kroone and F. A. Blakey, Proc. Am. Concrete Inst. **56,** 497–510 (1959).
[13] C. R. Hutchcroft and H. R. Anderson, Proc. Am. Concrete Inst. **37,** 597–604 (1941).
[14] L. E. Copeland and J. C. Hayes, Am. Soc. Testing Materials Bull. 194, p. 70 (1953); also Portland Cement Assoc. Bull. No. 47.
[15] I. M. Kolthoff and E. B. Sandell, Textbook of Quantitative Inorganic Analysis, 3d ed., p. 373, The MacMillan Co., New York (1952).
[16] C. M. Hunt, V. Dantzler, L. A. Tomes, and R. L. Blaine, J. Research NBS **60,** 441–446 (1958) RP2858.
[17] L. E. Copeland and J. C. Hayes, Proc. Am. Concrete Inst. **52,** 633–640 (1956).
[18] T. C. Powers and T. L. Brownyard, Proc. Am. Concrete Inst, **43,** 971–992 (1947), Portland Cement Assoc. Bull. No. 22.
[19] L. E. Copeland, Proc. Am. Concrete Inst. **52,** 863–874 (1956); Portland Cement Assoc. Bull. No. 75.
[20] T. C. Powers, L. E. Copeland, H. M. Mann, J. Portland Cement Assoc. Dev. Lab. **1,** 38–48 (1959).
[21] T. C. Powers, 4th International Symp. Chemistry of Cement, (1960).
[22] Nissan Zalmanoff, Rock Products **59,** 182–186 (1956).
[23] K. M. Alexander and J. Wardlaw, Australian J. Appl. Sci. **10,** 470–483 (1959).

(Paper 66A6–182)

JOURNAL OF RESEARCH of the National Bureau of Standards—A. Physics and Chemistry
Vol. 66A, No. 6, November–December 1962

Titanium Standards for Hydrogen Content

J. T. Sterling, F. J. Palumbo, and L. L. Wyman

(August 7, 1962)

This paper describes the preparation, analysis, and certification of a new series of standard samples. These samples consist of commercially pure titanium containing hydrogen at three levels (32 ppm, 98 ppm, and 215 ppm) and have been designated National Bureau of Standards Standard Samples Nos. 352, 353, and 354, respectively.

1. Introduction

The recent certification of National Bureau of Standards Standard Samples Nos. 352, 353, and 354, for hydrogen content in unalloyed titanium sheet marks the completion of (1) the lengthy process of developing suitable test methods, (2) selecting and producing adequate materials, and (3) the testing necessary for proving homogeneity and certification. The need for these standards resulted from the severe fabrication difficulties which occurred during production of titanium sheet as well as the usual desire to use these standards as reference material for specification compliance.

1.1. Government Titanium Sheet Program

Experiences in aircraft design during and subsequent to World War II indicated a need for materials for aeronautic developments that had a higher strength-weight ratio and better elevated temperature performance than that of the best aluminum or magnesium alloys. Since titanium and its alloys seemed to have these requirements, the Government sponsored extensive programs for the production of titanium sponge and for the fabrication of unalloyed and alloyed sheet.

Although the sponge production program progressed without too many difficulities, the sheet materials produced were so hard and brittle that they could not be fabricated into useful shapes. As a consequence, concerted efforts were exerted to identify and remedy the source of difficulty. Therefore, it was necessary to develop new analytical procedures and techniques for determining the amounts of impurities present in the material. The data obtained were then used for correlation purposes between the physical properties and composition. In essence, the presence of excessive amounts of hydrogen in the sheet was found to be the main offender. This early research indicated that vacuum annealing could be used as a remedial measure; however, the ultimate answer must lie in the development of metal-processing techniques, as shown by the analytical methods, which would prevent the metal and its alloys from initially accumulating hydrogen in deleterious amounts.

1.2. Analytical Commitee

In order to implement the analytical approach, a task group on gas analysis with Dr. T. D. McKinley, Chairman, was organized under the Metallurgical Advisory Committee on Titanium, Panel on Methods of Analysis with Mr. S. Vigo, Chairman. In brief, the efforts of this group resulted in the recommendations for analytical procedures which had been proven by a number of "round-robin tests" and by statistical analyses of the test results. These recommendations, in turn, created the need of reference standards for the hydrogen content of titanium and its alloy products. The Chemical Metallurgy Section was requested to prepare NBS Standard samples at three different levels of hydrogen content from sheet material prepared under the supervision of the Analytical Task Group.

2. Preparation of Materials

2.1. Fabrication

The titanium sheet used for making these standards was commercially pure titanium (RS–70, Heat No. R–11627) prepared by Republic Steel

Corporation, [1][1] South Division, Canton, Ohio under a contract funded and sponsored by Watertown Arsenal. The cost of the material for the samples was absorbed by Republic Steel Corporation, however, the processing (vacuum annealing, hydrogenation, surface grinding, and specimen cutting) was covered by the Watertown Arsenal contract and furnished to the National Bureau of Standards without charge.

One coil 33 in. wide was cold-rolled to 0.055 in. thickness, then mill annealed, descaled, and cut into twenty-four 96 in.-long sheets.

2.2. Hydrogen Equilibration

The program for this sheet material was directed towards the production of a series of samples at three different levels of hydrogen content in accordance with the following:

Sheet No.	Group	NBS sample No.	Hydrogen aim.	Permissible limits for hydrogen	Permissible limits for actual anal.
			ppm	*ppm*	%
1-8	III	352	30	25-45	±10
9-16	II	353	100	90-110	±5
17-24	I	354	200	190-210	±5

The sheet stock, as produced, contained 85 ppm of hydrogen; thus it was necessary to hydrogenate Groups I and II sheets to bring their hydrogen contents above the desired amounts. This operation consisted of submersion in a bath of sodium hydride, followed by a sulfuric acid wash to clean the sheets. Following the hydride treatment, the sheets were grit blasted in order to create a high surface-to-volume ratio which should enhance the out-gassing and equilibration treatments.

For the hydrogen equilibration treatment, the manufacturer has shown that at 1,300 ±5 °F (704 ±3 °C) the equilibration pressures were 1, 8, and 40μ for 30, 100, and 200 ppm hydrogen, respectively.

The procedure employed by the producer consisted of clamping each of four sheets at 2-in. intervals within a vertical retort annealing furnace; evacuating prior to heating to prove the furnace airtight and until a leak-rate of $<$ 60 μ/hr was achieved, then the heat was applied. As the load reached 750 °F (399 °C) the furnace was blanked off to insure against pumping off of any hydrogen. After stabilizing at the 1,300 °F (704 °C) level, oil-diffusion pumps were employed to attain the desired pressures. These conditions were maintained for 12 hr, following which the samples were cooled to room temperature over a period of 72 hr under conditions which maintained uniformity of temperature throughout the sheets to less than 10 °F (6 °C) in order to minimize nonuniform distribution of the hydrogen in the sheets.

The test results on Group III (30 ppm) sheets revealed a high degree of uniformity. These sheets were nibbled into ¼ in. squares, vapor degreased, dry-tumbled, and shipped to the National Bureau of Standards.

The preliminary test results on Group I and II indicated that a hydrogen content gradient was present in the sheets. In this instance it was decided, therefore, to cut the sheets into 12 to 14 pieces 12 in. × 15 in. and 18 in. × 15 in. Each of these sheets was then tested and only those which had hydrogen contents within the general limits set up for the two groups were processed into ¼ in. squares and forwarded to NBS. The identities of these sheets were maintained by packaging the squares from each 12 in. × 15 in. and 18 in. × 15 in. sheet separately. After each sheet had been tested at NBS it was then possible to narrow the limits of the hydrogen content even further for the final samples, which are the present published limits.

3. Test Method

There are four basic analytical procedures available for the determination of hydrogen content of titanium. These are the vacuum-fusion, hot-extraction, equilibrium-pressure measurement, and oxidation methods.

In order to compare these methods several "round robins" have been conducted by interested groups, among which are Materials Laboratory of Wright Air Development Center [2] an ad hoc group on chemical analysis of the Materials Advisory Board Titanium Alloy Sheet Rolling Panel, and an industrial group working with titanium. It was found that the hot extraction method at 1,400 °C appeared to be the most practical method in the case of hydrogen as a considerable number of specimens can be analyzed in one working day as against four or five for the vacuum-fusion method, and good reproducible results are obtainable.

It was decided, therefore, to use the hot-extraction method at 1,400 °C which is described in the following paragraphs. This method is now in the process of being recommended by the Metallurgical Advisory Committee on Titanium, Panel on Methods of Analysis to the American Society for Testing and Materials for certification as a standard method.

The specimens to be analyzed were selected at random from a particular group, cleaned of any oil, grease, and foreign matter by washing with ethyl ether, weighed, and inserted into the control arms of the vacuum fusion furnace. A quartz crucible was then packed with a new graphite crucible and graphite insulation inserted, and hung within the furnace assembly. The entire apparatus was then closed and vacuum slowly applied until a suitable vacuum (as observed with a McLeod gauge) was obtained with the mechanical pumps and the diffusion pumps. The furnace was slowly heated by induction to a temperature of 2,100 °C, which was maintained for approximately 1 to 1½ hr in order to outgas the graphite crucible and provide for a sufficiently low blank correction which was considered a constant. The temperature was then lowered to an operating temperature of 1,400 °C ±20 °C and the vacuum

[1] Figures in brackets indicate the literature references at the end of this paper.

checked to insure that an operating pressure of less than 1 x 10^{-3} mm Hg was maintained. The blank was then run, utilizing the method and collection times to be used with the specimens. If the blank was sufficiently low it was considered a constant and specimens run immediately. However, it was in the interest of accuracy and good practice that the blank correction be repeated every five or seven specimens in order to insure against any unusual or unexpected changes in values. If the blank correction was excessive, the furnace temperature was raised for another out-gassing until a suitably low blank correction was obtained.

When a suitable blank (approximately 2×10^{-7} g H_2) had been obtained, the specimen (being nonmagnetic) was moved along the control arm with a magnetic pusher and was introduced into the furnace at 1,400 °C. At this temperature, which was below the melting point of the specimen, only the hydrogen gas was liberated and collected as a total volume of gas in the Toeppler Pump for a period of 20 min. The gas was then transferred by the pump into a previously evacuated McLeod gage where it was measured as the total quantity of hydrogen liberated from the specimen. By using this figure and making suitable corrections for the blank and the calibration of the McLeod gauge, the percentage or parts per million of hydrogen gas in the specimen could be computed and reported.

4. Tests and Results

4.1. NBS Sample No. 352

The low hydrogen sample, designated Group III originally, now numbered NBS 352, was originally set up to have a hydrogen content in the range 25 to 45 ppm.

Because this material from the different sheets was mixed at the manufacturer's plant, it was not possible to segregate specific batches with respect to position in the original sheets. As a consequence, random samples were selected by a quartering process from the bulk after it had been subjected to through mixing. The test results from this material are given for the individual laboratories in tables 1 to 6, and the combined results by several cooperating laboratories are given in table 7.

4.2. NBS Sample No. 353

The intermediate hydrogen sample was prepared in the same manner as the low hydrogen material. However, the test samples were selected from the nibbled specimens from the 12 in. x 15 in. and 18 in. x 15 in. sections which were cut from the original sheets, as previously described.

The results for this selected material are given for the individual laboratories in tables 1 to 6, and the summary of results obtained from the combination of the test data from the various cooperating laboratories is given in table 8.

4.3. NBS Sample No. 354

The high hydrogen material was prepared in the same manner insofar as sampling is concerned as was sample No. 353. The results for the material selected for the standard are given for the individual laboratories in tables 1 to 6, and the results obtained by the combination of the results from the various laboratories is given in table 9.

5. Standard Samples

The availability of these three new standards for the hydrogen content of titanium has recently been announced by the National Bureau of Standards. A series of tests recently conducted by one of the leading producers of titanium, made on the material finally selected for the standards, gave excellent correlation with the test results shown in the following tables.

TABLE 1. *Battelle Memorial Institute*

	Observed values		
	Sample No. 352	Sample No. 353	Sample No. 354
	ppm	*ppm*	*ppm*
	30.8	99.5	204
	30.8	94.5	208
	31.8	96.5	211
	30.8	99.5	210
	30.0	92.7	213
	31.2	95.5	217
Total No. det.	6	6	6
Mean ppm	30.9	96.4	209.0
Standard dev. ppm	6	2.7	5.9
Coeff. of var. %	1.9	2.8	2.9
Range ppm	1.8	6.8	16
High value ppm	31.8	99.5	217
Low value ppm	30.0	92.7	201

NOTE: In tables 1 through 6 the standard deviation and coefficient of variation were computed as follows:

$$\text{Standard deviation} = s = \sqrt{\frac{\Sigma(X-\bar{X})^2}{n-1}}$$

where X = observed values,
$\bar{X}$ = average,
n = number of determinations

$$\text{Coefficient of variation} = \frac{s}{\bar{X}}$$

TABLE 2. *National Research Corporation*

	Observed values		
	Sample No. 352	Sample No. 353	Sample No. 354
	ppm	*ppm*	*ppm*
	35.9	106.4	218.6
	35.4	106.5	228.3
	34.4	94.2	219.8
	34.8	103.2	219.2
	35.3	97.2	217.3
	31.9	106.3	218.2
	33.6	83.1	221.9
	31.7	105.3	208.7
	33.4	93.9	224.1
	32.4	103.2	215.4
	34.6	104.0	214.9
	24.7	89.1	226.7
	29.0	98.4	213.5
		113.8	
Total No. det.	13	14	13
Mean ppm	32.9	100.3	219.0
Standard dev. ppm	3.1	8.1	5.4
Coeff. of var. %	9.4	8.1	2.5
Range ppm	11.2	30.7	19.6
High value ppm	35.9	113.8	228.3
Low value ppm	24.7	83.1	208.7

TABLE 3. *Dupont Company*

	Observed values		
	Sample No. 352	Sample No. 353	Sample No. 354
	ppm	*ppm*	*ppm*
	28	88	214
	34	92	207
	29	101	214
	30	97	210
	30	91	215
Total No. det	5	5	5
Mean ppm	30.2	93.8	212.0
Standard dev ppm	3.1	5.2	3.4
Coeff. of var %	7.7	5.5	1.6
Range ppm	6	13	8
High value ppm	34	101	215
Low value ppm	28	88	207

TABLE 4. *Allegheny Ludlum Corporation*

	Observed values		
	Sample No. 352	Sample No. 353	Sample No. 354
	ppm	*ppm*	*ppm*
	34.4	105	227
	34.2	104	226
	34.0	104	222
	33.7	103	220
	33.5	101	220
	32.7	101	219
Total No. det	6	6	6
Mean ppm	33.8	103.0	222.3
Standard dev ppm	0.6	1.7	3.3
Coeff. of var %	1.8	1.7	1.6
Range ppm	1.7	4	8
High value ppm	34.4	105	227
Low value ppm	32.7	101	219

TABLE 5. *Watertown Arsenal*

	Observed values		
	Sample No. 352	Sample No. 353	Sample No. 354
	ppm	*ppm*	*ppm*
	33.5	100.9	221.2
	33.4	98.3	216.7
	31.5	99.0	214.5
	29.7	101.1	213.0
	30.8	95.8	216.0
	31.8	102.2	214.7
	30.5	101.3	211.7
	29.8	95.4	221.2
	32.2	102.1	217.7
	32.1	99.8	212.0
	32.2	97.6	213.9
	30.4	106.2	214.0
	30.9	92.6	211.6
	35.0	101.3	215.6
		102.1	216.8
Total No. det	14	15	15
Mean ppm	31.7	99.7	215.3
Standard dev ppm	1.5	3.4	3.0
Coeff. of var %	4.7	3.4	1.4
Range ppm	5.3	13.6	9.6
High value ppm	35.0	106.2	221.2
Low value ppm	29.7	92.6	211.6

TABLE 6. *National Bureau of Standards*

	Sample No. 352		Sample No. 353		Sample No. 354	
	Observed values	Frequency	Observed values	Frequency	Observed values	Frequency
	ppm		*ppm*		*ppm*	
	27	3	88	1	190	1
	28	2	89	1	202	2
	29	7	90	3	205	4
	30	7	91	11	206	3
	31	6	92	11	207	1
	32	7	93	14	208	1
	33	6	94	9	209	10
	34	3	95	6	210	16
	35	3	96	10	211	11
			97	16	212	12
			98	12	213	8
			99	7	214	5
			100	3	215	10
			101	2	216	6
			102	1	217	6
					218	4
					219	1
					221	2
Total No. det	44		107		103	
Mean ppm	31.0		95.0		211.8	
Standard dev ppm	2.2		3.1		4.3	
Coeff. of var %	7.1		3.3		2.0	
Range ppm	8		14		31	
High value ppm	35		102		221	
Low value ppm	27		88		190	

TABLE 7. *Sample No. 352*

Group III

Laboratory	Mean	d	d^2
	ppm	*ppm*	
Nat'l Res. Corp	32.9	1.15	1.32
Watertown Arsenal	31.7	−0.05	------
Battelle Mem. Inst	30.9	−.85	0.72
Dupont Co	30.2	−1.55	2.40
Allegheny Ludlum Corp	33.8	2.05	4.20
Nat'l Bur. Standards	31.0	−0.75	0.56

$\Sigma = 190.5$ $\quad \Sigma d^2 = 9.20$

Average 31.75 $\quad$ Standard dev. = 1.356

Standard error = 0.554

95% confidence limits = 31.8±1.4 ppm.

Adopted value for Group III
32±2 ppm

NOTE: In tables 7 through 9 the 95 percent confidence limits were computed as follows:

$$95 \text{ percent Confidence limits} = \overline{X} \pm t\frac{s}{\sqrt{n}},$$

where $\overline{X}$ = average,
s = standard deviation,
n = number of laboratories,
t = 2.571 is the critical value of "t" as given, for example, by Youden [3].

TABLE 8. *Sample No. 353*

Group II

Laboratory	Mean	d	d^2
	ppm	*ppm*	
Nat'l Res. Corp	100.3	2.3	5.29
Watertown Arsenal	99.7	1.7	2.89
Battelle Mem. Inst	96.4	−1.6	2.56
Dupont Co	93.8	−4.2	17.64
Allegheny Ludlum Corp	103.0	5.0	25.00
Nat'l Bur. Standards	95.0	−3.0	9.00

$\Sigma = 588.2$ $\Sigma d^2 = 62.38$
Average 98.0
Standard dev. = 3.532
Standard error = 1.442
95% confidence limits = 98.0±3.7 ppm.

Adopted value for Group II 98±5 ppm

TABLE 9. *Sample No. 354*

Group I

Laboratory	Mean	d	d^2
	ppm	*ppm*	
Nat'l Res. Corp	219.0	4.1	16.81
Watertown Arsenal	215.4	0.5	0.25
Battelle Mem. Inst	209.0	−5.9	34.81
Dupont Co	212.0	−2.9	8.41
Allegheny Ludlum Corp	222.3	7.4	54.76
Nat'l Bur. Standards	211.8	−3.1	9.61

$\Sigma = 1289.5$ $\Sigma d^2 = 124.65$
Average 214.9
Standard dev. = 4.993
Standard error = 2.038
95% confidence limits = 214.9±5.2 ppm.

Adopted value for Group I 215±6 ppm

The authors are grateful to the Watertown Arsenal, Watertown 72, Mass., and S. W. Poole and R. S. Smith, Jr., of Republic Steel Corporation, South Division, Canton, Ohio, through whose cooperation the material for these samples was obtained. Also, we extend special thanks to Horace S. Harper of this laboratory, who performed many of the analyses, and also to the following laboratories which cooperated in the final analysis of the samples with great dispatch:

Allegheny Ludlum Steel Corporation, Research and Development Laboratories, Brackenridge, Pa.—W. A. Peifer; Battelle Memorial Institute, Columbus 1, Ohio—M. W. Mallett; E. I. du Pont de Nemours and Co., Pigments Department, Experimental Station, Wilmington 98, Delaware—T. D. McKinley; National Research Corporation, Cambridge 42, Massachusetts—J. P. Martin; Watertown Arsenal, Watertown 72, Massachusetts—S. Vigo.

6. References

[1] Final Technical Report, Republic Steel Corporation, South Division, Canton, Ohio, Watertown Arsenal Laboratories File No. 401/297.

[2] Titanium Metallurgical Laboratory Report No. 27 (Dec. 27, 1955) (PB–121607).

[3] Statistical Methods for Chemists, William J. Youden (John Wiley & Sons, Inc., New York, 1951).

(Paper 66A6–183)

JOURNAL OF RESEARCH of the National Bureau of Standards—A. Physics and Chemistry
Vol. 66A, No. 6, November–December 1962

Ultraviolet Stability of Crosslinked Polycaprolactam Systems

Stephen D. Bruck*

(August 2, 1962)

The relative ultraviolet stability of four chemically modified polycaprolactam (Nylon-6) systems is discussed: methylmethoxylated fibers and three other fibers having methylene, disulfide, and alkylene sulfide crosslinks, respectively. The ultraviolet degradation of these systems is studied by means of a sensitive analytical technique in which the methylene (—CH_2—) groups remaining in the chemically modified fibers after irradiation are converted to formaldehyde; the liberated formaldehyde is then reacted with chromotropic acid to give a colored product, the absorbancy of which can be determined spectrophotometrically. The results indicate that the data can be expressed by first order rate equations from which the rate constants may be calculated. The scission of the crosslinks is accompanied by a decrease in the internal orientation of the networks as shown by X-ray diffraction photographs.

1. Introduction

Previous communications from this laboratory [1 to 4] [1] described macroscopic deformations such as helical coiling and self-crimping of polycaprolactam (Nylon-6) fibers as a result of heterogeneous crosslinking in the swollen state. Among other fundamental properties of these crosslinked systems, their stability under ultraviolet radiation is of considerable interest. By studying such selected model systems, it might be possible to predict the behavior of others. It is the object of this paper to evaluate the relative ultraviolet stability of fibers having methylene, disulfide, and alkylene sulfide crosslinks, respectively, and also fibers with methylmethoxyl groups on the amide nitrogen atoms.

2. Discussion

The following structures are involved in this study:

I.

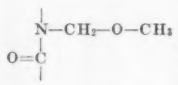

II.

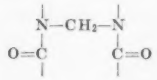

III.

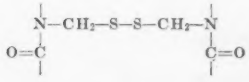

IV.

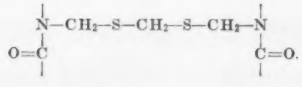

Structure (I) is a precursor in the preparation of the sulfur containing crosslinked structures (III, IV). The crosslinked unit (II) incorporates only one methylene group between the adjacent amide nitrogen atoms of two polymer chains; system (III) has a disulfide type crosslink and includes two methylene groups; finally structure (IV) has three methylene groups, one of which is interposed between two sulfur atoms. By such systematic variation of the type and length of crosslinks, it should be possible to evaluate their comparative ultraviolet stability and arrive at knetic deductions.

In order to study the ultraviolet degradation of these systems, use was made of a sensitive analytical technique described in detail elsewhere [5, 6]. In this method, the methylene (—CH_2—) groups in structures (I to IV) are hydrolyzed with sulfuric acid to yield one equivalent of formaldehyde per equivalent of methylene group. The formaldehyde so formed is then reacted with chromotropic acid (1,8,-dihydroxynaphthalene-3,6,disulfonic acid), and the absorbancy (log I_0/I.) of the resulting reaction product is subsequently determined at 570 mμ with a spectrophotometer. From the formaldehyde anaylsis it is possible to estimate the number of equivalents of crosslinks per 10^6 g of polymer. Although it was shown previously [7, 8] that in the case of a well-defined, fairly uniform crosslinked fiber the number of equivalents of crosslinks may be calculated from equilibrium swelling measurements, such an approach cannot be entirely relied upon when the crosslinking density across the fiber's cross section is nonuniform, as is the case with the systems having disulfide and alkylene sulfide type crosslinks [1, 2]. Futhermore, the ultraviolet irradiation may cause additional crosslinking not originally present in the system which, by participation in the swelling process, would obscure the calculations.

In the present work, two General Electric G25T8 germicidal, low-pressure mercury lamps were used. According to G.E. data, about 60 percent of the

*Present address: Applied Physics Laboratory, The Johns Hopkins University, 8621 Georgia Avenue, Silver Spring, Md.

[1] Figures in brackets indicate the literature references at the end of this paper.

input energy is transformed into a predominant wavelength of 2537 A, of which the special glass envelope transmits about 74 percent, or close to half of the total energy input. Thus, this type of lamp is a convenient source for nearly monochromatic ultraviolet radiation. Of the remainder of the energy, 2 percent is transmitted into visible light, and 48 percent is transformed into heat. Due to the special glass envelope, no energy was transmitted below 2000 A. The fibers were mounted on a specially designed stainless-steel holder in the manner illustrated by figure 1. The assembly was

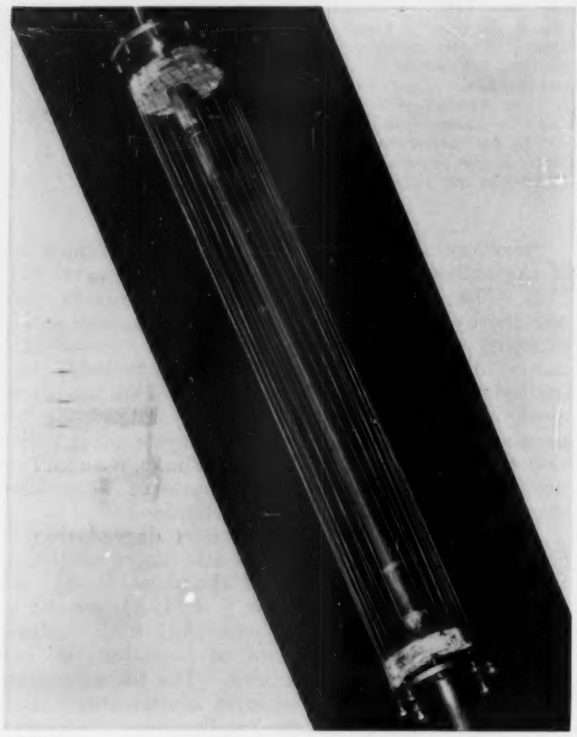

FIGURE 1. *Sample holder.*

then placed inside a quartz tube and slowly rotated in front of the mercury lamps by means of an electrically operated magnetic coupling. The lamps were placed approximately 2 in. away from the quartz tube and opposite each other.

During the irradiation, the pressure inside the apparatus was kept at 10^{-4} to 10^{-5} mm of Hg by means of an oil-diffusion and mechanical pumping system. The G25T8 mercury lamps permitted the use of samples large enough for subsequent analytical work. The average intensity of the illumination at the detector was measured by suspending a vacuum thermopile inside the quartz sample holder tube, and was found to be 6,800 $\mu w/cm^2$ or 6.80×10^4 ergs/cm^2-sec. It was also established that the intensity of the radiation along the axis of the lamp was uniform within 10 percent. Furthermore, the decrease in intensity of the lamps during the irradiation process was negligible and the temperature within the sample tube did not rise above 40 °C.

No attempt was made to determine quantum yields in the present work due to the fibrous nature of the samples which gives rise to considerable scattering of radiation that is difficult to measure. The fiber samples were irradiated in vacuum for up to 50 hr, treated for 0.5 hr in distilled water at 90 °C to remove the degradation products, dried, and then subjected to formaldehyde [5, 6] and methoxyl analyses [9]. Thus, the evolved quantities of formaldehyde represent the remaining (nonphotolysed) groups in structures I to IV. The results are summarized in table 1. In all cases there is a decrease in the methylene groups that are part of the crosslinks and also in the methylene groups that are part of the methylmethoxylated fiber, as indicated by the drop in formaldehyde concentration.

TABLE 1. *Kinetic data for ultraviolet degradation of chemically modified polycaprolactam fibers*

Sample No.	Type of modification [a]	Irradiation time	Sample weight	log I_0/I	% CH_2O	%—OCH_3 [b]
		hr	*mg*			
1	A	0	24.40	0.262	4.0±0.1	3.0±0.1
2	A	2	25.45	.236	2.5	2.4
3	A	4	22.82	.182	3.0	2.6
4	A	6	20.90	.146	2.6	2.3
5	A	8	22.90	.148	2.4	2.5
6	A	12	20.45	.125	2.3	2.1
7	A	16.3	25.95	.118	1.6	2.0
8	A	20	19.87	.098	1.8	1.9
9	A	30	25.10	.105	1.5	1.7
1	B	0	16.60	.251	5.6±0.1	
2	B	2	16.92	.210	4.6	
3	B	4	17.29	.179	3.8	
4	B	6	16.06	.143	3.3	
5	B	8.5	16.85	.160	3.5	
6	B	15	16.23	.113	2.5	
7	B	20	15.85	.103	2.3	
8	B	30	16.59	.089	2.0	
9	B	40	15.53	.082	1.9	
1	C	0	24.25	.161	2.4±0.1	
2	C	2.5	17.24	.097	2.0	
3	C	4	16.83	.092	2.0	
4	C	6.1	23.73	.132	2.0	
5	C	8	23.32	.109	1.7	
6	C	12	22.06	.091	1.5	
7	C	16	17.44	.069	1.4	
8	C	20	19.03	.068	1.3	
9	C	30	16.72	.051	1.0	
1	D	0	20.94	.150	2.6±0.1	
2	D	2	18.52	.114	2.3	
3	D	4	23.39	.130	2.0	
4	D	6	31.14	.148	1.8	
5	D	8	20.64	.106	1.9	
6	D	12	20.76	.097	1.7	
7	D	16	30.03	.101	1.2	
8	D	20	23.34	.078	1.2	
9	D	30	22.95	.088	1.3	

[a] A.

B.

C. 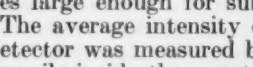

D. 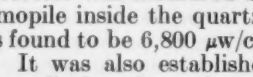

[b] Modified Clark apparatus used. Procedure: A. Steyermark, Quantitative Organic Microanalysis, p. 431 (Academic Press Inc., New York, 1961).

An uncrosslinked but irradiated control sample of polycaprolactam gave no positive test for formaldehyde but showed an increase in inherent viscosity, as seen in table 2. Small gel particles were observed in

TABLE 2. *Inherent viscosity of uncrosslinked (control) samples of polycaprolactam fibers*

Time of irradiation	Inherent viscosity (25 °C±0.1) 90% formic acid
hr	
0	1.005
2	1.145
12	1.230
20 [a]	1.400

[a] Filtered to remove gel particles.

the uncrosslinked control samples that had been irradiated for 20 hr, indicating the presence of radiation-induced crosslinks. This type of crosslinks differs from the chemically implanted ones as the former type represents actual "point-contacts" between two polymer chains as the result of recombination of free radicals, whereas the chemically implanted crosslinks have predetermined chemical composition and length.

The fact that chemically implanted crosslinks are broken by ultraviolet irradiation is also seen from equilibrium swelling measurements that were carried out by a photomicrographic technique described elsewhere [7, 8].

Figure 2 is a plot of the equilibrium volume swelling ratio, q_m (swelling agent: *m*-cresol) versus irradiation time for caprolactam fibers having methylene (—CH_2—) crosslinks. The symbol $q_m = V/Vo$, where V = the volume of the crosslinked network at equilibrium swelling, and Vo = the volume of the network before swelling. As figure 2 shows, the

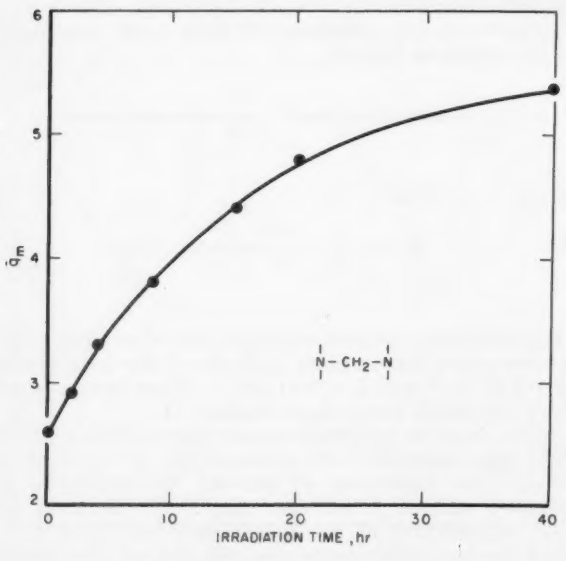

FIGURE 2. *Variation of equilibrium volume swelling ratio (q_m) with irradiation time for methylene-crosslinked polycaprolactam fibers.*

ultraviolet irradiation results in an increase in the q_m values, indicating a decrease in the crosslinking density. The sharp leveling off at approximately 20 hr of irradiation is most likely due to the appearance of radiation-induced crosslinking, the existence of which has already been shown by intrinsic viscosity measurements. In view of the fact that both the radiation-induced crosslinks and the chemically introduced crosslinks contribute to the swelling process, and because it is not possible to separate each of these variables, the equilibrium swelling measurements were not used in the calculation of the crosslinking density. Instead, the number of equivalents of chemically introduced crosslinks broken during the irradiation process was obtained from chemical analyses, as will be discussed below.

3. Kinetic Analysis of the Data

For the kinetic analysis of the data the logarithm of the percent formaldehyde was plotted against irradiation time. Figure 3 illustrates the data for the degradation of the methylmethoxyl groups in chemically modified polycaprolactam fibers when subjected to ultraviolet irradiation at 2537 A. If the methylmethoxylation process were free of side reactions, only one methylmethoxyl group would be attached to the amide nitrogen atom, which should yield one mole of formaldehyde (from the —CH_2— group) and one mole of methoxyl (—O—CH_3 group). However, the reaction conditions for the methylmethoxylation process [2, 10] do not entirely eliminate the formation of small amounts of polymethylol groups. The degradation of such groups will result in the evolution of formaldehyde but no methoxyl groups. Thus, the photolysis of the polymethylol and methylmethoxyl groups could be assumed to proceed according to two independent reactions as follows:

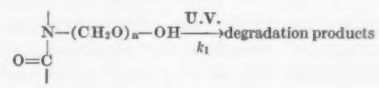

where $n = 1$ to 25

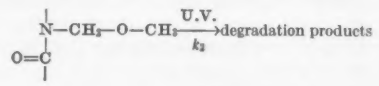

From Figure 3 it is noted that the unirradiated samples yielded approximately 4 percent (by weight) formaldehyde and 3 percent (by weight) methoxyl groups. However, after an irradiation period of approximately 5 hr, the samples continued to yield practically identical quantities of formaldehyde and methoxyl groups by weight. (It should be noted that the weight percent of both formaldehyde (M.W.=30) and methoxyl groups (M.W.=31) have very nearly the same relation to the mole percent of these materials.) An analysis of the data indicates the existence of two, simultaneous, but independent first order reactions (I and II, above), the effect of which may be mathematically expressed as follows

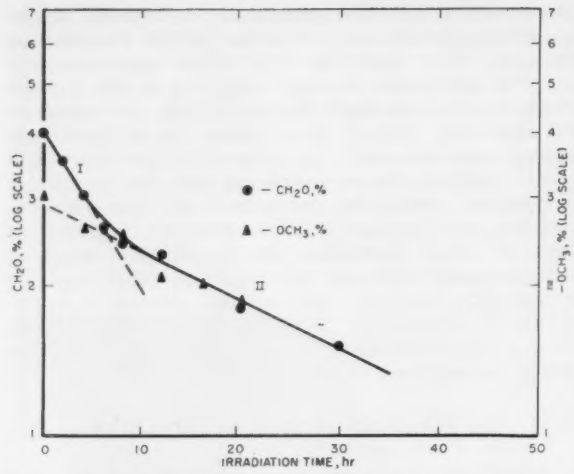

FIGURE 3. *Logarithmic plot of the ultraviolet degradation of methoxymethylated polycaprolactam fibers.*

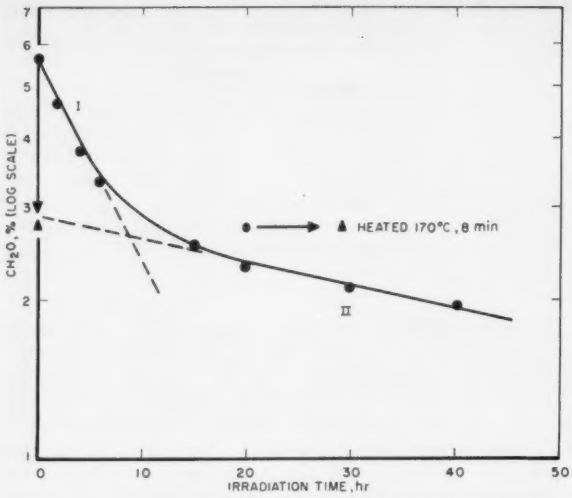

FIGURE 4. *Logarithmic plot of the ultraviolet degradation of methylene-crosslinked polycaprolactam fibers.*

provided the absorption is a small fraction of the incident light:

$$\text{I.} \qquad \frac{-dC_I}{dt}=k_1C_I$$

$$\text{II.} \qquad \frac{-dC_{II}}{dt}=k_2C_{II}$$

and,

$$\text{I.} \qquad C_I=A\exp(-k_1t)$$

$$\text{II.} \qquad C_{II}=B\exp(-k_2t)$$

where,

C_I=concentration of formaldehyde evolved by acid hydrolysis of the nonphotolysed polymethylol groups remaining in the fiber after irradiation.
C_{II}=concentration of formaldehyde evolved by acid hydrolysis of the nonphotolysed methylmethoxyl groups remaining in the fiber after irradiation.
k_1 and k_2=respective rate constants (hr^{-1})
A and B=constants
t=time of irradiation (hr).

Thus:

$$C=C_I+C_{II}=Ae^{-k_1t}+Be^{-k_2t}$$

where

C=total concentration of evolved formaldehyde.

From the above expression, k_1=0.18 hr^{-1}, and k_2=0.01 hr^{-1}, indicating that reaction I is much faster than reaction II.

A similar approach can be extended to the polycaprolactam system having methylene (—CH_2—) crosslinks. Although this type of crosslink is predominant in the fiber, the nature of the chemical reaction process [11] also gives rise to long polyformaldehyde crosslinks. Even relatively few of these crosslinks will result in the liberation of large quantities of formaldehyde upon irradiation. Furthermore, the polyformaldehyde type crosslinks are known to be heat-sensitive and can be converted to short methylene crosslinks upon heating. Advantage was taken of this property by heating the original, unirradiated, crosslinked sample at 170 °C for 8 min. in a vapor bath, whereupon its original formaldehyde content of 5.6 percent dropped to 2.8 percent. From figure 4 it is seen that this latter value forms a straight line with the rest of the points. Thus the existence of two independent first order reactions is indicated, as follows:

I. 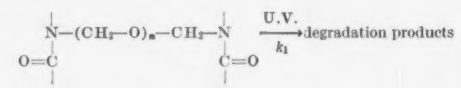

where n=1 to 25

II. 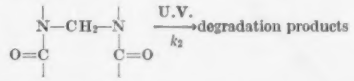

Application of the mathematical expression described above and a least square analysis of the data yields k_1=0.22 hr^{-1} and k_2=0.01 hr^{-1}. Here again, reaction I is much faster than reaction II.

The data on polycaprolactam fibers having disulfide type crosslinks are summarized by figure 5 in which the logarithm of percent formaldehyde is plotted against irradiation time. In contrast to the degradation of the methylene-crosslinked fiber and the methylmethoxylated sample, all the points fall on a straight line, indicating only one first order reaction without any apparent other reactions. The rate constant for this reaction is k=0.025 hr^{-1}.

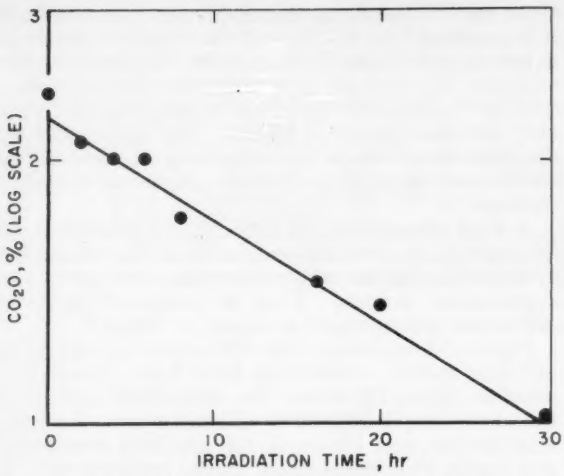

FIGURE 5. *Logarithmic plot of the ultraviolet degradation of disulfide-crosslinked polycaprolactam fibers.*

Additional evidence for the absence of other independent reactions was obtained from chemical analyses of residual sulfhydryl [12] and methoxyl groups remaining in the sample before and after irradiation. These groups are precursors in the formation of the disulfide crosslinks and could conceivably be present after the formation of these crosslinks. Appreciable amounts of such groups would be expected to follow a degradation pattern distinct from the crosslinks but similar to the degradation of the methylmethoxylated polycaprolactam samples shown earlier. Chemical analysis of the disulfide crosslinked samples (before and after irradiation) however, showed less than 0.3 weight percent methoxyl groups and less than 35 equivalents of free sulfhydryl groups per 10^6 g of polymer. These quantities are negligible and are expected to contribute little to the overall degradation of the disulfide crosslinks.

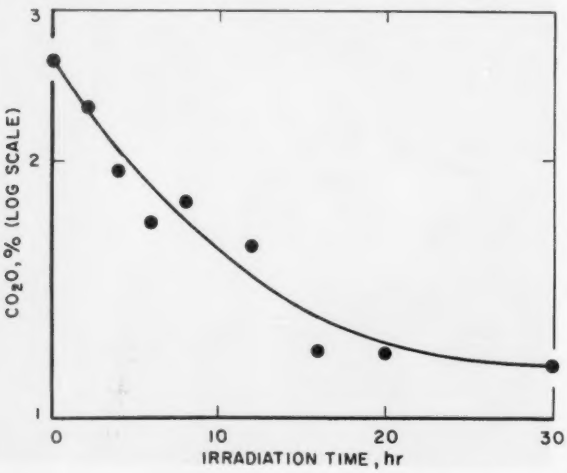

FIGURE 6. *Logarithmic plot of the ultraviolet degradation of alkylene sulfide-crosslinked polycaprolactam fibers.*

The ultraviolet degradation of polycaprolactam fibers having alkylene sulfide type crosslinks is illustrated by figure 6. The data are somewhat scattered and could not be analyzed on the basis of two independent first order reactions. Thus the ultraviolet degradation of this sample either does not follow first order kinetics or there are many other independent reactions that obscure interpretation. This latter possibility might indeed be operative inasmuch as the particular chemical reaction series leading to the introduction of the alkylene sulfide crosslinks also forms appreciable amounts of disulfide crosslinks and stabilized sulfhydryl groups [1]. The alkylene sulfide crosslinked fiber thus is expected to contain at least the following groups, all of which will yield various quantities of formaldehyde upon irradiation and subsequent hydrolysis:

I. 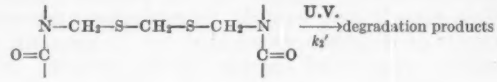

II. 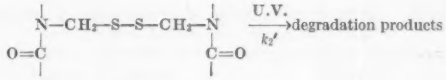

III. 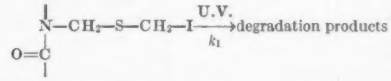

Considering the above factors, other techniques, for example radioactive tracer methods, would have to be applied in an attempt to separate the contributions of the above structures to the overall ultraviolet degradation process. However, it is interesting that, assuming the applicability of two first order reactions as in the other cases, a least square analysis of the data yields a rate constant of k_1=0.18–0.21 hr^{-1} that could probably represent the degradation of the stabilized sulfhydryl groups (reaction III).

The overall kinetic results are summarized in table 3. The data indicate that the values for k_1 (indicative of the degradation of secondary products) are between 0.18 and 0.22 hr^{-1} in all cases. The value for k_2 is 0.01 hr^{-1} for the degradation of both the methylmethoxylated and the methylene-crosslinked samples, indicating that in both cases the rate determining step is the scission of the N—C bond in the crosslinked part of the network.

TABLE 3. *Rate constants for the ultraviolet degradation of chemically modified polycaprolactam fibers*

Sample	k_1(hr^{-1})	k_2(hr^{-1})	k'_2(hr^{-1})
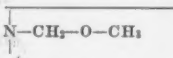	0.18	0.01	----------
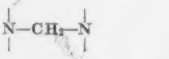	.22	.01	----------
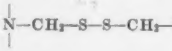	----------	.025	----------
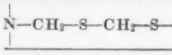	.18-0.21	----------	0-0.005

In the case of the disulfide crosslinked fibers, there is only one rate constant, with a value of 0.025 hr^{-1}, and there are no apparent side reactions.

Finally, in the case of the alkylene sulfide samples, the k_2' value (indicating the combined degradation of the alkylene sulfide and disulfide crosslinks) could not reliably be determined due to the heterogeneous nature of the fiber. However, assuming the existence of first order reactions, the k_2' value would be 0–0.005 hr^{-1}.

From chemical analysis of formaldehyde the number of equivalents of crosslinks present before and after irradiation can also be estimated by converting the crosslinks remaining after irradiation to formaldehyde. The results are summarized in table 4. The data indicate that after 30 hr of irradiation the crosslinking density in the fibers decreased for the methylene-crosslinked sample by 32 percent; alkylene sulfide crosslinked sample (containing appreciable amounts of disulfide crosslinks) by 55 percent; and disulfide crosslinked sample by 58 percent. From these results and from the calculated rate constants it is apparent that stability of the disulfide crosslinks is less (k_2=0.025 hr^{-1}) than either the methylmethoxylated (k_2=0.01 hr^{-1}), methylene crosslinked (k_2=0.01 hr^{-1}), or alkylene sulfide crosslinked (k_2' probably less than 0.01 hr^{-1}) fibers. This behavior of the disulfide crosslinks is not surprising in view of the well-known sensitivity of these groups to radiation damage.

TABLE 4. *Relative sensitivity of crosslinked polycaprolactam fibers towards ultraviolet irradiation*

Sample	Irradiation	Formaldehyde	Crosslinks
	hr	%	*equiv./10⁶g*
N–CH_2–N	[a] 0	3.0	1,000
"	30	2.1	682
N–CH_2–S–S–CH_2–N	0	2.4	392
"	30	1.0	167
N–CH_2–S–CH_2–S–CH_2–N	0	2.6	288
"	30	1.2	128

[a] Heated at 170 °C for 8 min.

A final observation of considerable interest is the decrease in the internal orientation of the crosslinked systems that apparently accompanies the ultraviolet degradation process. This is indicated by X-ray diffraction photographs as shown in figure 7.

Figure 7A represents the diffraction pattern of an alkylene sulfide crosslinked fiber *before* irradiation, whereas figure 7B shows the diffraction pattern of the same sample *after* 30 hr of irradiation. A similar relationship was observed for disulfide crosslinked and methylene crosslinked fibers, respectively. In all cases the broadening of the diffraction arcs after irradiation indicates a decrease in orientation. This phenomenon is attributed to a decrease in the internal stress in the network as a result of the scission of the crosslinks upon irradiation. Further work will have to be carried out to quantitatively measure this phenomenon.

The author thanks Mrs. Sally S. Flores, Donald A. Becker, and Sylvia M. Bailey for technical assistance in various phases of this work. Thanks are also due to H. Steffen Peiser for discussions on the X-ray diffraction patterns, Boris Paretzkin for the X-ray exposures, and to Frank L. McCrackin for the computer programing of the kinetic data.

A B

FIGURE 7. *X-ray diffraction photographs of alkylene sulfide-crosslinked polycaprolactam fibers before (A) and after (B) irradiation.*

3. References

[1] S. D. Bruck, J. Research NBS **66A** (Phys. and Chem.), No. 1, 77 (Jan.–Feb. 1962).
[2] S. D. Bruck, J. Research NBS **65A** (Phys. and Chem.), No. 6, 489 (Nov.–Dec. 1961).
[3] NBS Tech. News Bul. **45,** 152 (1961).
[4] Chemical and Engineering News, "Cross-links crimp and coil Nylon-6 Fiber," pp. 50–51, October 23, 1961.
[5] S. D. Bruck, J. Research NBS **66A** (Phys. and Chem.), No. 3, 251 (May–June 1962).
[6] S. D. Bruck, Paper No. 38, Abstract of Papers, Division of Analytical Chemistry, 141st Meeting, American Chemical Society, Washington, D.C., March 21–29, 1962.
[7] S. D. Bruck, J. Polymer Sci. **55,** S29 (1961).
[8] S. D. Bruck, J. Research NBS **65A** (Phys. and Chem.), No. 6, 485 (Nov.–Dec. 1961).
[9] A. Steyermark, Quantitative Organic Microanalysis, p. 431 (Academic Press Inc., New York, 1961).
[10] W. R. Sorenson and T. W. Campbell, Preparative Methods of Polymer Chemistry, p. 64 (Interscience Publ., Inc., New York, 1961).
[11] B. Graham and O. E. Schupp, Jr., U.S. Patent 2,540,726 Example 1.
[12] S. D. Bruck and S. M. Bailey, J. Research NBS **66A** (Phys. and Chem.), No. 2, 185 (March–April 1962).

(Paper 66A6–184)

JOURNAL OF RESEARCH of the National Bureau of Standards—A. Physics and Chemistry
Vol. 66A, No. 6, November–December 1962

Spectral-Line Intensities and gf-Values in the First Spectrum of Copper

Charles H. Corliss

(July 23, 1962)

Relative intensities are reported for 180 lines of Cu I between 2600 A and 7200 A, observed in a 10-ampere copper arc. Oscillator strengths, normalized as closely as possible to the absolute scale, are derived from the observations.

1. Introduction

The line intensities reported in the NBS Tables of Spectral-Line Intensities [1] [1] were observed in a 10-amp arc in air between copper electrodes containing one atom of an added element for every 1,000 atoms of copper. In order to reduce the original observations to a true scale of relative intensities, numerous lines in the first spectrum of copper were selected to serve as reference standards of intensity. The relative power radiated by these lines was measured by comparing the copper spectrum with the spectra from an incandescent ribbon-filament lamp operated at a known temperature and from a calibrated hydrogen-lamp continuum. The measurements were made by the standard methods of heterochromatic photographic photometry and are described in detail in the NBS Tables [1] and elsewhere by Meggers, Corliss, and Scribner [2].

From 2 to 24 determinations were made on each of 207 lines of Cu I between 2600 and 8100 A, with an average of about 9 determinations per line. A section of a typical plate is shown in figure 1.

The spectrum of copper consists of sharp lines and diffuse lines. In this investigation the spectrograph slit was adjusted to a sufficient width to form flat-topped images of the sharp lines. Intensities measured in the plateau of these images are proportional to the total intensities integrated over the widths of the lines. Measurements were not made on the diffuse lines.

[1] Figures in brackets indicate the literature references at the end of this paper

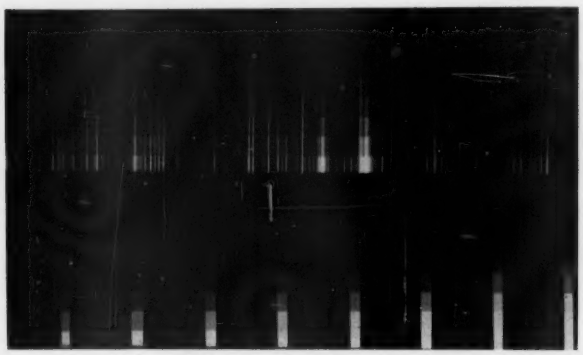

FIGURE 1. *Typical plate for the measurement of spectral-line intensities in copper.*

Spectral range 3400 to 3850 A. Above, arc spectrum of copper through rotating stepped sector. Below, spectrum of standard ribbon-filament lamp through a mask at intervals of 50 A and with the same sector.

2. Self-absorption in Strong Lines

The particle density of neutral copper atoms in the positive column of our 10-amp copper arc is about 10^{15} cm^{-3} [3]. At this density the gas is optically thick at the wavelengths of the strong lines and they are affected by self-absorption, as shown in figure 2. In this figure, I is the intensity of a strong copper line measured in the copper arc and I_0 is the intensity of the same line measured on the same intensity scale in a similar arc between silver electrodes to which one atom of copper was added for every 1000 atoms of silver. The copper lines in silver were measured relative to the intensities of lines of other elements also added to the silver and previously measured relative to copper lines in a copper arc. By this procedure we would expect copper lines that are free of absorption in the copper arc to be 1,000 times as strong in the copper arc as in the silver arc.

Inspection of figure 2 discloses that the ratio I/I_0 approaches 1,000 as I_0 diminishes. I_0 is actually the

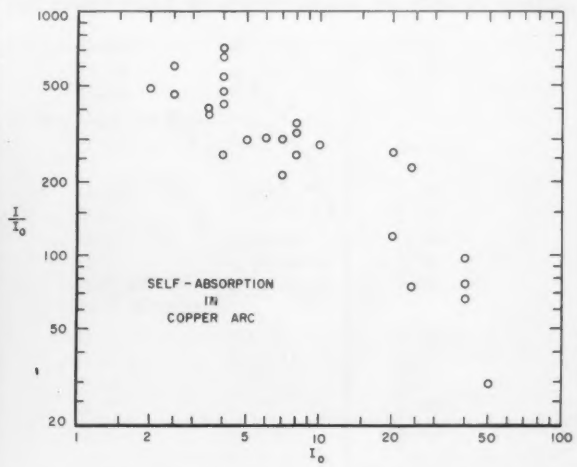

FIGURE 2. *Self-absorption in a 10-amp copper arc, showing how the amount of self-absorption diminishes for fainter lines.*

The points represent 27 lines over the wavelength range from 2824 to 8092 A, and having upper energy levels between 30 and 72 kK.

scale of intensity of the NBS Tables. This scale has a lower limit of the order of one. We may say then that copper lines too faint to appear in the NBS Tables will not be perceptibly affected by self-absorption in the 10-amp copper arc in air. Of the 207 lines measured in the copper arc, 27 appear in the NBS Tables. The remaining 180 lines will be unaffected by self-absorption and it is for these lines only that we will derive oscillator strengths. Figure 2 is plotted for the 27 strong reference standard lines without regard to wavelength or excitation potential.

3. Derivation of Oscillator Strengths From Intensities

The following formula has been developed [4, 5] for deriving absolute gf-values from the intensities in the NBS Tables of Spectral-Line Intensities:

$$gf = C(u/Np) I\lambda^3 e^{E/kT}$$

where u is the partition function at 5100 °K for the atom or ion under consideration, N is the percent of the element in the neutral or ionized state, p is the persistence of the atom in the arc relative to copper, I is the intensity of the line on the scale used in the NBS Tables, E is the value of the upper energy level, k is Boltzmann's constant, and T is the effective temperature of the arc. The effective temperature of our copper arc has been determined to be 5100 °K [6]. For Cu I, u is 2.4, N is 93 percent, and p is of course unity. N is calculated from Saha's ionization equation in which the electron density is taken to be 2.4×10^{14} cm^{-3} [3].

C is a normalization function, determined from absolute gf-values for 21 different elements in the NBS Tables, that adjusts the scale to an absolute basis. In the case of our copper lines, we must divide this C (shown in figure 3) by 1,000 since the particle density of copper atoms is 1,000 times the density of the atoms for which the formula was developed, and the intensity scale is increased correspondingly. The drooping characteristic of this function at large values of E is caused by preferential excitation of lines from high levels close to the electrodes of the arc. Over 90 percent of our copper lines fall on this nonconstant portion of the function.

The results are given in table 1. In the columns are listed in the following order the intensity on the scale of the NBS Intensity Tables, the wavelength to two decimal places and the two energy levels to the nearest kayser taken from Shenstone [7], $gA\times10^{-8}$ sec^{-1}, gf, and log gf. The transition probability, g_nA, is related to g_mf by Ladenburg's equation

$$g_nA = 0.667\times10^{16}\, g_mf/\lambda^2 \text{ sec}^{-1},$$

where g_n is $(2J+1)$ for the upper level, A is Einstein's transition probability of spontaneous emission, g_m is $(2J+1)$ for the lower level, and f is the absorption oscillator strength.

4. Accuracy of Results

No extensive intensity measurements have been reported heretofore for these lines. Allen and Asaad [8] have reported gf-values measured in a 3-amp copper arc and adjusted to an absolute scale, for 135 lines, of which about 80 are found in our list. A comparison of the two sets of values shows a systematic difference which is a function of E and reproduces our normalization function C. This discrepancy arises from the fact that Allen and Asaad used a constant normalization factor. The discrepancy is particularly severe because most of the lines originate above 50 kK, where the value of C is changing rapidly. If this discrepant factor is removed, there is a remaining constant difference; the Allen and Asaad log gf is 0.5 less than ours.

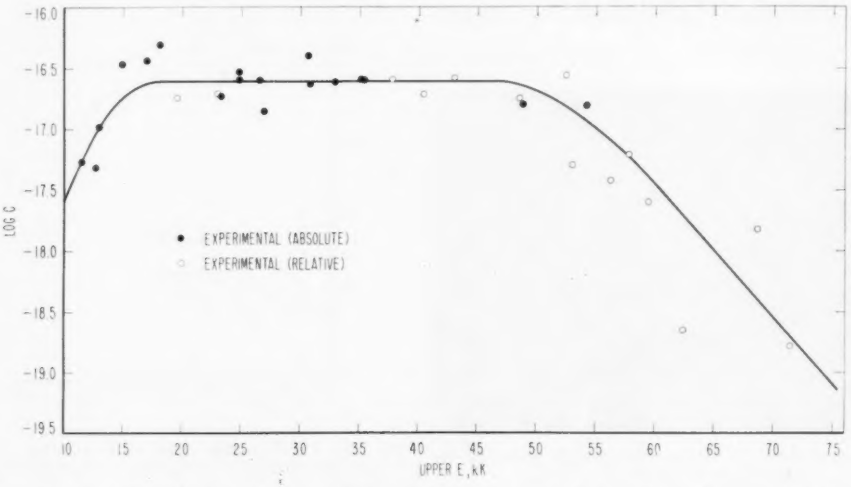

FIGURE 3. *Normalization function for establishing an absolute scale and correcting for departure from thermodynamical equilibrium at high energy levels.*

TABLE 1. *Transition probabilities of copper*

Intensity	Wavelength A	Energy Levels K	gA 10^8/sec	gf	Log gf
78	2626.68	40944 – 79003	0.042	0.0043	−2.36
131	2630.00	39019 – 77031	0.070	0.0073	−2.14
145	2634.93	39019 – 76959	0.078	0.0081	−2.09
41	2645.30	40114 – 77905	0.022	0.0023	−2.63
60	2649.84	40114 – 77841	0.033	0.0034	−2.47
15	2846.48	40944 – 76064	0.0087	0.0011	−2.98
139	2858.22	39019 – 73995	0.080	0.0097	−2.01
185	2858.73	11203 – 46173	0.010	0.0013	−2.89
65	2890.84	44406 – 78988	0.038	0.0048	−2.32
56	2891.64	44544 – 79116	0.033	0.0042	−2.38
11	2931.70	40944 – 75044	0.0065	0.00084	−3.08
29	2933.06	39019 – 73103	0.017	0.0022	−2.66
119	2978.30	43514 – 77080	0.072	0.0096	−2.02
103	2979.38	43514 – 77068	0.063	0.0083	−2.08
98	2998.38	11203 – 44544	0.0036	0.00048	−3.32
161	3012.00	40114 – 73305	0.096	0.013	−1.88
54	3014.85	41153 – 74313	0.033	0.0045	−2.35
191	3021.54	40909 – 73995	0.12	0.016	−1.80
179	3022.61	39019 – 72093	0.11	0.015	−1.84
90	3024.99	30535 – 63585	0.044	0.0060	−2.22
43	3030.26	40114 – 73105	0.026	0.0036	−2.45
37	3044.03	41153 – 73995	0.023	0.0031	−2.50
33	3047.80	30784 – 63585	0.016	0.0022	−2.65
17	3052.55	41563 – 74313	0.010	0.0015	−2.84
13	3053.38	42302 – 75044	0.0080	0.0011	−2.95
27	3068.91	13245 – 45821	0.0014	0.00020	−3.69
980	3073.80	11203 – 43726	0.029	0.0041	−2.39
141	3088.13	40944 – 73316	0.087	0.012	−1.91
838	3099.93	39019 – 71268	0.50	0.073	−1.14
78	3113.48	39019 – 71128	0.047	0.0068	−2.17
78	3120.44	40114 – 72151	0.048	0.0070	−2.16
1294	3126.11	39019 – 70998	0.78	0.11	−0.94
461	3128.70	40114 – 72067	0.28	0.041	−1.38
302	3140.31	39019 – 70853	0.18	0.027	−1.57
638	3142.44	40114 – 71927	0.39	0.058	−1.24
358	3146.82	40114 – 71883	0.22	0.033	−1.49
19	3148.33	41563 – 73316	0.012	0.0018	−2.75
44	3149.51	41563 – 73305	0.028	0.0041	−2.39
286	3156.63	13245 – 44916	0.012	0.0018	−2.74
47	3160.05	41563 – 73199	0.029	0.0044	−2.35
378	3169.68	41563 – 73103	0.24	0.036	−1.45
22	3171.66	44544 – 76064	0.014	0.0021	−2.67
214	3223.44	42302 – 73316	0.14	0.021	−1.67
266	3224.66	42302 – 73305	0.17	0.027	−1.58
501	3231.18	41153 – 72093	0.32	0.050	−1.30
164	3233.90	41153 – 72067	0.10	0.016	−1.79
700	3235.71	42302 – 73199	0.45	0.071	−1.15
1538	3243.16	41153 – 71979	0.98	0.15	−0.81
434	3268.28	41563 – 72151	0.28	0.045	−1.35
1114	3282.72	41563 – 72017	0.72	0.12	−0.94

TABLE 1. *Transition probabilities of copper*—Continued

Intensity	Wavelength A	Energy Levels K	gA 10^8/sec	gf	Log gf
1514	3290.54	40909 – 71291	0.97	0.16	−0.80
116	3292.39	41563 – 71927	0.075	0.012	−1.92
557	3292.83	11203 – 41563	0.0096	0.0016	−2.81
746	3317.22	41153 – 71291	0.48	0.079	−1.10
483	3319.68	41153 – 71268	0.31	0.051	−1.29
206	3329.64	41153 – 71178	0.13	0.022	−1.66
213	3335.22	41153 – 71128	0.14	0.023	−1.64
348	3349.28	42302 – 72151	0.23	0.038	−1.41
703	3365.34	41153 – 70860	0.46	0.077	−1.11
68	3375.67	41563 – 71178	0.044	0.0076	−2.12
308	3381.42	41563 – 71128	0.20	0.035	−1.46
20	3392.02	43726 – 73199	0.013	0.0023	−2.63
37	3396.32	41563 – 70998	0.024	0.0042	−2.38
118	3413.34	45821 – 75109	0.081	0.014	−1.85
177	3440.51	13245 – 42302	0.0039	0.00070	−3.16
531	3457.85	11203 – 40114	0.0064	0.0011	−2.94
49	3459.43	44406 – 73305	0.034	0.0061	−2.22
115	3472.14	44406 – 73199	0.079	0.014	−1.84
22	3474.58	44544 – 73316	0.015	0.0028	−2.56
510	3476.00	44544 – 73305	0.35	0.064	−1.19
750	3483.76	44406 – 73103	0.52	0.094	−1.03
81	3488.86	44544 – 73199	0.056	0.010	−1.99
95	3498.06	43514 – 72093	0.065	0.012	−1.92
71	3500.32	44544 – 73105	0.049	0.0091	−2.04
36	3507.41	43514 – 72017	0.025	0.0046	−2.34
564	3512.12	43514 – 71979	0.39	0.072	−1.14
92	3517.04	43726 – 72151	0.063	0.012	−1.93
367	3520.03	44916 – 73316	0.26	0.048	−1.32
796	3524.23	43726 – 72093	0.55	0.10	−0.99
371	3527.48	43726 – 72067	0.26	0.048	−1.32
1897	3530.38	13245 – 41563	0.035	0.0065	−2.18
360	3533.75	43726 – 72017	0.25	0.047	−1.33
130	3544.96	43726 – 71927	0.090	0.017	−1.77
40	3546.43	44916 – 73105	0.028	0.0053	−2.27
71	3594.02	11203 – 39019	0.00065	0.00013	−3.90
115	3609.30	13245 – 40944	0.0018	0.00036	−3.45
141	3610.81	44406 – 72093	0.100	0.020	−1.71
441	3613.76	43514 – 71178	0.31	0.060	−1.22
168	3614.22	44406 – 72067	0.12	0.023	−1.63
160	3620.35	43514 – 71128	0.11	0.022	−1.66
364	3621.24	44544 – 72151	0.26	0.051	−1.29
30	3629.77	43726 – 71268	0.021	0.0042	−2.38
192	3635.92	45821 – 73316	0.14	0.028	−1.56
105	3641.69	43726 – 71178	0.074	0.015	−1.83
132	3645.23	45879 – 73305	0.096	0.019	−1.72
92	3648.38	43726 – 71128	0.065	0.013	−1.89
312	3655.86	43514 – 70860	0.22	0.044	−1.36
113	3656.78	44544 – 71883	0.081	0.016	−1.79
110	3659.35	45879 – 73199	0.080	0.016	−1.79
26	3664.08	45821 – 73105	0.019	0.0038	−2.42

TABLE 1. *Transition probabilities of copper*—Continued

Intensity	Wavelength A	Energy Levels K	gA 10^8/sec	gf	Log gf
88	3665.74	43726 – 70998	0.062	0.013	−1.90
89	3671.95	45879 – 73105	0.065	0.013	−1.88
32	3695.36	44963 – 72017	0.023	0.0047	−2.32
32	3699.10	46173 – 73199	0.024	0.0048	−2.32
173	3700.54	44963 – 71979	0.13	0.026	−1.59
62	3712.01	46173 – 73105	0.046	0.0094	−2.03
88	3720.77	13245 – 40114	0.0011	0.00024	−3.63
27	3721.67	44406 – 71268	0.019	0.0040	−2.39
120	3734.18	44406 – 71178	0.087	0.018	−1.74
214	3741.24	44406 – 71128	0.15	0.033	−1.49
84	3759.49	44406 – 70998	0.061	0.013	−1.89
100	3771.90	46598 – 73103	0.075	0.016	−1.80
35	3799.88	44544 – 70853	0.026	0.0055	−2.26
71	3800.50	44963 – 71268	0.052	0.011	−1.95
100	3805.23	45879 – 72151	0.075	0.016	−1.79
32	3813.54	44963 – 71178	0.024	0.0052	−2.29
83	3820.88	44963 – 71128	0.061	0.013	−1.87
16	3837.98	45879 – 71927	0.012	0.0027	−2.58
342	3860.47	44963 – 70860	0.25	0.057	−1.25
22	3881.71	46173 – 71927	0.017	0.0038	−2.42
44	3921.27	46598 – 72093	0.034	0.0078	−2.11
52	3925.27	46598 – 72067	0.040	0.0092	−2.03
27	3933.03	46598 – 72017	0.021	0.0048	−2.32
16	3946.94	46598 – 71927	0.012	0.0029	−2.54
7	3951.62	45879 – 71178	0.0054	0.0013	−2.90
11	3979.95	45879 – 70998	0.0084	0.0020	−2.70
5	3993.69	45821 – 70853	0.0038	0.00092	−3.04
10	3998.02	46173 – 71178	0.0077	0.0019	−2.73
53	4003.03	45879 – 70853	0.041	0.0098	−2.01
52	4027.03	46173 – 70998	0.040	0.0098	−2.01
49	4050.62	46173 – 70853	0.038	0.0094	−2.03
52	4052.38	46598 – 71268	0.041	0.010	−2.00
141	4075.57	46598 – 71128	0.11	0.028	−1.56
85	4104.22	40114 – 64472	0.058	0.015	−1.84
37	4121.74	46598 – 70853	0.029	0.0075	−2.13
176	4177.76	39019 – 62948	0.12	0.030	−1.52
432	4248.96	40944 – 64472	0.30	0.082	−1.08
101	4259.40	40114 – 63585	0.069	0.019	−1.73
462	4378.20	40114 – 62948	0.32	0.091	−1.04
92	4415.54	40944 – 63585	0.065	0.019	−1.72
589	4480.35	30535 – 52849	0.19	0.057	−1.24
640	4509.37	42302 – 64472	0.48	0.15	−0.84
263	4539.70	41563 – 63585	0.19	0.059	−1.23
603	4586.97	41153 – 62948	0.43	0.14	−0.86
205	4674.72	41563 – 62948	0.15	0.049	−1.31
84	4697.49	42302 – 63585	0.063	0.021	−1.68
753	4704.59	41153 – 62403	0.54	0.18	−0.74
39	4797.04	41563 – 62403	0.029	0.0099	−2.01
268	5016.61	44544 – 64472	0.22	0.084	−1.08
58	5034.36	43726 – 63585	0.047	0.018	−1.75

TABLE 1. *Transition probabilities of copper*—Continued

Intensity	Wavelength A	Energy Levels K	gA 10^8/sec	gf	Log gf
162	5111.91	44916 – 64472	0.14	0.054	−1.27
138	5144.12	43514 – 62948	0.11	0.044	−1.36
114	5200.87	43726 – 62948	0.093	0.038	−1.42
70	5352.67	43726 – 62403	0.057	0.025	−1.61
30	5354.95	44916 – 63585	0.026	0.011	−1.96
43	5360.03	45821 – 64472	0.038	0.016	−1.78
11	5376.87	45879 – 64472	0.0098	0.0042	−2.37
67	5391.62	44406 – 62948	0.057	0.025	−1.61
38	5432.05	44544 – 62948	0.032	0.014	−1.84
28	5463.14	46173 – 64472	0.025	0.011	−1.95
49	5554.94	44406 – 62403	0.042	0.019	−1.71
40	5732.33	44963 – 62403	0.035	0.017	−1.76
14	6223.66	56030 – 72093	0.017	0.0099	−2.00
12	6325.45	46598 – 62403	0.012	0.0070	−2.16
18	6474.20	56651 – 72093	0.023	0.014	−1.84
12	6485.18	56651 – 72067	0.015	0.0096	−2.02
3.0	6506.14	56651 – 72017	0.0038	0.0024	−2.61
4.7	6544.51	56651 – 71927	0.0060	0.0039	−2.41
4.1	6550.98	56030 – 71291	0.0052	0.0034	−2.47
4.3	6583.54	58119 – 73305	0.0056	0.0037	−2.44
3.4	6599.68	56030 – 71178	0.0043	0.0028	−2.55
30	6621.61	56030 – 71128	0.038	0.025	−1.60
6	6629.67	58119 – 73199	0.0079	0.0052	−2.28
24	6672.23	58119 – 73103	0.032	0.021	−1.67
101	6741.42	56030 – 70860	0.13	0.089	−1.05
8	6881.94	56651 – 71178	0.011	0.0076	−2.12
8	6890.90	57419 – 71927	0.011	0.0077	−2.11
44	6905.94	56651 – 71128	0.059	0.042	−1.38
3.8	6968.34	56651 – 70998	0.0051	0.0037	−2.43
4.5	7154.29	58119 – 72093	0.0063	0.0048	−2.31

The accuracy of the intensity measurements made in the copper arc is discussed in references [1] and [2]. Comparison of repeated determinations indicates that the standard deviation of an individual determination of the intensity of copper lines is about 2 or 3 percent.

The accuracy of the *gf*-values derived from intensity measurements is discussed in references [4] and [5]. In the case of our copper lines, about 2/3 of them arise from levels between 70 and 80 kK above the ground state. For these lines the standard deviation in log *gf* that arises from the uncertainty in T is about 0.18 (50 percent in *gf*) and the error due to the uncertainty in the intensity (0.01) is negligible. To estimate the absolute error in these high level lines we add again the error due to the uncertainty of T in the Boltzmann factor in Saha's equation (0.18) and the error introduced by the uncertainty in the value of the electron density in Saha's equation (0.17). Adding these as the square root of the sums of the squares we find the standard deviation of an individual determination of the absolute value of log *gf* is 0.3, or about a factor of 2 in *gf*.

The results in table 1 were calculated from the formulas in section 3 by W. R. Bozman using a modification of the program he developed for NBS Mono. 53 [4].

5. References

[1] W. F. Meggers, C. H. Corliss, and B. F. Scribner, Tables of spectral-line intensities, NBS Mono. 32 (1961).
[2] W. F. Meggers, C. H. Corliss, and B. F. Scribner, Spectrochim. Acta **17,** 1137 (1961).
[3] C. H. Corliss, J. Research NBS **66A** (Phys. and Chem.), 169 (1962).
[4] C. H. Corliss and W. R. Bozman, Experimental transition probabilities for spectral lines of seventy elements, NBS Mono. 53 (1962).
[5] C. H. Corliss, Astrophysical J. (Nov. 1962).
[6] C. H. Corliss, J. Research NBS **66A** (Phys. and Chem.) 5 (1962).
[7] A. G. Shenstone, Phil. Trans. Roy. Soc. London **241A,** 297 (1948).
[8] C. W. Allen and A. S. Asaad, Monthly Notices Roy. Astron. Soc. **117,** 36 (1957).

(Paper 66A6–185)

JOURNAL OF RESEARCH of the National Bureau of Standards—A. Physics and Chemistry
Vol. 66A, No. 6, November–December 1962

Batch Adsorption From Solution

William V. Loebenstein

(August 7, 1962)

A batch adsorption equation was derived by integrating an irreversible rate equation obtained by neglecting the desorption term of the Langmuir adsorption-rate equation. The integrated equation was in reasonably good agreement with experiment and provided a means for determining from the data the parameters q_0 and k_1. These constants, namely, the adsorptive capacity and the adsorption rate constant, completely characterized the adsorption system at that temperature. Agreement was found between these *batch* adsorption parameters and their counterparts previously derived from *column* adsorption experiments when both types of adsorption were performed simultaneously.

1. Introduction

The study of adsorption from solution of one or more solutes by solid adsorbents has lagged in comparison with the advances made in gas adsorption. The problem is more complicated for a number of reasons: (1) The systems of interest are invariably multi-component and, hence, the possibility of competition exists for the available adsorption sites if, indeed, the same sites are involved. (2) Equations of state are less well understood for liquid systems than for gases. (3) The isotherms applicable to gas adsorption have been studied in great detail. The differences between physical and chemical adsorption are usually well defined and the parameters of the isotherm equation are meaningful. In contrast, the isotherms applicable to adsorption from solution are complicated by the fact that no clean-cut distinction can generally be made between physical adsorption and chemisorption. Complete reversibility is seldom if, indeed, ever attained. A Freundlich adsorption equation which often fits the data well is limited in its usefulness because its parameters lack physical significance. (4) The additional complications resulting from the greater viscosity in liquids than in gases as well as the contribution to the overall complexity attributable to diffusion can well be appreciated.

Adsorption from solution is customarily conducted either as a column or as a batch operation In the former instance the solution is allowed to percolate through a column usually held in a vertical position such as is the common practice with ion exchange columns. In a batch operation, a quantity of adsorbent is mixed all at once with a quantity of solution and the system kept in agitation for a convenient period of time. Separation of the resultant solution is accomplished by filtering, centrifuging, or decanting.

It should be possible to characterize a solution-adsorbent system by either column or batch technique and arrive at the same result since the physical and/or chemical forces applicable in each case must be identical. Furthermore, the results obtained from a batch experiment should be somewhat more reliable because of several reasons. Among the most serious objections to column experiments are: (1) The overall complexity and expense of experimental equipment; (2) the inherent difficulties associated with maintaining a constant flow rate; (3) the difficulty of assuring a constant temperature throughout the column; (4) the appreciable probability of channeling within the packed column; (5) the variability in the results associated with classification by particle size during settling of the column; (6) the errors inherent in any of the various methods of settling of the column; and (7) the relatively large expenditure both in time and manpower required for a column experiment.

Previous attempts to solve the kinetics of batch adsorption from solution have been, for the most part, disappointing. A certain measure of success was reported by Dryden and Kay [1] [1] despite the fact that their equation (based on a solution of the finite bath theory) assuming a *linear* adsorption isotherm was applied to systems which obeyed the *Freundlich* isotherm. Their use of the "fractional approach to equilibrium" was a refinement of the work of Eagle and Scott [2] which, in turn, was an outgrowth of the earlier application by Geddes [3].

The aforementioned approach while providing a measure of the adsorption rate constant can give no estimate of the maximum extent of adsorption which might conceivably correlate with surface area. Other investigators assuming either a Langmuir representation [4, 5, 6, 7] or (less frequently) a B.E.T. behavior [8, 9, 10, 11] applied to solutions were able to estimate adsorptive capacities. However, since their applications were made using the equations derived for $t=\infty$, no kinetic information can be expected.

2. Theoretical Development

The present investigation treats the problem of batch adsorption in a manner analogous to that recently found extremely useful in column adsorption [12]. The kinetic form of an adsorption equation which may reasonably be expected to fit the data is integrated subject to a "conservation" equation, i.e.,

[1] Figures in brackets indicate the literature references at the end of this paper

a conservation of mass equation applied to the adsorbable solute.

2.1. Adsorption Rate

The kinetic form of a Langmuir adsorption equation before attainment of equilibrium may be represented as follows:

$$\frac{dq}{dt}=k_1c(q_0-q)-k_2q \tag{1}$$

where

q=the amount of solute adsorbed per gram of the adsorbent at any time, t;
q_0=the maximum value q would have if all the adsorption sites were filled;
c=the solute concentration at any time, t; and
k_1, k_2=the specific adsorption and desorption rate constants.

While eq (1) can be handled in its complete form [2] as shown, the result is unwieldy and some doubt exists that the additional precision that may result in some instances can justify the resultant increase in complexity. Furthermore, the presence of the last term of eq (1) implies *complete* reversibility, a condition which is rarely encountered in any practical case concerned with adsorption from solution. Accordingly, the kinetic equation adopted in this work is, simply:

$$\frac{dq}{dt}=k_1c(q_0-q). \tag{2}$$

Further justification for this simplification is the fact that in the column work already mentioned [12] quite satisfactory agreement was found in comparing columns of different dimensions, although the desorption rate constant k_2 had been eliminated from the integrated equation in that case also. Equation (2) simply states that the rate of adsorption is proportional at any instant to the concentration of the solute and to the number of unfilled adsorption sites.

The "conservation equation" for batch adsorption may be expressed in the form:

$$c_0V=cV+qW \tag{3}$$

where c_0 is the initial concentration of the solute, V the volume of solution, and W the mass of the adsorbent.

Equation (2) is easily integrated subject to eq (3) and the boundary conditions that $q=0$ and $c=c_0$ when $t=0$. This resultant integrated equation may be expressed as:

$$\ln\frac{\frac{c}{c_0}}{1-\frac{q}{q_0}}=-\left(\frac{Wq_0}{Vc_0}-1\right)c_0k_1t. \tag{4}$$

[2] See eq 19.

Perhaps the best representation of the adsorption equation is obtained by eliminating c, entirely, between eqs (3) and (4) to obtain:

$$\frac{q}{q_0}=\frac{1-e^{-\left(\frac{Wq_0}{Vc_0}-1\right)c_0k_1t}}{\frac{Wq_0}{Vc_0}-e^{-\left(\frac{Wq_0}{Vc_0}-1\right)c_0k_1t}}. \tag{5}$$

At $t=0$, the numerator of the fraction vanishes, so $q=0$.

When $Wq_0/Vc_0>1$, the exponent of e is negative, so that the exponential terms are always less than unity. Thus the denominator is always greater than the numerator and $0<q/q_0<1$. Furthermore, under these conditions there is not enough adsorbate in the system to satisfy the capacity of the adsorbent, so as $t\to\infty$ the value of q tends toward Vc_0/W. Conversely, when $Wq_0/Vc_0<1$, the exponent of e is positive and the exponential terms become greater than unity and increase in magnitude with time. Again the quotient is always positive with a value between zero and one. Now, however, as $t\to\infty$ the limiting value of q is q_0 as expected.

Also from eq (5) it can be seen that: [3]

$$\lim_{\frac{W}{V}\to 0}\frac{q}{q_0}=1-e^{-c_0k_1t}. \tag{6}$$

The slope of the curve $q=f(t)$ is even more revealing. By differentiating eq (5) with respect to t, one obtains:

$$\frac{\partial q}{\partial t}=q_0c_0k_1\left[\frac{\frac{Wq_0}{Vc_0}-1}{\frac{Wq_0}{Vc_0}-e^{-\left(\frac{Wq_0}{Vc_0}-1\right)c_0k_1t}}\right]^2e^{-\left(\frac{Wq_0}{Vc_0}-1\right)c_0k_1t}. \tag{7}$$

Now if the exponent in eq (7) is greater than zero, then at relatively large values of t

$$\frac{\partial q}{\partial t}\approx\frac{q_0c_0k_1\left(\frac{Wq_0}{Vc_0}-1\right)^2}{e^{-\left(\frac{Wq_0}{Vc_0}-1\right)c_0k_1t}} \tag{8}$$

which, in turn, goes to zero as $t\to\infty$.

If the exponent in eq (7) is less than zero, then as t grows large

$$\frac{\partial q}{\partial t}\approx q_0c_0k_1\left[\frac{\frac{Wq_0}{Vc_0}-1}{\frac{Wq_0}{Vc_0}}\right]^2e^{-\left(\frac{Wq_0}{Vc_0}-1\right)c_0k_1t} \tag{9}$$

which, in the limit as $t\to\infty$, again goes to zero.

The integrated equation corresponding to eq (5) which was found to apply to *column* [12] adsorption is repeated here for convenience:

[3] This is essentially the equation derived by Harned [13] in 1920.

$$\ln\left(\frac{c_0}{c}-1\right)=\frac{k_1 q_0 x}{\dot{V}}-\frac{k_1 c_0 y}{\dot{V}} \qquad (10)$$

where $\dot{V}$ is the volume velocity; x is the mass of adsorbent upstream from the point at which effluent is collected; and y is the throughput or volume of effluent which has passed up to that time. Since the effluent in column adsorption is usually collected only at the end of the column, the value of x is constant. Thus, eq (10) is readily adapted for evaluating the parameters q_0 and k_1 from the linear plot of $\ln\left(\frac{c_0}{c}-1\right)$ against y. For the present work where batch adsorption is involved, no simple linear representation of eq (4) or (5) is possible for testing goodness of fit and for evaluating the parameters q_0 and k_1. Consequently it was necessary to resort to methods of successive approximations. Two such methods which were found to be helpful are given in the appendix.

3. Experimental Techniques

The batch adsorption experiments were conducted in stoppered erlenmeyer flasks agitated mechanically by means of a water bath shaking apparatus thermostated at 80 °C. The older experiments involved the use of a service bone char (Char 32) as the adsorbent in various U.S. sieve fractions both separately and in recombined mixtures. The adsorbate was the colorant in a Louisiana raw sugar liquor (of 60 Brix sucrose concentration). The concentration of the colorant was considered to be proportional to the optical density (or attenuation index assuming no scattering) as measured by a Beckman DU spectrophotometer at 560 mμ wavelength. The resonableness of this assumption was discussed in some detail in the previous work [12]. The proportionality constant, k_0, is not known, so that only comparative results are possible from all the colorant adsorption experiments. The length of time of each adsorption measurement was limited, in the earlier work, to 3 hr and the volume of solution was fixed as was the initial concentration. Six different weights of adsorbent were used in each experiment. A comparison was also made at that time with an activated carbon, namely Darco S–51, in an otherwise identical system.

The more recent series of experiments was designed to compare the results of batch adsorption with column adsorption for the same systems. Again a service bone char (Char 117–B) was used in all comparisons. A particular Hawaiian raw sugar liquor (Sugar 17) was tested both by batch and by column experiments all at 80 °C. Time, as well as weight of adsorbent, was allowed to vary among batches. The adsorption of colorant (optical density at 420 mμ wavelength), sulfate ion, and total cations, were determined independently for the two methods. The $[SO_4]^=$ determination was made by a turbidimetric method applied to suspensions of precipitated $BaSO_4$ as described by Gee et al. [14]. Total cations were determined by an ion exchange technique using Amberlite IR–120 in the hydrogen-form followed by titration with a standard base [15].

4. Comparison of Parameters Derived From Related Batch Experiments

4.1. Comparison Among Sieve Sizes of the Same Adsorbent

Table 1a gives the data obtained from one of the colorant adsorption batch experiments in the older series. The first method described in the appendix for determining the values of q_0 and k_1 from the experimental data was applied here. After four or five trials, the improved choice of $q_0 \approx 9.80\ k_0$ resulted in the quantities computed as shown in table 1b. In comparison with previous trials the quantity computed for Δq_0 was sufficiently close to zero, that no further refinement was deemed to be justified.

The data of table 1a were used to plot q against c/c_0 as shown by the open circles and curve of figure 1.

The corresponding values of q computed according to eq (5) using the two parameters q_0 and k_1 from table 1b are shown in crosses. The agreement is seen to be quite good except at the tail end of the curve where the amount of adsorbent used was small.

Table 2 summarizes the results for the same bone char but for various sieve sizes (both separately and in combination) tested with the same sugar solution for adsorption of colorant. The values listed for q_0 and k_1 were derived in each case by a method described in the appendix.

For the case of sieve fraction (30 on 35), the value of $8.58\ k_0$ for q_0 seems somewhat low in line with the other members of the series. Likewise its k_1 value of $0.182\ 1/k_0$ appears to be high. Interestingly enough, the values derived by application of the theory to the reconstituted 50 percent mixtures agree rather well with the arithmetic means of the independently determined separate fractions. It should be noted in the last line of table 2 that the mixture included the (30 on 35) fraction which exhibited the anomalous behavior already mentioned. Its contribution in the case of the mixed sample must have been consistent with its separate behavior to have resulted in such close agreement between derived value and averaged value for q_0.

It is seen that the value of q_0 varied about 2½-fold between the coarser and finer fractions as shown in Figure 3. If the entire surface within a porous adsorbent particle were accessible to the adsorbate, the particle size should have little (if any) influence on the capacity for adsorption per unit mass of adsorbent providing the surface area were large. The sample of bone char used in this work had a B.E.T. total area (determined with N_2 gas at 77 °K) of about $80\ m^2 \cdot g^{-1}$. It can easily be shown that the external or boundary area of (48 on 80) mesh char particles is about $0.01\ m^2 \cdot g^{-1}$. A 3½-fold increase in particle size to (20 on 30) mesh would decrease this particle

TABLE 1a. *Typical data obtained by varying the amount of adsorbent from batch to batch*

Expt. (22-29), char 32 through 20 on 30 with Louisiana raw sugar liquor. $c_0 = k_0(-\log t_{580}) = 0.349 k_0$ mM·ml^{-1}; $V = 78$ ml; $q = (c_0 - c) \div (W/V)$.

Batch No.	W	c	$c_0 - c$	W/V	q	t	c/c_0	$\ln c_0/c$
	g	*mM·ml*$^{-1}$		*g·ml*$^{-1}$	*mM·g*$^{-1}$	*hr*		
1	2.00	0.302 k_0	0.047 k_0	0.026	1.808 k_0	3.00	0.865	0.145
2	5.00	.257 k_0	.092 k_0	.064	1.438 k_0	3.00	.736	.307
3	10.02	.195 k_0	.154 k_0	.128	1.203 k_0	3.00	.559	.582
4	14.99	.143 k_0	.206 k_0	.192	1.073 k_0	3.00	.410	.892
5	19.99	.105 k_0	.244 k_0	.256	0.953 k_0	3.00	.301	1.200
6	24.98	.0802 k_0	.269 k_0	.320	.841 k_0	3.00	.230	1.470

TABLE 1b. *Improved estimate of parameters (method 1) applied to data of table 1a for* $q_0 = 9.80$ k_0 mM·g^{-1}

Batch No.	Order of computations														
	1	2	3	4	6	9	10	11	12	13	5	7	8	14	15
	q/q_0	q/q_0^2	$1-q/q_0$	$-\ln(1-q/q_0)$	$\partial F/\partial k_1$	F	ΔF	$(W/V)k_1 t$	$\frac{q/q_0^2}{1-q/q_0}$	$\partial F/\partial q_0$	$\ln c_0/c + \ln(1-q/q_0)$	Eq. (7a)		Eq. (9a)	
1	0.184	0.0188	0.816	0.203	−0.283	0.156	−0.011	0.0130	0.0230	−0.0100	−0.058	$141.179 k_1 = 23.5897$	$k_1 = 0.16709\ 1/k_0$ ml·mM^{-1}·hr^{-1}	$4.630\times10^{-4}\Delta q_0 = 25.8\times10^{-4}$	$\Delta q_0 = 5.57\times10^{-4} k_0$ mM·g^{-1}
2	.147	.0150	.853	.159	.835	.299	.008	.0321	.0176	.0145	.148				
3	.123	.0126	.877	.131	2.716	.585	−.003	.0642	.0144	.0498	.451				
4	.109	.0111	.891	.115	4.598	.883	.009	.0962	.0125	.0837	.777				
5	.0972	.00992	.903	.102	6.479	1.185	.015	.1283	.0110	.1173	1.098				
6	.0858	.00876	.914	.0900	8.361	1.487	−.017	.1604	.0096	.1508	1.380				

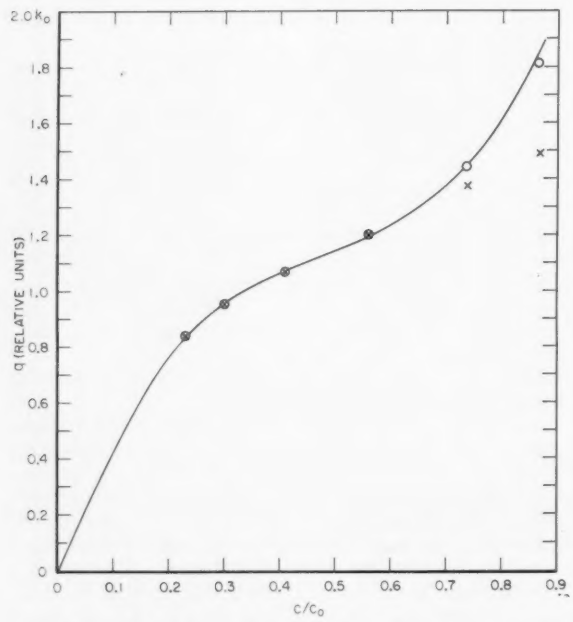

FIGURE 1. *Batch adsorption curve for colorant (contained in a Louisiana raw sugar liquor) using a (20 on 30) mesh service bone char.*

Three hour experimental points are shown by circles, calculated points by crosses.

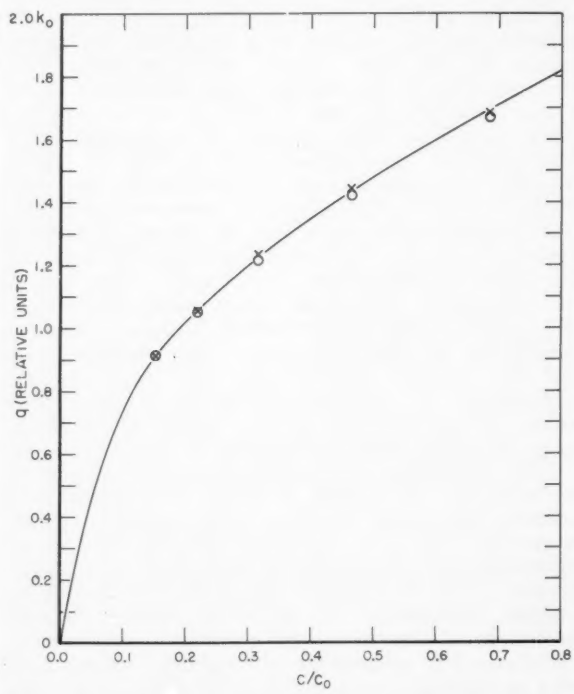

FIGURE 2. *Batch adsorption curve for colorant (contained in a Louisiana raw sugar liquor) using a 50 percent mixture of (20 on 30) mesh and (48 on 80) mesh service bone char.*

Three hour experimental points are shown by circles, calculated points by crosses.

area to 0.003 $m^2 \cdot g^{-1}$ and result in a decrease in B.E.T. area of less than 0.01 percent. It is interesting to speculate whether the observed variation of capacity for adsorption with sieve fraction was caused by the possibility that the service char may have restricted access to its interior brought on by the building up of mineral deposits, etc., resulting from repeated cycles of raw sugar filtration and high temperature kilning.

TABLE 2. *Relative values of adsorptive capacity* q_0 *and rate constant* k_1 *for the adsorption of colorant from a Louisiana raw sugar liquor on service bone char 32 of various sieve fractions*

Sieve sizes (US standard mesh) single closely sieved fractions	q_0 determined values		k_1 determined values	
	$mM \cdot g^{-1}$		$ml \cdot mM^{-1} \cdot hr^{-1}$	
(20 on 30)	9.90 k_0		0.165 $1/k_0$	
(30 on 35)	8.58 k_0		.182 $1/k_0$	
(35 on 48)	10.25 k_0		.144 $1/k_0$	
(48 on 80)	23.00 k_0		.0895 $1/k_0$	
Fines (smaller than 80 mesh)	24.79 k_0		.227 $1/k_0$	
	q_0		k_1	
50% mixtures of sieve fractions	Determined values	Average of individual values	Determined values	Average of individual values
(20 on 30) and (48 on 80)	17.30 k_0	16.5 k_0	0.118 $1/k_0$	0.127 $1/k_0$
(30 on 35) and (48 on 80)	16.00 k_0	15.8 k_0	.105 $1/k_0$	0.136 $1/k_0$

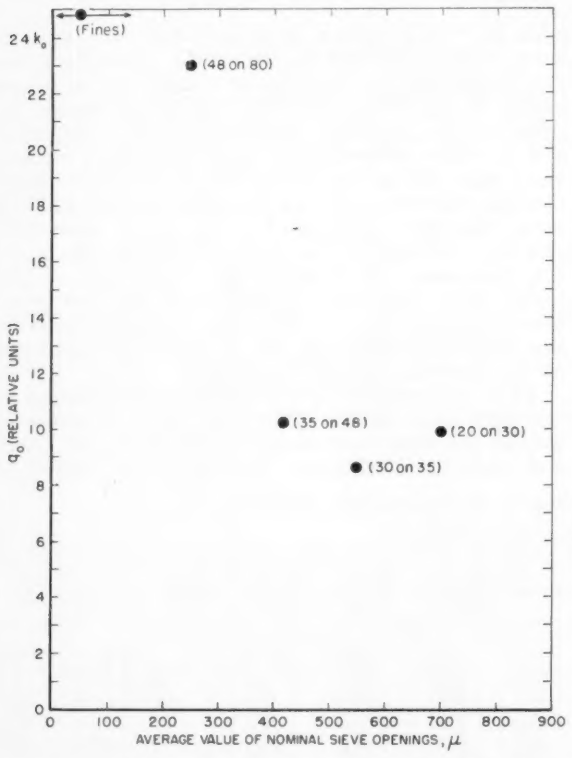

FIGURE 3. *Adsorption capacity of various sieve fractions of a service bone char for colorant plotted against mean particle diameter within each fraction.*

5. Comparison Between Two Different Adsorbents

It is interesting to compare the behavior of a decolorizing carbon (Darco S–51) with a service bone char in connection with the same sugar solution and under identical conditions in all other respects. The observed curve and calculated points for q of the decolorizing carbon are shown in figure 4. The magnitude of q_0 and k_1 are in qualitative agreement with known behavior when activated carbon is compared with bone char.

If the relative number of adsorption sites (as estimated by the magnitude of q_0) were a constant fraction of the surface area for different carbon adsorbents, one might hope to use this as a tool to compare surface areas. The ratio of their relative colorant adsorptive capacities of 53.5 k_0 for Darco S–51 to, say, 10 k_0 for (20 on 30) mesh service bone char would predict a surface area for the activated carbon of $80 \times 53.5/10 = 428$ $m^2 \cdot g^{-1}$. Published values of about 500 $m^2 \cdot g^{-1}$ [16] based on B.E.T. nitrogen adsorption isotherms have been given for the surface area of Darco S–51. Of course, considerably more work would have to be done in this connection before such an inference could be verified.

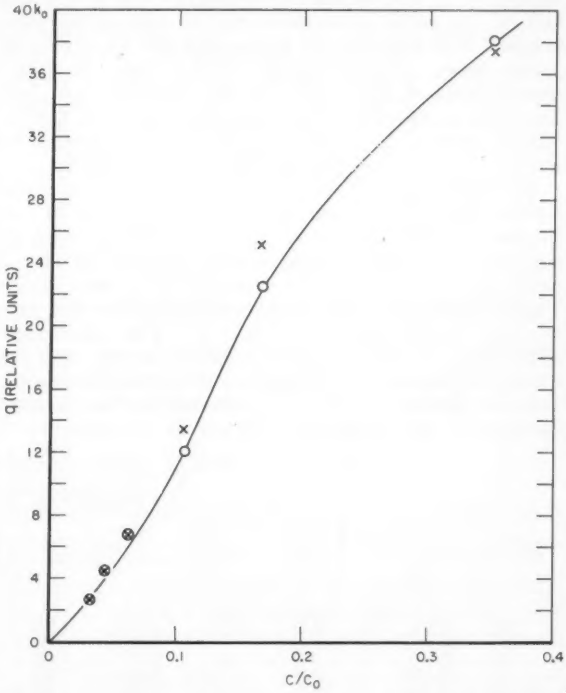

FIGURE 4.—*Batch adsorption curve for colorant (contained in a Louisiana raw sugar liquor) using a decolorizing (vegetable) carbon.*

Three hour experimental points are shown by circles, calculated points by crosses.

6. Batch Versus Column Adsorption—Comparison of q_0 and of k_1

A Hawaiian raw sugar solution was studied by means of a column experiment and a batch experiment using a service bone char as the adsorbent in each case. The adsorption of colorant as well as certain inorganic components, notably sulfate ion and alkaline-earth cations, were determined at the same time. The alkaline-earth cations consisted almost entirely of calcium ions and (to a much lesser extent) magnesium.

6.1. Colorant Adsorption Parameters

For the column experiment a cylindrical column of 500 ml capacity was used with 562 g of char leaving a total void volume of about 300 ml. The flow rate of sugar solution was held at 300 ml·hr^{-1}. When plotted according to eq (10), the results are shown in figure 5. The last seven points form a reasonably good straight line. From the slope of this line and its intercept on the zero-throughput axis, a value of 4.66 k_0 for q_0 and 0.0685 $1/k_0$ for k_1 were estimated. The first three points corresponding to no more than one column displacement are probably too high. Remnants of the settling liquor not completely displaced would make c abnormally low and, consequently, $\left(\frac{c_0}{c}-1\right)$ would be too high.

The data of the batch experiment (26–B_2) performed with aliquots of the same raw sugar solution and of the same bone char carried out at the same temperature and on the same day are available for comparison. It should be noted that in batch experiments of the recent work, time was not held constant in all of the samples, but was deliberately varied from ½ hr to 4 hr. The data collected are shown to the left of the double rule in table 3.

By applying the methods of successive approximation described in the appendix the values of 8.52 k_0 and 0.0490 $1/k_0$ were obtained for q_0 and k_1, respectively. These parameters applied to eq (5) were used to calculate the quantity q for each batch. These calculations and results are shown to the right of the double rule in table 3. The differences between $q_{(obs)}$ and $q_{(calc)}$ are given in the last column. The sum of the squares of these differences is 1.83 k_0^2, hence the mean square deviation between calculated and observed values of q amounts to

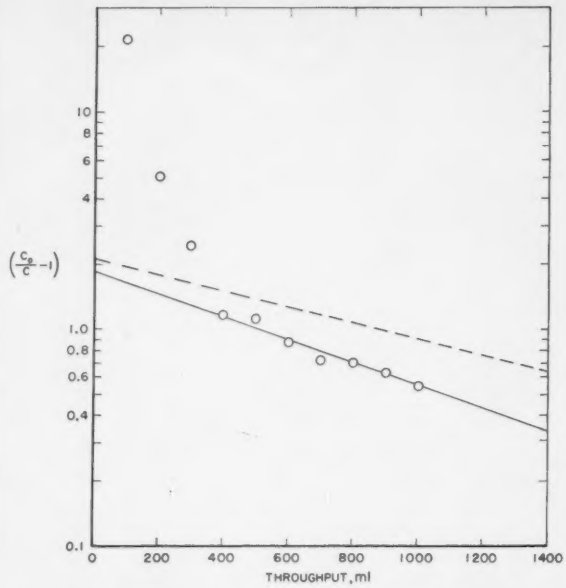

FIGURE 5. *Column adsorption of colorant (contained in a Hawaiian raw sugar liquor) by a service bone char shown by experimental points.*

Solid line was selected as best fit for these data. (Perfect agreement with batch adsorption would have required the experimental column points to have fallen on broken line.)

0.305 k_0^2. This yields a value of 0.55 k_0 as "standard error of estimate" for the quantity q based on the above calculations, although it should not be interpreted as experimental error. Attention should be called to the apparent anomaly between samples 4 and 5. The concentration may have been erroneously recorded as the same, but it is equally likely that the experimental error was great enough to have given identical readings for the 1½-hr and 2-hr samples. The data were treated as though the latter was the case. It is significant that even if the 1½-hr point had been omitted and the computations had been based on the seven remaining batches, the value thus obtained for q_0 would have differed by no more than about 3½ percent.

All in all, considering the assumptions inherent in the derivation of the adsorption rate equation as well as the experimental errors present in the batch and column adsorption methods, the values of

TABLE 3. *Batch adsorption of colorant and test of improved estimate of parameters*

Batch expt 26 B_2; V=49.5 ml; c_0=5.21 k_0 mM·ml^{-1}.

Sample No.	W	t	c	W/V	$q_{(obs)}$	$\frac{Wq_0}{Vc_0}$	$\left(\frac{Wq_0}{Vc_0}-1\right)c_0k_1t$	Exponential term of eq (5)	Numerator of eq (5)	Denominator of eq (5)	q/q_0 (calculated)	$q_{(calc)}$	Δq
	g	hr	mM·ml^{-1}	g·ml^{-1}	mM·g^{-1}							mM·g^{-1}	mM·g^{-1}
2	50.0	0.5	3.68 k_0	1.010	1.515 k_0	1.652	0.0832	0.920	0.0798	0.732	0.109	0.929 k_0	0.561 k_0
3	50.0	1.0	3.32 k_0	1.010	1.871 k_0	1.652	.1664	0.847	.153	.805	.190	1.619 k_0	.252 k_0
4	50.0	1.5	2.66 k_0	1.010	2.525 k_0	1.652	.2497	0.779	.221	.873	.253	2.156 k_0	.369 k_0
5	50.0	2.0	2.66 k_0	1.010	2.525 k_0	1.652	.3329	0.717	.283	.935	.303	2.582 k_0	−.057 k_0
7	50.0	4.0	1.99 k_0	1.010	3.188 k_0	1.652	.6658	0.514	.486	1.138	.427	3.638 k_0	−.450 k_0
6	60.0	4.0	1.62 k_0	1.212	2.962 k_0	1.982	1.0026	0.367	.633	1.615	.392	3.340 k_0	−.378 k_0
8	40.0	4.0	2.59 k_0	0.808	3.243 k_0	1.321	0.3278	0.721	.279	0.600	.465	3.962 k_0	−.719 k_0
9	30.0	4.0	2.21 k_0	0.606	4.950 k_0	0.9910	−.00919	1.0092	−.0092	−.0182	.505	4.303 k_0	.647 k_0

$8.52k_0$ versus $4.66k_0$ for q_0 and 0.0490 $1/k_0$ versus 0.0685 $1/k_0$ for k_1 derived from batch and column, respectively, are rather encouraging. If the column experiment had yielded results for q_0 and k_1 in identical agreement with those obtained from the batch experiment, the dashed line shown in figure 5 would have resulted.

6.2. Sulfate Adsorption Parameters

The results obtained in the adsorption of sulfate ion by bone char from raw sugar solution are especially significant. Since the concentration of sulfate can be measured in *absolute* units (only relative units for colorant concentration), a means was available for the first time for estimating that fraction of the surface of the adsorbent on which sulfate-adsorption sites existed.

Data collected from the column experiment are given in table 4. A semi-logarithmic plot of the dimensionless quantity $\left(\frac{c_0}{c}-1\right)$ against throughput gave a reasonably good straight line (in accordance with eq (10)) with intercept on the zero-throughput ordinate of ln 10 (or 2.303) and with a slope of -2.373×10^{-3} ml^{-1}. From these results the values of q_0 and k_1 were easily determined:

$$q_0=34.1\ \mu\text{eq}\cdot\text{g}^{-1}$$

$$k_1=0.036\ \text{ml}\cdot\mu\text{eq}^{-1}\ \text{hr}^{-1}.$$

TABLE 4. *Column adsorption of sulfate*

Weight of adsorbent, 562 g; flow rate 300 ml·hr^{-1}; concentration of $[SO_4]^=$ in on-liquor, $c_0=9.88$ mM·l$^{-1}\approx 19.76$ μeq·ml^{-1}; temperature=80 °C.

Throughput	$\left(\frac{c_0}{c}-1\right)$
ml	
100	8.69
200	5.81
300	4.68
400	3.22
500	2.97
600	2.17
900	1.66
1,200	0.871
1,500	.680
1,800	.607
1,900	.116

The corresponding batch adsorption experiment for sulfate ion was performed, the data of which are given in table 5 (to the left of the double rule). By use of the methods described in the appendix, the final values obtained were

$$q_0=35.4\ \mu\text{eq}\cdot\text{g}^{-1}$$

$$k_1=0.0287\ \text{ml}\cdot\mu\text{eq}^{-1}\cdot\text{hr}^{-1}.$$

With these numerical values for the batch adsorption capacity and rate constant, the remainder of table 5 (to the right of the double rule) was calculated. A comparison between the calculated values of q and the corresponding observed values discloses a mean square deviation of 1.75 $\mu\text{M}^2\cdot\text{g}^{-2}$ (with six degrees of freedom). Considering the number of variables involved and the experimental difficulties associated especially with column adsorption, the agreement attained for $[SO_4]^=$ between column and batch adsorption is very good. In kinetic studies of this type, agreement within the same order of magnitude is often acceptable.

6.3. Alkaline Earth Cation Adsorption Parameters

The adsorption of calcium and magnesium ions should in all fairness be treated separately, since each ion must follow its own unique adsorption isotherm. The only justification that could be given for treating the mixture as a composite would be the assumption that the individual ion adsorption characteristics might not be too different one from the other. Furthermore, since the data were already available, they were tested according to the present theory. The data for the column experiment when plotted according to eq (10) were reasonably well fitted by a straight line as shown in figure 6. From this it may be estimated:

$$q_0\approx 8.6\ \mu\text{eq}\cdot\text{g}^{-1}$$

and

$$k_1\approx 0.0059\ \text{ml}\cdot\mu\text{eq}^{-1}\cdot\text{hr}^{-1}$$

for the adsorptive capacity and rate constant, repectively.

The corresponding batch experiment was applied to the adsorption of [calcium plus magnesium] with the data shown in the left half of table 6 subjected

TABLE 5. *Batch adsorption of sulfate and test of improved estimate of parameters*

Batch experiment 26 B_3; $V=49.5$ ml; $c_0=9.90$ μM·ml^{-1} [a, b]

Sample No.	W	t	c	W/V	$^aq_{(obs)}$	$\frac{Wq_0}{Vc_0}$	$\left(\frac{Wq_0}{Vc_0}-1\right)c_0k_1t$	Exponential term of eq (5)	Numerator of eq (5)	Denominator of eq (5)	q/q_0 (calculated)	$^aq_{(calc)}$	$^a\Delta q$
	g	*hr*	μM·ml^{-1}	g·ml^{-1}	μM·g^{-1}							μM·g^{-1}	μM·g^{-1}
2	50.0	0.5	5.07	1.010	4.78	1.809	0.229	0.796	0.204	1.013	0.201	3.56	1.22
3	50.0	1.0	3.36	1.010	6 47	1.809	.459	.632	.368	1.177	.313	5.55	0.92
4	50.0	1.5	2.88	1.010	6.95	1.809	.688	.503	.497	1.306	.381	6.76	.19
5	50.0	2.0	2.73	1.010	7.10	1.809	.918	.400	.600	1.409	.426	7.55	−.45
7	50.0	4.0	1.86	1.010	7.96	1.809	1.836	.160	.840	1.649	.509	9.03	−1.07
6	60.0	4.0	1.35	1.212	7.05	2.171	2.657	.070	.930	2.101	.442	7.84	−0.79
8	40.0	4.0	3.27	0.808	8.21	1.447	1.014	.363	.637	1.084	.588	10.43	−2.22
9	30.0	4.0	2.07	.606	12.92	1.085	0.1929	.826	.174	0.259	.672	11.92	1.01

[a] Computations have been carried in units of micromoles, but these dimensions were converted to micro equivalents in reporting q_0 and k_1.
[b] Slight difference in values of c_0 between column and batch experiments is a result of heated blank sample No. 1 in batch experiment redetermined.

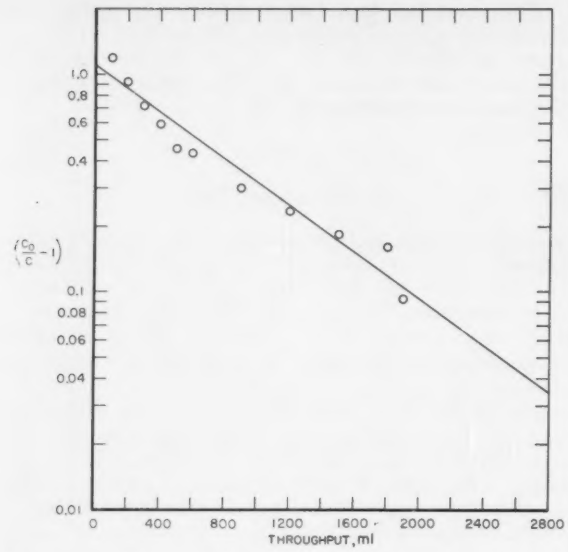

FIGURE 6. *Column adsorption of total cations (principally calcium and magnesium) from a Hawaiian raw sugar liquor by a service bone char.*

to the method of calculation already described. The right half of table 6 (to the right of the double rule) was computed corresponding to

$$q_0 \approx 70.3\ \mu\text{eq}\cdot\text{g}^{-1}$$

and

$$k_1 \approx 0.0030\ \text{ml}\cdot\mu\text{eq}^{-1}\cdot\text{hr}^{-1}$$

after several successive approximations. No appreciable improvement in the degree of fit was indicated although, in this case, a mean square deviation as large as 58.1 $\mu\text{eq}^2\cdot\text{g}^{-2}$ (with six degrees of freedom) was estimated between the observed and calculated values of q.

A comparison of batch with column-derived parameters in this instance discloses a twofold discrepancy in the rate constant, while the adsorptive capacities disagreed by almost an order of magnitude.

7. Fraction of Surface Area Available for Adsorption

It was stated at the beginning of the section on sulfate adsorption that the capacity for adsorption in absolute units could be used to estimate the fraction of the surface to which the adsorption of each species was confined. In the case of $[SO_4]^=$, for example, it was found that the maximum capacity, q_0, amounted to about 35 $\mu\text{eq}\cdot\text{g}^{-1}$ for a service bone char (Char 117–B) whose B.E.T. area is about 80 $\text{m}^2\cdot\text{g}^{-1}$ (measured by nitrogen adsorption at 77 °K). If the effective area of an adsorption site for the nitrogen molecule is taken as 16.2 A^2, there would be required 812 μM of nitrogen per gram of char to cover a monolayer for the particular bone char used. The sulfate ion is a tetrahedron with a sulfur-oxygen interatomic separation of 1.51 A [17] and an oxygen radius of 1.32 A. If the effective area of an adsorption site for the sulfate ion is roughly 28 A^2, then the fraction of the total surface that could accommodate sulfate adsorption at the maximum adsorptive capacity of the char (measured by q_0) would amount to only about 3¾ percent.

8. Temperature Dependence

Very little has been said here concerning k_1, the adsorptive rate constant. Data at several temperatures would certainly be of prime importance in order to ascertain whether eq (5) might be made even more general. It would be anticipated that k_1 might be replaced by an exponential Arrhenius type formulation to describe the temperature dependence of adsorption providing temperature has no more than a trivial effect upon q_0, as was found by Hirst and Lancaster [18].

9. Shapes of Adsorption Curves

The practical (finite time) adsorption curves, some examples of which are given here in figures 1, 2, and 4, should not be confused with equilibrium adsorption isotherms. The experimentally observed curves may have so many different shapes that they are difficult to catalog. Figure 7, for example, is a plot of the results already given for the batch adsorption of sulfate ion by bone char from a raw

TABLE 6. $[Ca]^{++}$ *plus* $[Mg]^{++}$ *composite adsorption and test of improved estimate of parameters*

Batch experiment 26 B_2; V=49.5 ml; c_0=64.50 $\mu\text{eq}\cdot\text{ml}^{-1}$

Sample No.	W	t	c	W/V	$q_{(obs)}$	$\frac{Wq_0}{Vc_0}$	$\left(\frac{Wq_0}{Vc_0}-1\right)e^{ak_1t}$	Exponential term of eq (5)	Numerator of eq (5)	Denominator of eq (5)	q/q_0 (calculated)	$q_{(calc)}$	Δq
	g	hr	$\mu\text{eq}\cdot\text{ml}^{-1}$	$g\cdot\text{ml}^{-1}$	$\mu\text{eq}\cdot\text{g}^{-1}$							$\mu\text{eq}\cdot\text{g}^{-1}$	$\mu\text{eq}\cdot\text{g}^{-1}$
2	50.0	0.5	48.9	1.010	15.4	1.101	0.0099	0.9902	0.00985	0.111	0.0887	6.2	9.2
3	50.0	1.0	45.1	1.010	19.2	1.101	.0198	.9804	.0196	.121	.162	11.4	7.8
4	50.0	1.5	41.9	1.010	22.4	1.101	.0297	.9708	.0292	.130	.225	15.8	6.6
5	50.0	2.0	41.7	1.010	22.6	1.101	.0396	.9612	.0388	.140	.277	19.5	3.1
7	50.0	4.0	39.6	1.010	24.7	1.101	.0792	.9239	.0761	.177	.430	30.2	−5.5
6	60.0	4.0	37.5	1.212	22.3	1.321	.2517	.778	.222	.543	.409	28.8	−6.5
8	40.0	4.0	45.0	0.808	24.1	0.881	−.0933	1.0977	−.0977	−.217	.450	31.6	−7.5
9	30.0	4.0	41.7	.606	37.6	.6605	−.2662	1.3000	−.3000	−.6395	.469	33.0	4.6

sugar solution. The 4-hr experimental points (circles) show a maximum appearing at about 0.3 on the c/c_0 axis. Similar maxima have shown up in numerous other investigations reported in the literature [19–26] for which various explanations have been proposed. The present theory, i.e. eq (5), does not predict these phenomena despite the fact that it appears to do so, as in figure 7. This is a result of the fact that the value of c in the abscissa is the *observed* concentration. The maximum in the calculated values would disappear if plotted against recomputed values of c determined from these least-square q-values according to eq (3). A horizontal shift would then result in the position of each of the calculated points (squares in fig. 7). The resultant adsorption curve connecting these new positions would resemble, in general appearance, the shape of the familiar Freundlich Isotherm.

From a physical point of view, the observed concentration c is not an independent variable, since its values cannot be preselected as can values of W/V and of c_0. It is significant that no maximum in the observed adsorption curve appears when q is plotted as a function of W/V instead of c for the 4-hr points of figure 7.

Regardless of whether the batch experiment is performed by holding c_0 constant (as was done here) or by holding W/V constant if in each case the time is held constant, the slope of the adsorption curve is always greater than zero according to eq (5). This may be proved by the following considerations:

At constant t, eq (5) expresses q as a function of two variables. Therefore, a differential change in q is given by eq (11)

$$dq=\left.\frac{\partial q}{\partial(W/V)}\right|_{c_0} d(W/V)+\left.\frac{\partial q}{\partial c_0}\right|_{W/V} dc_0. \qquad (11)$$

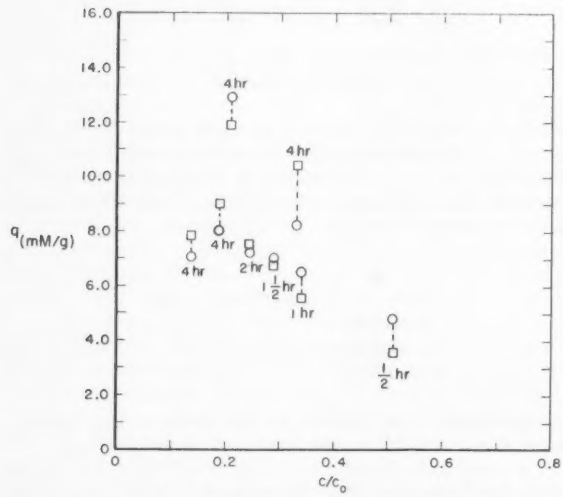

FIGURE 7. *Batch adsorption results for sulfate ion (contained in a Hawaiian raw sugar liquor) by a service bone char at designated durations of contact time.*

Experimental points are shown by circles, calculated points by squares.

When each variable, in turn, is held constant the slope of the adsorption curve may be expressed as

$$\left.\frac{\partial q}{\partial c}\right|_{c_0}=\left.\frac{\partial q}{\partial(W/V)}\right|_{c_0}\left.\frac{\partial(W/V)}{\partial c}\right|_{c_0} \qquad (12)$$

and

$$\left.\frac{\partial q}{\partial c}\right|_{W/V}=\left.\frac{\partial q}{\partial c_0}\right|_{W/V}\left.\frac{\partial c_0}{\partial c}\right|_{W/V} \qquad (13)$$

It is clear from inspection that $\left.\frac{\partial(W/V)}{\partial c}\right|_{c_0}$ is negative and that $\left.\frac{\partial c_0}{\partial c}\right|_{W/V}$ is positive. Now if it can be shown that $\left.\frac{\partial q}{\partial(W/V)}\right|_{c_0}$ is always negative and that $\left.\frac{\partial q}{\partial c_0}\right|_{W/V}$ is always positive, then it must follow that $\frac{dq}{dc}$ is greater than zero throughout its entire range.

Equation (5) may be differentiated with respect to w/v to obtain:

$$\left.\frac{\partial q}{\partial(W/V)}\right|_{c_0} =\frac{\left[\frac{q_0^2}{c_0}(c_0k_1t)\left(\frac{Wq_0}{Vc_0}-1\right)+\frac{q_0^2}{c_0}\right]e^{-\left(\frac{Wq_0}{Vc_0}-1\right)c_0k_1t}-\frac{q_0^2}{c_0}}{\left[\frac{Wq_0}{Vc_0}-e^{-\left(\frac{Wq_0}{Vc_0}-1\right)c_0k_1t}\right]^2} \qquad (14)$$

from which it can be shown that eq (14) is indeed negative providing its numerator is negative. This reduces to the requirement that:

$$e^{+\left(\frac{Wq_0}{Vc_0}-1\right)c_0k_1t}>1+\left(\frac{Wq_0}{Vc_0}-1\right)c_0k_1t.$$

When $\frac{Wq_0}{Vc_0}>1$ and the exponential term is expressed as a series expansion, the proof is self-evident. When $\frac{Wq_0}{Vc_0}<1$, the above inequality is rearranged to an equivalent form, namely:

$$\frac{1}{e^{+\left(1-\frac{Wq_0}{Vc_0}\right)c_0k_1t}} >\frac{1}{1+\left(1-\frac{Wq_0}{Vc_0}\right)c_0k_1t+\left(1-\frac{Wq_0}{Vc_0}\right)^2(c_0k_1t)^2+\ldots}$$

where the power series results from the reciprocal of $1-\left(1-\frac{Wq_0}{Vc_0}\right)c_0k_1t$. Again the inequality is proved by a term-for-term comparison with the series expansion of the exponential.

For the case where W/V is held constant, it can be shown again from eq (5) that:

$$\left.\frac{\partial q}{\partial c_0}\right|_{W/V} = \frac{\frac{q_0}{c_0}\left(\frac{Wq_0}{Vc_0}\right) - \left[\frac{q_0}{c_0}\left(\frac{Wq_0}{Vc_0}\right) + \frac{q_0}{c_0}(c_0 k_1 t)\left(\frac{Wq_0}{Vc_0} - 1\right)\right] e^{-\left(\frac{Wq_0}{Vc_0} - 1\right) c_0 k_1 t}}{\left[\frac{Wq_0}{Vc_0} - e^{-\left(\frac{Wq_0}{Vc_0} - 1\right) c_0 k_1 t}\right]^2} \tag{15}$$

and by the same type of reasoning as in the previous case, it follows that $\left.\frac{\partial q}{\partial c_0}\right|_{W/V} > 0$.

10. Simplified Method for Evaluating Parameters

Most of the present treatment included in eqs (11) through (15) has been concerned with the special requirements of eq (5) that q be considered a function of the ratio W/V or of c_0, but that t be held constant. The least-squares method (method 2 illustrated in the appendix) of determining the optimum values for q_0 and k_1 is exact and applicable in all cases—even when the values of the three independent variables are simultaneously changed from batch to batch. At best, however, the method is laborious, since it is based on a process of successive approximations. The experimental arrangement also is somewhat inefficient in that it limits each batch to one experimental point. The experimental setup would be much simpler if, say, only one flask were used and the course of adsorption as a function of time were measured *in situ*. This would be equivalent to the consideration of q as a function only of t. This gives rise to the simplest and quickest determination of q_0 and k_1 from only two measurements by judicious choice of the intervals. Let q_1 correspond to the time t_1, and q_2 to time t_2 such that $t_2 = 2t_1$. If eq (5) is solved for its exponential term and the data of these two experimental points are substituted back, the following pair of equations results:

$$\left.\begin{aligned} e^{-\left(\frac{Wq_0}{Vc_0} - 1\right) c_0 k_1 t_1} &= \frac{q_0 - q_1\left(\frac{Wq_0}{Vc_0}\right)}{q_0 - q_1} \\ e^{-2\left(\frac{Wq_0}{Vc_0} - 1\right) c_0 k_1 t_1} &= \frac{q_0 - q_2\left(\frac{Wq_0}{Vc_0}\right)}{q_0 - q_2} \end{aligned}\right\}. \tag{16}$$

They may be solved simultaneously by squaring both sides of the first equation and eliminating the exponent. The equation which remains may be solved directly for q_0 to yield eq (17).

$$q_0 = \frac{q_1^2\left[q_2\left(\frac{W}{Vc_0}\right) - 1\right]}{q_1^2\left(\frac{W}{Vc_0}\right) - 2q_1 + q_2}. \tag{17}$$

Then, by back substitution it can be shown that:

$$k_1 = \frac{\ln\left[\frac{q_0 - q_1\left(\frac{Wq_0}{Vc_0}\right)}{q_0 - q_1}\right]}{c_0 t_1\left(1 - \frac{Wq_0}{Vc_0}\right)}. \tag{18}$$

An excellent opportunity for testing the self-consistency of eqs (17) and (18) is afforded by the previously cited reference of Dryden and Kay [1]. They used a conductivity cell head attached to the adsorption flask to measure changes in concentration of aqueous acetic acid as a function of time. The adsorbent was steam-activated coconut carbon. The total duration of their adsorption experiment was 60 min (at 30±0.5 °C) at the end of which time, adsorption was virtually complete. The weight, W, of the carbon was 3.00 g; the volume V of solution was 100 ml; and the initial concentration c_0 of acetic acid was 0.0306 N. After the first 5 min, Dryden and Kay measured the following concentrations at the times indicated:

t	c
min	meq·ml^{-1}
10.0	0.0200
15.0	.0185
20.0	.0166
30.0	.0155
45.0	.0147
60.0	.0140

The 10.0 and 20.0 min data give rise to q_1 and q_2 values of 0.3533 and 0.4667 meq·g^{-1}, respectively, by application of eq (3). These, in turn, may be substituted in eqs (17) and (18) to yield q_0 and k_1 directly. A second independent determination results from the 15.0 and 30.0 min data and a third determination from the 30.0 and 60.0 min data. These determinations are, respectively:

q_0	k_1
meq·g^{-1}	ml·meq^{-1}·min^{-1}
0·576	3·94
·573	3·55
·565	3·74

In dimensions comparable to the work of the present paper this would correspond to about 570 μeq·g^{-1} for q_0 and about 0.22 ml·μeq^{-1}·hr^{-1} for k_1. It is seen, for example, that Dryden and Kay's charcoal exhibited about ten times the capacity for acetic acid adsorption from aqueous solution as did our service bone char for sulfate from a raw sugar liquor. Also, their rate constant was greater by about the same

factor despite their lower temperature, as might have been anticipated qualitatively because of the differences in viscosities.

The methods given in the appendix for determining the parameters from batch adsorption were devised for desk calculator computation. Where many batch experiments are to be made on a routine basis, or where it may be preferred to use eq (19) in place of eq (5) it is more practical to enlist the services of a digital computer.

11. General Equation When Desorption Is Appreciable

In the event that the desorption rate constant k_2 is retained in the integration of eq (1), the resultant adsorption equation becomes:

$$\frac{(M-N)-q}{(M+N)-q}=\frac{M-N}{M+N}\,e^{-2N\left(\frac{W}{V}\right)k_1t} \tag{19}$$

where

$$M=\frac{V}{2W}\left[\frac{k_2}{k_1}+c_0\left(1+\frac{Wq_0}{Vc_0}\right)\right]$$

and

$$N=\left(M^2-\frac{V}{W}\,q_0c_0\right)^{\frac{1}{2}}.$$

Equation (19) reduces to eq (5), as expected, when k_2 is set equal to zero. By the same token W/V is eliminated by means of eq (3), and it is interesting to show that as time, t, goes to infinity, equation (19) reduces to the familiar Langmuir adsorption isotherm:

$$\frac{q}{q_0}=\frac{Kc}{1+Kc} \tag{20}$$

where the equilibrium constant K is defined in the usual way as the ratio of the individual rate constants, k_1/k_2.

12. Summary

A batch adsorption equation was derived which expresses the amount of solute adsorbed per unit weight of adsorbent at constant temperature as a function of solution volume, concentration, amount of adsorbent, and time of contact. The equation is given in terms of only two constants, both of which have physical significance and are extremely useful in adsorption work. One of these parameters, q_0, is a measure of the maximum adsorptive capacity of the adsorbent for the solute or species adsorbed, while the other parameter, k_1, is the specific adsorption rate constant applicable at that temperature.

For known mixtures of different mesh (or grain size) of the same adsorbent the adsorptive capacity appeared to be an additive property.

The relative abundance of adsorption sites exhibited by a family of carbonaceous adsorbents for adsorption of organic colorant molecules was approximately proportional to the known surface areas of the adsorbents.

Adsorptive capacities and rate constants obtained from the batch adsorption equation were in substantial agreement with the numerical values for the same parameters obtained from column adsorption experiments performed simultaneously under identical conditions.

13. Appendix. General Methods for Calculating q_0 and k_1

13.1. Method 1

The first method illustrated is applicable to eq (4). Let $F_{(\mathrm{exp})}$ and $F_{(\mathrm{cal})}$ be defined such that

$$F_{(\mathrm{exp})}=\ln c_0/c \tag{1a}$$

and

$$F_{(\mathrm{cal})}=-\ln\,(1-q/q_0)+k_1\frac{\partial F_{(\mathrm{cal})}}{\partial k_1} \tag{2a}$$

$$\frac{\partial F_{(\mathrm{cal})}}{\partial k_1}=\left(\frac{W}{V}\,q_0-c_0\right)t \tag{3a}$$

$$\frac{\partial F_{(\mathrm{cal})}}{\partial q_0}=\frac{W}{V}\,k_1t-\frac{q/q_0^2}{1-q/q_0} \tag{4a}$$

and

$$\Delta F=F_{(\mathrm{exp})}-F_{(\mathrm{cal})} \tag{5a}$$

A value for q_0 is assumed. Now in the equation:

$$\Delta F=\ln c_0/c+\ln\,(1-q/q_0)-k_1\frac{\partial F_{(\mathrm{cal})}}{\partial k_1} \tag{6a}$$

which may be separately determined for each point, numerical values are assignable to all quantities except k_1 and ΔF. A "best" value of k_1 consistent with the initial choice of q_0 is obtained by least-squaring ΔF over all points. This results in the equation:

$$k_1\sum\left(\frac{\partial F_{(\mathrm{cal})}}{\partial k_1}\right)^2=\sum\left\{\frac{\partial F_{(\mathrm{cal})}}{\partial k_1}\,[\ln\,c_0/c+\ln\,(1-q/q_0)]\right\} \tag{7a}$$

from which the first k_1 is evaluated.

If both q_0 and k_1 were now to be "corrected" by adding to each the quantities Δq_0 and Δk_1, respectively, according to the first terms of a Taylor's expansion in two variables [27], one of the resultant normal equations obtained from all the points would be:

$$\Delta q_0\sum\left(\frac{\partial F_{(\mathrm{cal})}}{\partial q_0}\right)^2+\Delta k_1\sum\left(\frac{\partial F_{(\mathrm{cal})}}{\partial q_0}\,\frac{\partial F_{(\mathrm{cal})}}{\partial k_1}\right)=\sum\left(\frac{\partial F_{(\mathrm{cal})}}{\partial q_0}\cdot\Delta F\right) \tag{8a}$$

However, in the present application k_1 is held constant temporarily while q_0 is allowed to vary, hence the second term of eq (8a) vanishes and there results:

$$\Delta q_0 \sum \left(\frac{\partial F_{(calc)}}{\partial q_0}\right)^2 = \sum \left(\frac{\partial F_{(calc)}}{\partial q_0} \cdot \Delta F\right) \qquad (9a)$$

from which a Δq_0 is computed.

The sign of Δq_0 indicates the direction of the next choice for q_0 although its magnitude usually will grossly underestimate the extent of the correction. However, a plot of Δq_0 against q_0 quickly discloses, after a few trials, the choice of q_0 which causes Δq_0 to vanish. Concurrently, it can be verified that as successive q_0 choices are made closing the gap between the plus and minus values of Δq_0, the magnitude of the corresponding new sums computed for $\Sigma(\Delta F)^2$ tend toward a minimum.

Method 1 is subject to some bias, partly because it compares solution concentrations instead of amounts absorbed per gram and partly because the comparison is logarithmic. Despite these disadvantages, it requires successive choices of q_0 only, and it is applicable over wide ranges. An example of the application of method 1 was indicated in table 1b.

13.2. Method 2

The second method is applicable to eq (5). It is free from the serious limitations of method 1 and follows a more conventional procedure, as given by Scarborough [27]. The value of q obtained by substituting the experimentally observed value of c into eq (3) is termed $q_{(obs)}$. For a given choice of k_1 and q_0, eq (5) may be used to calculate a q for each combination of W, V, t, and c_0, and this value is designated $q_{(calc)}$. Thus, $\Delta q = q_{(obs)} - q_{(calc)}$. By obtaining partial derivatives of q in eq (5) it can be verified that:

$$\frac{\partial q}{\partial k_1} = \frac{\left(\frac{Wq_0}{Vc_0}-1\right)^2 c_0 q_0 t\, e^{-\left(\frac{Wq_0}{Vc_0}-1\right) c_0 k_1 t}}{\left[\frac{Wq_0}{Vc_0} - e^{-\left(\frac{Wq_0}{Vc_0}-1\right) c_0 k_1 t}\right]^2} \qquad (10a)$$

and

$$\frac{\partial q}{\partial q_0} = \frac{q_{(calc)}}{q_0} + \frac{\frac{Wq_0}{Vc_0}\left\{\left[\left(\frac{Wq_0}{Vc_0}-1\right) c_0 k_1 t + 1\right] e^{-\left(\frac{Wq_0}{Vc_0}-1\right) c_0 k_1 t} - 1\right\}}{\left[\frac{Wq_0}{Vc_0} - e^{-\left(\frac{Wq_0}{Vc_0}-1\right) c_0 k_1 t}\right]^2}. \qquad (11a)$$

For a particular choice of k_1 and q_0, the quantity $\Sigma(\Delta q)^2$ (summed over all n measurements) is a measure of goodness to fit . . . the smaller the summation value, the better the choice of k_1 and q_0. The initial choice of these parameters has been successively improved by adding to k_1 the quantity:

$$\Delta k_1 = \frac{\Sigma\left(\frac{\partial q}{\partial k_1} \cdot \Delta q\right)}{\Sigma\left(\frac{\partial q}{\partial k_1}\right)^2} \qquad (12a)$$

and by adding to q_0 the quantity:

$$\Delta q_0 = \frac{\Sigma\left(\frac{\partial q}{\partial q_0} \cdot \Delta q\right)}{\Sigma\left(\frac{\partial q}{\partial q_0}\right)^2}. \qquad (13a)$$

It should be pointed out that this procedure assigns *all* of the variability of q first to one parameter and then to the other. Thus, it tends to *over-correct*, but by a lesser amount each trial. After a few such trials have been made, in a given experiment, if is usually possible to converge more quickly by a weighted averaging of the results so far. This separate adjustment has been found to work consistently better than by assigning the variability in q to a *simultaneous* adjustment in k_1 and q_0.

Example: In a batch experiment for adsorption of sulfate ion on service bone char 117–B the following data were obtained: $c_0 = 9.90\ \mu M.ml^{-1}$.

Sample No.	W/V	t	c/c₀	q(obs)
	g·ml⁻¹	hr		μM.g⁻¹
2	1.010	0.5	0.512	4.78
3	1.010	1.0	.339	6.47
4	1.010	1.5	.291	6.95
5	1.010	2.0	.244	7.10
7	1.010	4.0	.188	7.96
6	1.212	4.0	.135	7.05
8	0.808	4.0	.330	8.21
9	.606	4.0	.209	12.92

By starting with an initially assumed value for q_0 of about 33 using the first method, a corresponding value of 0.017 for k_1 was determined. After four trials had been made, improved values of $q_0 \approx 15.5$ and $k_1 \approx 0.0437$ were obtained. For most purposes these approximate values might be sufficient and consistent with experimental error. However, for purposes of illustration, the second method was used to refine these results still further. The following table summarizes the successive improvements:

Trial	Values assumed		Σ(Δq)²	Resultant corrections	
	q_0	k_1		Δq_0	Δk_1
	μM·g⁻¹	ml·μM⁻¹·hr⁻¹	μM²·g⁻²	μM·g⁻¹	ml·μM⁻¹·hr⁻¹
1	15.53	0.0437	21.63	+3.99	+0.0186
2	19.32	.0623	12.20	−2.39	−.0105
3	16.93	.0518	11.56	+1.43	+.0083
4	18.36	.0601	10.57	−1.10	−.0043
5	17.73	.0573	10.29	−0.017	+.0011

Thus it is seen after the fifth trial that even though the degree of fit (as measured by $\Sigma(\Delta q)^2$) had been improved by a factor of two, the values of q_0 and k_1 had only changed from 15.5 to 17.7 and from 0.044 to 0.057, respectively. In addition, the final

Δq_0 and Δk_1, quantities amounted to changes of less than 0.1 and 2 percent, respectively, in q_0 and k_1. Further refinement could not be justified.

The author thanks members of the Bone Char Research Project for their assistance in carrying out much of the experimental work.

14. References

[1] C. E. Dryden and W. B. Kay, Ind. Eng. Chem. **46**, 2294 (1954).
[2] S. Eagle and J. W. Scott, Ind. Eng. Chem. **42**, 1287 (1950).
[3] R. L. Geddes, Trans. Am. Inst. Chem. Engrs. **42**, 88 (1946).
[4] W. D. Harkins and D. M. Gans, J. Am. Chem. Soc. **53**, 2804 (1931).
[5] H. A. Smith and J. F. Fuzek, J. Am. Chem. Soc. **68**, 229 (1946).
[6] E. B. Greenhill, Trans. Faraday Soc. **45**, 625 (1949).
[7] E. R. Linner and A. P. Williams, J. Phys. & Colloid. Chem. **54**, 610 (1950).
[8] Y. Fu, R. S. Hansen, and F. E. Bartell, J. Phys. & Colloid. Chem. **52**, 374 (1948).
[9] R. S. Hansen, Y. Fu, and F. E. Bartell, J. Phys. & Colloid. Chem. **53**, 769 (1949).
[10] F. E. Bartell and D. J. Donahue, J. Phys. Chem. **56** 665 (1952).
[11] W. W. Ewing and F. W. J. Liu, J. Colloid. Sci. **8**, 209 (1953).
[12] W. V. Loebenstein, Proc. of Fifth Tech. Sess. on Bone Char, 253 (1957).
[13] H. S. Harned, J. Am. Chem. Soc. **42**, 372 (1920).
[14] A. Gee, L. P. Domingues, and V. R. Deitz, Anal. Chem. **26**, 1487 (1954).
[15] L. P. Domingues, Proc. of Fourth Tech. Sess. on Bone Char, 347 (1955).
[16] V. R. Deitz, Ann. N.Y. Acad. Sci. **49**, 315, (1948).
[17] Linus Pauling, The Nature of the Chemical Bond, Cornell Univ. Press (1948) p 240.
[18] W. Hirst and J. K. Lancaster, Research (London) **3**, 337 (1950).
[19] M. L. Corrin, E. L. Lind. A. Roginsky and W. D. Harkins, J. Colloid. Sci. **4**, 485 (1949).
[20] F. H. Nestler and H. G. Cassidy, J. Am. Chem. Soc. **72**, 680 (1950).
[21] R. S. Hansen and W. V. Fackler, Jr., J. Phys. Chem. **57**, 634 (1953).
[22] R. D. Vold and A. K. Phansalkar, Rec. Trav. Chim. **74**, 41 (1955).
[23] A. Fava and H. Eyring, J. Phys. Chem. **60**, 890 (1956).
[24] B. Tamamushi and K. Tamaki, Trans. Faraday Soc. **55**, 1007 (1959).
[25] F. H. Sexsmith and H. J. White, Jr., J. Colloid. Sci. **14**, 598 (1959).
[26] Y. Gotshal, L. Rebenfeld, and H. J. White, Jr. *ibid*, 619 (1959).
[27] J. B. Scarborough, Numerical Mathematical Analysis 2d Ed., The Johns Hopkins Press, Baltimore (1950) pp 451–469.

(Paper 66A6–186)

JOURNAL OF RESEARCH of the National Bureau of Standards—A. Physics and Chemistry
Vol. 66A, No. 6, November–December 1962

Separation of Hafnium from Zirconium and Their Determination: Separation by Anion-Exchange

Lawrence A. Machlan and John L. Hague

(August 2, 1962)

A procedure is described for the separation of hafnium from zirconium and their individual determination. The sample is dissolved in sulfuric and hydrofluoric acids and the hydrofluoric acid removed by fuming. After dilution with water, the solution is transferred to a column containing a strong quaternary amine anion-exchange resin (Dowex-1). The hafnium is eluted with diluted (3.5 percent by volume) sulfuric acid solution. Zirconium is removed by elution with 10 percent by volume sulfuric acid solution. The elements are precipitated with cupferron, ignited, and weighed as the oxides. For samples containing from twenty to eighty percent of zirconium, a second separation of the hafnium fraction using the column is necessary.

1. Introduction

The use of hafnium and zirconium in nuclear applications has made the separation and determination of the two an important problem. Because hafnium and zirconium are very difficult to distinguish chemically, they can, for many uses, be considered as one constituent. However, since hafnium and zirconium have very different nuclear properties, it is important to know the relative amounts of each present in materials used in the nuclear reactor field.

The difficulties encountered in separating hafnium from zirconium are well known [6, 7].[1] It has been shown [1] that a separation of hafnium and zirconium can be obtained by anion-exchange in sulfuric acid solution.

The method described here has been used to determine hafnium and zirconium in mixtures of the two elements containing 80 percent or less of zirconium. Work is in progress to apply the method to materials containing more than 80 percent of zirconium.

The samples are dissolved in a sulfuric-hydrofluoric acid solution and the hydrofluoric acid is fumed off. The solution is diluted with water to 3.5 percent by volume of sulfuric acid and transferred to an anion-exchange column. The hafnium is eluted with a 3.5 percent sulfuric acid solution and then the zirconium is eluted with a 10 percent sulfuric acid solution. For samples containing more than about 20 percent of zirconium the hafnium fraction may contain some zirconium and a second separation using the column is necessary to insure complete separation. The hafnium and zirconium are precipitated with cupferron, ignited, and weighed as HfO_2 and ZrO_2.

The procedure for samples containing less than 20 percent of zirconium requires approximately 3 days to carry to completion, as about 12 hr are required for the ion-exchange separation, and the remaining time is required for dissolving the sample and for making the cupferron precipitations.

[1] Figures in brackets indicate the literature references at the end of this paper.

2. Procedures

2.1. Ion-Exchange Columns

The columns used in these experiments were constructed of polystyrene tubes approximately 12 in. long and 1 in. i.d. A simple column can be prepared from such tubing as follows: Insert a piece of polystyrene tubing 6 in. long, 3/16 in. o.d. (with a 1/16 in. wall) through a No. 5 waxed, rubber stopper, so that one end of the tubing is flush with the small end of the stopper. Attach another 6 in. length of the same tubing with a 2-in. length of Tygon R tubing. Insert the rubber stopper into the bottom of the 1-in. i.d. tube. Attach a hose-cock clamp, used to control the flow rate, to the Tygon tubing. Columns suitable for continuous operation have previously been described for both glass [4] and plastic [5] assemblies, and these are convenient to use if a number of analyses are to be performed.

The anion-exchange resins used were Dowex-1, 200- to 400-mesh, having 8 percent of divinylbenzene crosslinkages. Experience during several years has shown that the mesh size of these resins may vary considerably from lot to lot. To select resin of suitable size, the material as received is air-dried, and sieved through a 270-mesh sieve. Most of the very fine material is removed from the fraction passing the 270-mesh sieve, as follows: Prepare a suspension of the resin in diluted [2] hydrochloric acid (1 + 19). The coarser fraction is allowed to settle for 10 to 15 min, and the fines removed by decantation. Repeat the process several times, until most of the very fine material is removed.

Load the column with resin as follows: Cover the bottom of the column with a 1/4- to 3/8-in. layer of acid-resistant, polyvinyl chloride plastic "wool." Add

[2] Diluted hydrochloric acid (1 + 19) denotes 1 volume of concentrated hydrochloric acid, sp gr 1.18, diluted with 19 volumes of water. If no dilution is specified, the concentrated analytical reagent is meant.

portions of the resin suspension so as to obtain a settled column of the resin that is 22 cm high. Wash the loaded column with approximately 100 ml of diluted nitric acid (1+9), and then perform several washing cycles by alternate additions of diluted hydrochloric acid (1+9) and diluted hydrochloric acid (3+1) to remove the remaining fines. Finally, wash the column with diluted sulfuric acid (7+193), to convert the resin to the sulfate form. Approximately 350 to 400 ml of sulfuric acid solution will be required, and the removal of the chloride can be followed by testing portions of the eluate with silver nitrate solution. The resin charge should not be allowed to become dry.

2.2. Reagents

Sulfuric acid solution (3.5 percent).—Add 70 ml of sulfuric acid to 1,930 ml of water, mix well, and cool to room temperature. This solution is referred to as 3.5 percent sulfuric acid solution in the procedure.

Cupferron solution (60 g/liter).—Dissolve 30 g of cupferron in 450 ml of water, dilute to 500 ml, and filter through a dry filter. This solution should be cooled to about 5 °C and prepared as needed, as the solution is not stable.

Cupferron wash solution.—Add 25 ml of cupferron solution to 975 ml of cold (5 °C) diluted hydrochloric acid (1+9). Prepare as needed.

2.3. Procedure

Transfer 0.5 g of the metal sample (accurately weighed) to a covered 25-ml platinum crucible and add a suitable quantity (14 ml for samples containing less than 20 percent of zirconium, 21 ml for samples containing from 20 to 60 percent of zirconium, and 28 ml, with some evaporation, for samples containing from 60 to 80 percent of zirconium) of diluted sulfuric acid (1+3) and 5 to 6 drops of hydrofluoric acid. The sample will dissolve at room temperature. (If the sample is in the oxide form transfer an amount of sample equal to 0.5 g of hafnium and zirconium to the crucible, and add a suitable quantity (see above) of diluted sulfuric acid (1+3) and 2 to 3 ml of hydrofluoric acid. Heat gently on an air bath to dissolve.) After the sample dissolves, wash the cover with water and place the uncovered crucible on a sand or air bath. Evaporate the solution to fumes of sulfuric acid, cool, and wash down the walls of the crucible with water. Evaporate the solution to fumes again, cool, quantitatively transfer the solution to a 400-ml beaker, and add sufficient water to give a 3.5 percent sulfuric acid solution.

Transfer the solution of the sample in small increments (10 to 15 ml) to the equilibrated ion-exchange column. Wash the beaker four or five times with 5-ml portions of the 3.5 percent sulfuric acid solution, transferring the washings to the column and allowing the solution to drain to the top of the resin each time. Finally wash down the sides of the column several times with a total of approximately 50 ml of the same solution.

a. For Samples Containing Less Than 20 Percent of Zirconium

Discard the first 125 ml[3] of solution from the column. Continue adding the 3.5 percent sulfuric acid solution. Collect the second fraction of 550 ml (see footnote 3), containing the hafnium, in an 800-ml beaker. Replace the beaker with a 600-ml beaker to catch the zirconium fraction. Allow the solution to drain to the top of the resin and wash the sides of the column with 3 or 4 portions (a total of about 20 ml) of diluted sulfuric acid (1+9), allowing the solution to drain to the top of the resin each time. Add a total of 250 ml of diluted sulfuric acid (1+9) and remove the beaker containing the zirconium fraction. Equilibrate the ion-exchange column for the next elution cycle by passing 400 ml of 3.5 percent sulfuric acid solution through the resin and allowing the solution to drain to the top of the resin.

To the second fraction, containing the hafnium, add 65 ml of hydrochloric acid. Cool to 5 °C, and add slowly while stirring, 100 ml of cupferron solution. Add a ball of paper pulp equivalent to about one 11-cm filter paper, stir until the pulp is well dispersed, and allow the precipitate to settle. Filter through a double 7-cm close-textured filter paper fitted to a Büchner funnel and precoated with some paper pulp. Transfer the precipitate to the funnel and wash, using 300 ml of cupferron wash solution. Transfer the precipitate and paper to a weighed 25-ml platinum crucible, and ignite at a low temperature until the carbon is gone. Finally ignite to constant weight at 1,100 °C, and weigh as hafnium dioxide.

To the third fraction, containing the zirconium, add 15 ml of hydrochloric acid. Cool to 5 °C and add slowly with stirring 50 ml of cupferron solution. Add a ball of paper pulp equivalent to about one 11-cm filter paper, stir, and allow the precipitate to settle. Filter, wash, and ignite the zirconium precipitate as described for hafnium. Weigh the zirconium as the dioxide.

b. For Samples Containing From 20 to 80 Percent of Zirconium

Discard the first 125 ml (see footnote 3) of solution from the column. Add a sufficient[4] quantity of 3.5 percent sulfuric acid solution to elute all of the hafnium and some (10 to 50 mg) of the zirconium. Collect this second fraction in an 800-ml beaker. Replace the beaker with a 600-ml beaker and continue the elution of zirconium as described in section 2.3a.

To the second fraction, containing the hafnium, and some zirconium, add 65 ml of hydrochloric acid, and continue the procedure as described for hafnium in section 2.3a, until the precipitate is ignited at low temperature. Reserve the oxides for a second separation using the column.

To the third fraction, containing zirconium, precipitate using 50 to 100 ml of cupferron solution,

[3] Each column must be calibrated to determine the volume of solution needed to elute the hafnium and zirconium. This is necessary because the resins and column loadings vary somewhat with different lots of resin.

[4] The quantity, approximately 500 to 600 ml, will depend on resin, column loading, and relative amounts of hafnium and zirconium.

filter, and ignite as described for zirconium in section 2.3a. This is zirconium fraction one.

To the reserved oxides from the second fraction, add 14 ml of diluted sulfuric acid (1+3) and 1 to 2 ml of hydrofluoric acid. Heat gently on an air bath to dissolve. After the oxides dissolve, wash the cover with water and place the uncovered crucible on a sand or air bath. Evaporate the solution to fumes of sulfuric acid, cool, and wash down the walls of the crucible with water. Evaporate the solution to fumes again, cool, quantitatively transfer the solution to a 250-ml beaker, and dilute to 100 ml with water.

Transfer the solution in small increments (10 to 15 ml) to the equilibrated ion-exchange column. Wash the beaker four or five times with 5-ml portions of the 3.5 percent sulfuric acid solution, transferring the washings to the column. Finally wash down the sides of the column several times with approximately 50 ml of the same solution. Continue as described in section 2.3a to obtain the hafnium fraction and zirconium fraction two. Calculate the zirconium percentage from the sum of the two zirconium fractions and the hafnium percentage from the final hafnium fraction.

3. Elution of Elements With Sulfuric Acid Solutions

It has been shown previously [1] that hafnium can be separated from zirconium using 3.5 percent sulfuric acid solution to elute from resin having 8 percent of divinylbenzene crosslinkages having a maximum particle-sizing of about 50μ (passing through a 270-mesh sieve). To obtain more separation the height of the resin column was increased to 22 cm. This separation, while not as great as other separations using ion-exchange [2, 3, 8, 9], is adequate if care is taken in setting up the columns, calibrating each column, and in preparing the solution used for the ion-exchange separation. The first three curves in figure 1 give the separation of hafnium from zirconi-

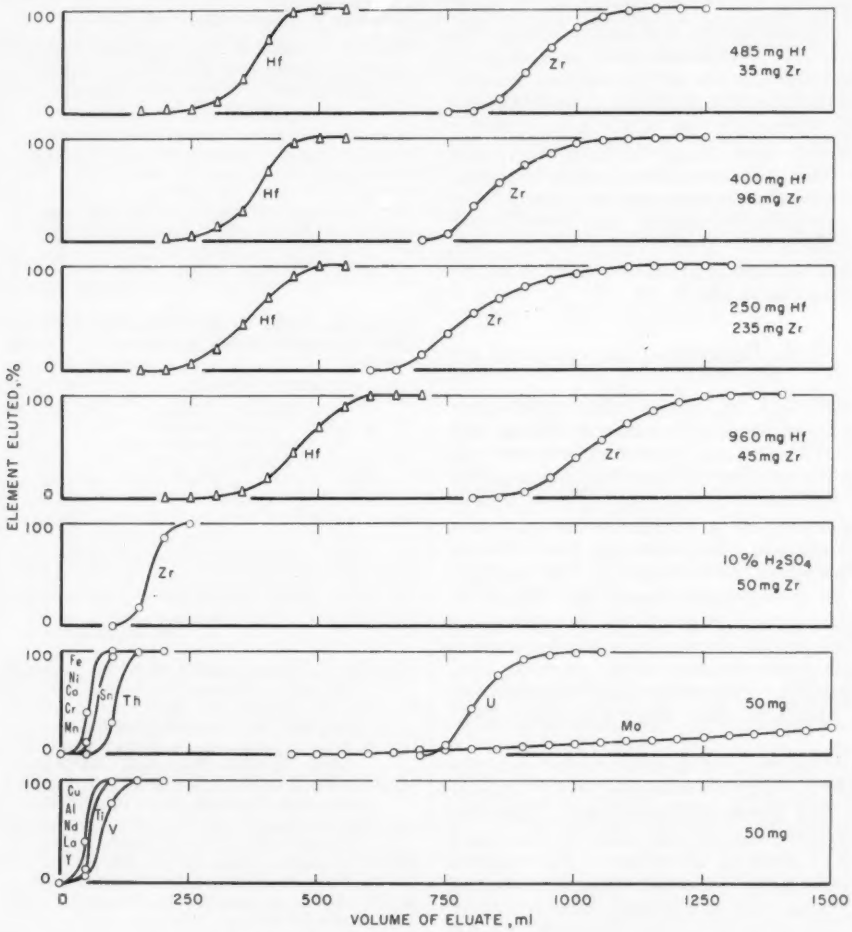

FIGURE 1. *Elution behavior of elements.*

um in 0.5 g samples of increasing zirconium-hafnium ratio by elution with 3.5 percent sulfuric acid solution. The fourth curve shows the separation obtained on a 1 g sample of hafnium metal by elution with 3.5 percent sulfuric acid solution. To obtain a reasonable volume of separation between the hafnium and the zirconium fractions, it is recommended that 0.5 g samples be used and that samples containing more than 20 percent of zirconium be determined by a double ion-exchange separation. To reduce the volume of solution needed to elute the zirconium, it was eluted with a 10 percent sulfuric acid solution. The fifth curve gives the zirconium elution curve in 10 percent sulfuric acid solution.

The last two curves give the elution characteristics of some other elements in 3.5 percent sulfuric acid solution. Iron (3), nickel (2), cobalt (2), chromium (3), manganese (2), copper (2), aluminum (3), neodymium (3), lanthanum (3), and yttrium (3) are eluted from the column without delay. Tin (4), thorium (4), titanium (4), and vanadium (5) are only slightly absorbed, all being eluted in 3 or 4 column volumes. Uranium (6) and molybdenum (6) are strongly absorbed. Elements that do not precipitate with cupferron, such as chromium, nickel, and cobalt, will not interfere with the determination of hafnium and zirconium by the recommended procedure. Elements that do precipitate with cupferron, such as iron, titanium, and molybdenum, would interfere in the recommended procedure. These elements are partially eluted into the discard fraction but to eliminate these interferences, the oxides can be redissolved and a mandelic acid or phosphate precipitation made.

4. Results

The results obtained by the recommended procedure on a series of synthetic oxide mixtures are given in table 1. The first six experiments were done by the procedure recommended for samples containing less than 20 percent of zirconium. These values require little comment, being within the usual limits of gravimetric methods. Experiments 7 to 10 were done by the procedure recommended for samples containing from 20 to 80 percent zirconium. These results show that for these compositions recoveries are within 2 to 5 parts per thousand. The oxides used in these experiments were obtained from previous ion-exchange separations. Spectrographic examination of these oxides indicated less than 100 ppm cross contamination.

The results obtained on synthetic metal samples are given in table 2. The metals used were "reactor grade" metals. The zirconium was nearly hafnium-free and the hafnium (sample 1 in table 3) contained approximately 2.14 percent zirconium. The zirconium added was calculated from the zirconium in the hafnium metal and the zirconium metal added. Spectrographic examination of the recovered oxides indicated less than 100 ppm zirconium in the hafnium fraction and less than 1 percent hafnium in the zirconium fraction.

The results obtained on two "reactor grade" hafnium metals is given in table 3.

TABLE 1. *Results of determinations of zirconium and hafnium by the recommended procedure in various synthetic oxide mixtures*

Experiment	Hafnium oxide			Zirconium oxide		
	Added	Found	Difference	Added	Found	Difference
	mg	*mg*	*mg*	*mg*	*mg*	*mg*
1[a]	575.3	574.9	−0.4	33.6	33.7	+0.1
2[a]	574.9	574.7	−.2	33.9	33.6	−.3
3[a]	574.7	574.6	−.1	33.5	33.4	−.1
4[a]	476.8	476.6	−.2	133.2	133.2	.0
5[a]	476.6	476.3	−.3	132.2	132.0	−.2
6[a]	476.2	475.6	−.6	127.2	127.2	.0
7[b]	294.9	295.6	+.7	334.1	335.3	+1.2
8[b]	294.0	293.8	−.2	331.8	331.6	−.2
9[b]	146.0	146.2	+.2	502.1	502.8	+.7
10[b]	146.2	146.4	+.2	499.4	498.6	−.8

[a] Experiments using the procedure: "For samples containing less than 20 percent of zirconium."
[b] Experiments using the procedure: "For samples containing from 20 to 80 percent of zirconium."

TABLE 2. *Results of determinations of zirconium and hafnium by the recommended procedure in synthetic metal samples*

Experiment	Hafnium			Zirconium		
	Added	Found	Difference	Added	Found	Difference
	mg	*mg*	*mg*	*mg*	*mg*	*mg*
1	473.8	474.7	+0.9	36.2	35.6	−0.6
2	464.2	465.2	+1.0	36.1	35.6	−.5
3	479.9	479.8	−0.1	28.5	28.6	+.1

TABLE 3. *Results of determinations of zirconium and hafnium by the recommended procedure in "reactor grade" hafnium metals*

Sample number	Sample weight	Hafnium	Zirconium
	g	%	%
1	0.5	97.97	2.15
1	.5	97.98	2.06
1	.5	97.81	2.21
1	.5	97.85	2.16
2	.5	95.26	4.82
2	.5	95.29	4.79
2	.5	95.35	4.77

5. References

[1] John L. Hague and Lawrence A. Machlan, J. Research NBS **65A** (Phys. and Chem.) No. 1, 75 (1961).
[2] John L. Hague and Lawrence A. Machlan, J. Research NBS **62,** 53 (1959) RP2929.
[3] John L. Hague, E. D. Brown, and H. A. Bright, J. Research NBS **53,** 262 (1952) RP2542.
[4] John L. Hague, E. E. Maczkowske, and H. A. Bright, J. Research NBS **53,** 353 (1954) RP2552.
[5] John L. Hague and Lawrence A. Machlan, J. Research NBS **62,** 13 (1959) RP2923.
[6] R. B. Hahn, Anal. Chem. **23,** 1259 (1951).
[7] G. Hevesy, Chem. Revs. **2,** 12 (1925).
[8] K. A. Kraus and G. E. Moore, J. Am. Chem. Soc. **75,** 1460 (1953).
[9] G. E. Moore and K. A Kraus, J. Am. Chem. Soc. **74,** 843 (1952).

(Paper 66A6–187)

JOURNAL OF RESEARCH of the National Bureau of Standards—A. Physics and Chemistry
Vol. 66A, No. 6, November–December 1962

Publications of the National Bureau of Standards*

Selected Abstracts

Structure shielding against fallout radiation from nuclear weapons, L. V. Spencer, *NBS Mono. 42 (June 1, 1962) 75 cents.*
The theory of structure shielding from fallout gamma radiation is developed to the point of applications to elementary structure types. Examples discussed in the text include the density interface, shielded foxhole or basement, light superstructure, vertical wall, blockhouse, vents, compartmentalization effects, and mazes. A large number of engineering charts and graphs are presented for engineering calculations, including many obtained from angular distributions of the exposure dose. Results are given for a fission spectrum, and for Co^{60} and Cs^{137} sources. This information has been obtained almost completely by machine calculations utilizing basic cross section data. A number of sources of experimental data are mentioned, but detailed comparisons with experiment are not included.

Basic magnetic quantities and the measurement of the magnetic properties of materials, R. L. Sanford and I. L. Cooter, *NBS Mono. 47 (May 21, 1962) 30 cents.*
This paper gives general information regarding the two basic quantities, magnetic induction, B, and magnetizing force, H, and also the magnetic constant Γ_m (often designated by the symbols μ_s and μ_0. Information is also given regarding the magnetic properties of various materials and methods and apparatus commonly used in the Magnetic Measurements Section for measuring these properties by means of reversed direct current or alternating currents of low frequency. Magnetic measurements peculiar to high frequencies are not discussed. In view of the gradual adoption of the rationalized mksa system of units, this system is included as well as the classical cgs electromagnetic system.

Determination of total X-ray beam energy with a calibrated ionization chamber, J. S. Pruitt and S. R. Domen, *NBS Mono. 48 (June 5, 1962) 20 cents.*
This report describes the use of an air-filled aluminum-alloy ionization chamber to determine the energy transported by a bremsstrahlung beam with maximum photon energy in the range 6 to 170 Mev. The experimental calibrations of this chamber over this energy range are given, as well as the results of calibration experiments made with a 250-kv constant-potential X-ray tube and with Cs^{137} and Co^{60} gamma-rays. Information is presented about the change in calibration when the chamber is used with different experimental conditions, and when either its dimensions or its alloy composition are changed slightly. This report can be used to construct a replica chamber and to determine its absolute calibration between 6 and 170 Mev under a variety of experimental conditions.

Annotated bibliography on soft X-ray spectroscopy, H. Yakowitz and J. R. Cuthill, *NBS Mono. 52 (June 29, 1962) $1.00.*
About 550 references are contained in this bibliography which includes, it is believed, a complete coverage of the soft X-ray literature since 1950 and through 1960. Some references to earlier work are given but the general review references, listed separately, give an adequate coverage of the earlier work.
The emphasis is on the application of soft X-ray spectroscopy to the study of valence band electronic states in metals and alloys and therefore the spectral region of 25 to 800 angstroms involving ruled glass grating spectrometers is of principal interest. However, a wealth of data have been gathered, primarily by the Russians, on valence electronic states by means of high energy transitions where crystal spectrometers are satisfactory. These references and any X-ray work leading to the distribution of valence electronic states are included regardless of the transitions employed.
In addition to soft X-ray data, references on all pertinent aspects of the apparatus and experimental problems are included. Also listed separately are references of value in corroborating soft X-ray data with other results, such as energy band calculations.
Subject, author, X-ray band, material, and other indices are included.

Weights and measures administration, *NBS Handb. 82 (June 22, 1962) $1.75. (Supersedes H26)*
This Handbook presents a comprehensive picture of what an effective weights and measures program should embrace. The principles set forth are specifically recommended by the National Conference on Weights and Measures to all weights and measures officials and to the legislative bodies of States, counties, and cities. The Handbook should be helpful to agencies and individuals interested in setting up weights and measures supervision in a State or sub-division thereof, or concerned with strengthening such supervision where it now exists. It should also be useful as a training manual for new weights and measures officials and as a manual for review training for experienced officials, in the area of fundamental principles and general procedures.

OMNIFORM I: A general purpose machine program for the calculation of tables of functions given explicitly in terms of one variable, J. Hilsenrath and G. M. Galler, *NBS Tech. Note 125 (PB161626) (1962) $1.00.*
A general purpose computer program, designed for use by non-programmers requiring computation of tables of functions written explicitly in terms of one variable, is described. The program features include: 22 types of elementary and special functions; provision for taking of functions of functions, table read-in, flexible print-out; and standardized input to a variety of problems. The use of the program is illustrated with a number of sample problems.

The thermodynamic properties of nitrogen from 64 to 300 °K between 0.1 and 200 atmospheres, T. R. Strobridge, *NBS Tech. Note 129 (PB161630) (1962) $2.25.*
The internal energy, enthalpy, entropy, and specific volume of molecular nitrogen are derived and tabulated as functions of temperature and pressure. In addition to a mathematical model for the pressure-volume-temperature surface, accurate functions are given for the representation of the vapor pressure, density of saturated liquid, specific heat of saturated liquid, and the specific heat at zero pressure.
Tabular values in British units over the same pressure and temperature range are available as Supplement A of this Technical Note.

Detailed techniques for preparing and using hard gallium alloys, G. G. Harman, *NBS Tech. Note 140 (PB161651) (1962) 75 cents.*
This report presents an expansion and clarification of techniques for preparing and using dental-amalgam-type gallium alloys for industrial and scientific uses that were previously published in the *Review of Scientific Instruments.* In addition, new material, such as hardness of the alloys and discussions of the bonding mechanism are presented. A different class of bonding alloys based on the same principals but not incorporating gallium are described, along with application details.

Dielectric constant of liquid parahydrogen, R. J. Corruccini, *NBS Tech. Note 144 (PB161645) (1962) 50 cents.*
It is shown that the available data on the dielectric constant of hydrogen conform to the Clausius-Mossotti equation within the probable experimental errors. The published data cover temperatures from the triple point ($\sim$14 °K) to well above room temperature and a thousandfold range of densities.

Using an average value of the specific polarization, tables of the dielectric constant of the liquid have been computed for temperatures from the triple point (13.803 °K) to 32 °K (58 °R) and pressures from saturation to 340 atmospheres.

A wire exploder for generating cylindrical shock waves in a controlled atmosphere, D. L. Jones and K. B. Earnshaw, *NBS Tech Note 148 (PB161649) (1962) 50 cents.*
A design for a rugged exploding wire device is given. This device permits the study of strong cylindrical shock waves in controlled atmospheres using optical and microwave techniques. Adequate detail and pictures are given to allow construction of the device.

Utilization of tritium and carbon-14 in studies of isotope effects, H. S. Isbell, H. L. Frush, and L. T. Sniegoski, *Book, Tritium in the Physical and Biological Sciences II, 94–101 (International Atomic Energy Agency, Vienna, Austria, 1962).*
The utility of tritium in organic research has been augmented by the development of a simple method for determining C^{14} and tritium in the same sample. The non-volatile, radioactive material, in a film that is "infinitely thick" to tritium radiation, is counted in a windowless, gas-flow proportional counter; the film is then re-counted when covered with an absorber that stops all radiation from tritium, but allows a fraction of that from C^{14} to pass. The absorber used was ¼-mil, double-aluminized "Mylar" film.
By introduction of one isotope at a point removed from the reaction center, an isotope effect for the other can be determined from changes in the tritium-C^{14} ratio in the reactant and/or products as the reaction proceeds. Carriers of reactant, products or derivatives can be added at any point to facilitate isolation, because the analytical method depends primarily on the tritium-C^{14} ratio.
The isotope-effects in the bacterial oxidation of six C^{-14}-or tritium-labeled D-mannitols and three tritium-labeled D-glucitols have been studied. Primary isotope effects (large for tritium, small for carbon-14) were found when the radioisotope was at the position of oxidation. A secondary isotope-effect was found for tritium at C3 of D-mannitol. A hypothesis is advanced to explain the difference in the oxidation behavior of the D-mannitols labeled with tritium at C1 and at C3.

Entropies, heats of sublimation and dissociation energies of the cesium halides, M. D. Scheer and J. Fine, *J. Chem. Phys.* **36**; *No. 6, 1647–1753 (Mar. 15, 1962).*
The vapor pressures of the crystalline cesium halides have been measured in the 700–900°K temperature range. The salt vapor effusing from a Knudsen effusion cell was accurately collimated into a molecular beam with a well defined cross sectional area. Beam intensities were determined from the positive ion currents produced by dissociation of the halide and ionization to Cs^+ on a tungsten surface at 1700°K. From the experimental vapor pressures and heats of sublimation, the crystal entropies, dissociation energies, and heats of sublimation at 298°K were computed using available spectroscopic and thermal data.

Deactivation of Hg (6^3P_1) by CO and N_2 M. D. Scheer and J. Fine, *J. Chem. Phys.* **36**; *No. 5, 1264–1267 (Mar. 1962).*
Atoms of Hg (6^3P_0) produced by collisions between Hg (6^3P_1) and either N_2 or CO were detected by measuring the electrons ejected from a silver surface. From the pressure dependence of this effect, it was shown that the quenching of Hg (6^3P_1) to Hg (6^3P_0) by collision with CO occurs at about the same rate as with N_2. Since CO is twenty times more efficient than N_2 in the quenching of 2537Å fluorescence, the process [Hg (6^3P_1) + CO→Hg (6^1S_0) + CO*] must be much faster than the corresponding reaction with N_2. A possible explanation of this effect is the intermediate formation of HgCO* which dissociates to Hg (6^1S_0) and vibrationally excited CO (v = 20). This could account for the fact that H_2CO and $(HCO)_2$ are formed in the Hg photosensitized reaction of N_2 and CO and not in the electric discharge experiments of H atoms reacting with ground state CO.

The heat capacity of diamond at high temperatures, A. C. Victor, *J. Chem. Phys.* **36,** *No. 7, 1903–1911 (Apr. 1962).*
The enthalpy of gem diamonds has been measured from 273 to 1073°K using a "drop" method and a Bunsen ice calorimeter. The derived heat-capacity values, which are believed to be accurate to ±0.5 percent, are used to calculate the thermal functions of diamond above 298.15°K. Values of C_v^0 (harmonic) derived from the present investigation and recent measurements of the thermal expansion and the elastic constants of diamond are compared with theoretical treatments. Reasonably good agreement in the temperature range of this study can be obtained with a single Debye function ($\Theta_D = 1860$) obtained from the measured elastic constants. Extrapolation of the data gives $\Theta_\infty = 1880 \pm 10$.

Millimeter wave techniques, W. Culshaw, *Book, Advances in Electronics and Electron Physics* **XV,** *197–263 (Academic Press, Inc., New York, N.Y., 1961).*
The importance of millimeter waves both in research and in technology is outlined, and the difficulties experienced in the exploitation of these short wavelengths are made evident. Considerable attention is given to transmission and measurement problems, since conventional waveguide methods have serious limitations at short mm wave lengths. Optical and quasi-optical methods are discussed, and applications of mm wave interferometers and a mm wave spectrometer are considered, and diffraction effects treated in detail. The great potential use of the mm wave Fabry-Perot interferometer in precision measurements, and in maser research is made evident. Total reflection phenomena at mm wavelengths are presented and applications such as attenuation standards, phase changers, and polarizers are discussed. A re-entrant biconical spherical resonator is considered for operation at mm and sub-mm wavelengths, at high orders of interference. Expressions for the Q and shunt impedance are given, and results indicate that it could have direct application to the mm wave generation problem, and to solid state research at these wavelengths. Finally some practical aspects of mm wave detection and possible levels of sensitivity are given, together with some concluding remarks on millimeter wave research.

Transition probabilities for permitted and forbidden lines of Si X, Fe XIV and Fe X, R. H. Garstang, *Extrait des Ann. d'Astrophys.* **25,** *No. 2, 109–117 (1962).*
Transition probabilities have been calculated for forbidden transitions within the $2s^22p$ and $2s2p^2$ configurations and for permitted transitions in the array $2s^22p$—$2s2p^2$ of Si X. The energy levels of the $3s3p^2$ and $3s^23d$ configurations in Fe XIV have been predicted by extrapolation along the isoelectronic sequence. Transition probabilities have been calculated for forbidden transitions within the ($3s3p^2 + 3s^23d$) configurations and for permitted transitions in the arrays $3s^23p - 3s3p^2$ and $3s^23p - 3s^23d$ of Fe XIV. Some preliminary results are given for the $3s^23p^5 - 3s3p^6$ and $3s^23p^5 - 3s^23p^4\,3d$ arrays in Fe X. The effect of departures from LS-coupling due to spin-orbit interaction and configuration interaction is discussed.

The influence of temperature and pressure on the rheological properties of polymers, R. S. Marvin, *J. Japan Soc. Testing Materials, Rheology Issue* **11,** *303–307 (May 1962).*
The influence of temperature and pressure on viscosity and their corresponding influence on time dependent rheological properties is reviewed in terms of the free volume theory. Measurements obtained at the National Bureau of Standards on the effect of pressure on the dynamic bulk modulus of natural rubber and poly (vinyl acetate) are used to illustrate the usefulness of the free volume concept and to give some clues as to its validity. The results for natural rubber seem to agree very well with the predictions of the free volume theory; those for poly (vinyl acetate) show an unexplained discrepancy which indicates the need for further studies of other polymeric systems.

Plural scattering of 20-kev electrons in aluminum, L. Marton, J. A. Simpson, H. A. Fowler, and N. Swanson, *Phys. Rev.* **126,** *No. 1, 182–192 (Apr. 1, 1962).*
The angular and energy-distrubution of 20 kev electrons, scattered at very small angles ($\angle 10^{-2}$, radians) by transmission through aluminum foils are compared with the theory of plural inelastic scattering, under the following assumptions: (a) The probability of elastic scattering at very small angles is negligibly small in comparison with the probability of

inelastic scattering. (b) Inelastic scattering occurs predominantly through sharply-defined "characteristic" energy losses, whose number follows a Poisson statistical distribution. (c) The angular distribution in each loss follows a simple law: $\Phi(\theta) \propto 1/(\theta_E^2+\theta^2)$, where $\theta_E=\Delta E/2E$. (d) The cumulative angular distribution from plural inelastic scattering is obtained by repeated "folding" of $\Phi(\theta)$ with the angular spread of the incident beam. The angular distribution of zero-loss electrons is found to be substantially independent of the foil thickness; the normalized angular distributions of the 1- and 2-loss peaks are accurately fitted by the "folding" calculation; Poisson statistics give a good approximation to the observed numbers of energy losses. The value of λ for five observations on foils of thicknesses 650–2580 A is approximately 810 A, independent of thickness; systematic errors in the method of observation may render this value up to 20% higher than the mean free path corresponding to the total cross-section.

The international standard of light, R. P. Teele, *J. Opt. Soc. Am.* **52,** *No. 7, 826 (July 1962).*
In 1931 Wensel et al. reported the practical realization of the suggestion, made in 1908 by Waidner and Burgess, that a blackbody radiator at the freezing point of pure platinum be used as a standard of light. Subsequently such a standard was adopted internationally, effective January 1, 1948. From 1957 to the present time investigations of factors affecting the reproducibility of the standard have been conducted at the National Bureau of Standards. The previous work was extended to include crucibles and sight tubes of different dimensions and immersed to various depths, and the use of various freezing patterns. The application of corrections for the necessary viewing aperture, for the temperature drop in the walls of the sight tube, and for the unimmersed portion of the sight tube, enable us to evaluate the ideal blackbody radiator from observed values obtained with practical radiators. Appropriate modification of the freezing pattern yields improved precision. It is found that the standard is reproducible to well within 0.1 percent.
It is planned to present a complete discussion and results in the Journal of Research of the NBS.

Effect of gamma radiation on chemical structure of plastics, V. J. Krasnansky, M. S. Parker, and B. G. Achhammer, *SPE Trans.* **1,** *133–138 (July 1961).*
Twelve plastics representing various chemical structures were studied as part of a program to determine the utility of plastics as packaging materials in the high energy radiation preservation of food. The plastics were exposed to selected dosages of Cobalt-60 gamma radiation, in vacuum and in air. Gas evolution and changes in infrared spectra as a result of irradiation were used to hypothesize the relative stability of these plastics to irradiation. On the basis of these criteria it was found that plastics containing conjugated ring systems, ionic linkages, and chlorine in side groups were the most stable.

Thermal degradation of polymers at temperatures up to 1200 °C, S. L. Madorsky, *Soc. Chem. Ind. Mono. No. 13, 60–74 (1961).*
A study was made of the thermal degradation of polymers in a vacuum and in some cases in helium at atmospheric pressure, using 10 to 50 mg samples. Polymethylene, a noncrosslinked polymer, when heated for about half an hour in a vacuum or in helium at 500 °C, vaporizes without leaving a residue. The volatile products consist of a series of saturated and unsaturated hydrocarbons of various molecular weights. At 800 °C and higher, pyrolysis gives similar results; however, the products are more fragmented, and the higher the temperature and pressure the greater is this fragmentation. Polytrivinylbenzene, which is a highly crosslinked polymer, and poly(vinylidene fluoride), which is one that develops crosslinkings during pyrolysis, both yield on heating in a vacuum at any pyrolysis temperature various volatile fragments and a more or less carbonized residue. Here too, as in the case of polymethylene, a higher temperature produces greater fragmentation of the volatile products. The more volatile products were analyzed by mass spectrometry, and the less volatile products were tested for their average molecular weight by a microcryoscopic method. Elemental analysis of residues were made by a microchemical method.

Growth rates of zinc crystals from the vapor phase, R. L. Parker and L. M. Kushner, *J. Chem. Phys.* **35,** *No. 4, 1345 (Oct. 1961).*
The rate of growth of zinc crystals from the vapor phase has been studied as a function of the vapor supersaturation σ at a temperature of 390 °C. The σ-values ranged between 0.009 and 0.09. The rate R was found to vary approximately linearly with σ, permitting estimates to be made of the two parameters σ_1 and βC_0, appearing in the Burton, Cabrera and Frank theory of crystal growth. The results indicate that surface nucleation was not operative in either the nucleation or the growth of these crystals.

Heats of formation of inorganic fluorine compounds—A survey, G. T. Armstrong and L. A. Krieger, *Progress on Intern. Research on Thermodynamics and Transport Properties, p. 8–77 (ASME & Academic Press, Inc., New York, N.Y., 1962).*
This paper demonstrates the present state of measurements leading to heats of formation for the inorganic fluorine compounds. An attempt is made to show the relative magnitudes of the areas in which measurements are lacking, as compared to the areas in which data exist. No attempt is made to indicate the best values to be assigned where conflicting data exist. As a group, the binary compounds have been the most thoroughly studied. The coverage of thermodynamic information decreases rapidly as the complexity of the compounds increases. Organic compounds aside from the substituted methanes are not discussed.
A bibliography containing 513 entries dealing with thermochemical work on fluorine compounds published in the last decade is included. A lengthy table is given in which are listed fluorine and compounds, in which fluorine is combined with one, two, three and more other elements, and aqueous species of these same classes of substances. For each substance, references are given to experimental and theoretical work and other reviews giving the heat of formation or other data directly applicable to the calculation of the heat of formation.

Vibration-rotation spectra of BrCN, A. G. Maki and C. T. Gott, *J. Chem. Phys.* **35,** *No. 9, 2282–2285 (1962).*
The vibration-rotation structure of the infrared absorption bands due to $\nu_2^1+\nu_3$, $2\nu_2^0+\nu_3$, and $\nu_1+\nu_3$ have been observed and measured for $Br^{79}CN$ and $Br^{81}CN$. The average value of α^3 for these two isotopes was found to be $+0.000677$ cm^{-1}. The Fermi resonance constant for the resonance diad was calculated to be $W_{12}=35.41$ cm^{-1} for $Br^{79}CN$ and $W_{12}=35.48$ cm^{-1} for $Br^{81}CN$. The positions of the Q branches of a number of other bands were also measured.

Electron spin resonance studies of γ-irradiated small molecules at 4 °K and 77 °K, R. E. Florin, D. W. Brown, and L. A. Wall, *Proc. 5th Intern. Symp. on Free Radicals, Paper No. 18, 1–17 (Almquist and Wiksell, Stockholm, Sweden, July 6–7, 1961).*
Electron spin resonance spectra were observed for the species H, D, N, CH_3, CF_3, and SiF_3, produced by gamma irradiation of H_2, D_2, N_2, CH_4, CF_4, and SiF_4, respectively, at 4 °K, and of CH_4, CF_4, and SiF_4 mixed with Xe at 77 °K. The yields of CH_3 and CF_3 radicals per 100 ev absorbed (G-values) were much lower at 77 °K. No radicals were found at 77 °K in pure CH_4 and CF_4. The CH_3 and CF_3 spectra are closely similar to each other in Xe mixtures at 77 °K. The spectrum from CF_4 irradiated at 4 °K is totally different from the spectrum at 77 °K. SiF_3 has a characteristic complicated spectrum at all temperatures. Decay phenomena are mentioned briefly.

Direct measurement of line intensities and widths in the first overtone band of CO, H. J. Kostkowski and A. M. Bass, *J. Quant. Spectry. Radiative Transfer* **1,** *177–184 (1961).*
The absolute intensities and widths of self-broadened lines in the first overtone band of carbon monoxide were measured directly with a small grating monochromator to an estimated accuracy of 5 percent. The intensities were obtained at CO pressures below one atmosphere and the widths at pressures from 2½ to 20 atmospheres. Slit function corrections were

made using the results of a paper previously published by the authors. The intensities were found to fit the results of the rotation-vibration interaction calculation of Herman and Wallis. Spectral transmission calculations assuming a Lorentz shape for all the lines fit the observed data up to 20 atmospheres pressure.

Dislocations and stacking faults in aluminum nitrides, P. Delavignette, H. B. Kirkpatrick, and S. Amelinckx, *J. Appl. Phys.* **32,** *No. 6, 1098–1100 (June 1961).*
The recently developed methods for the direct observation of dislocations by means of transmission electron microscopy have now been applied to aluminium nitride single crystal plates, obtained by growth from the vapour phase. The crystal plates, which were developed parallel to the c-face, were thin enough to transmit electrons as grown.

Absolute isotopic abundance ratio and the atomic weight of chlorine, W. R. Shields, E. L. Garner, and V. H. Dibeler, *J. Am. Chem. Soc.* **84,** *1510–1522 (1962).*
An absolute value is obtained for the isotopic abundance ratio of natural chlorine by surface emission mass spectrometry and by the use of calibration samples of known isotopic composition prepared from nearly pure separated chlorine isotopes. The data result in the absolute value for the Cl^{35}/Cl^{37} ratio $=3.1272^{+0.0062}_{-0.0075}$. The atomic weight on the unified scale ($C^{12}=12$) is $35.45273^{+0.00073}_{-0.00089}$. The indicated uncertainties are over-all limits of error based on 95% confidence limits for the mean and on allowances for effects of known sources of possible systematic error.

Temperature dependence of electron emssion in the field emission region, R. Klein and L. B. Leder, *Phys. Rev.* **124,** *1046–1049 (Nov. 1961).*
The variation in field emission current as a function of the temperature of the emitter has been measured for tungsten over the range from 4.2 °K to 400 °K. The expected form of the temperature dependence of the emission current confirms the relationship previously postulated on theoretical grounds. This is $j(T)=j(o)\frac{KT}{\sin KT}$ where K is a constant depending on the work function and the field at the surface of the emitter. A current-increment method, in which the increase of current is plotted against the square of the temperature increase at constant field, gives a straight line whose slope permits surface field calculations more precise than heretofore possible by electron microscope measurement of tip radius.

Ultra-high vacuum ultraviolet monochromator, L. Marton, J. A. Simpson, J. A. Suddeth, and L. B. Leder, *1961 Trans. 8th Natl. Vacuum Symp., 2d Intern. Congress, Ed. L. E Prauss, p. 633–639 (Pergamon Press, Inc., New York, N.Y., 1962).*
A 1-meter, normal incidence vacuum ultraviolet monochromator having a sample chamber pressure of approximately 1×10^{-9} mm Hg is described. The entrance and exit slits are on the Rowland circle while the center floats. Wavelength is scanned by moving the grating along the circle. All moving parts are external to the vacuum chamber. The high vacuum conditions are obtained by several stages of differential pumping from the lamp housing to the sample chamber. The entire monochromator is of stainless steel with welded joints. Interesting vacuum features are the flange design, liquid nitrogen traps and rotary sea.

Field emission from niobium in the normal and superconducting states, R. Klein and L. B. Leder, *Phys. Rev.* **124,** *No. 4, 1050–1052 (Nov. 1961).*
The change of field emission current from a superconductor as a result of a transition to the normal state under constant field and temperature conditions was calculated. The derivation is based on the Bardeen-Cooper-Schrieffer formulation of the density of states and band gap model for a superconductor. The experimental method for determining the current charge consisted in measuring the current increment between a niobium field emitter in the superconducting state at 4.2 °K and in the normal state at a temperature T above the transition. After correcting for the current increase occurring as a result of the temperature increase alone, the residual would be that associated with the superconducting-normal transition. This was less than the detectability of the measurements, although the calculations indicated an expected increase in current easily measurable if the superconducting-normal transition had occurred at the emitter surface. It is speculated that under high field conditions, the superconducting state is quenched at the surface.

On the self-diffusion of ions in a polyelectrolyte solution, S. Lifson and J. L. Jackson, *J. Chem. Phys.* **36,** *No. 9, 2410–2414 (May 1962).*
The self-diffusion of ions in a polyelectrolyte solution is investigated both with respect to the average time an ion is associated with a particular polyelectrolyte molecule and with respect to the effect of the electrostatic field of the macroions on the macroscopic self-diffusion constant. The results on the macroscopic self-diffusion constant are shown to be generally compatible with experiments on self-diffusion of counterions in polyelectrolyte solutions. On the other hand, the study of the time of association of a counterion with a particular macroion yields results which cannot be reconciled with the common interpretation of transference experiments on the same solutions.

Time resolved electron optical image of a pulsed atomic beam in flight, L. Marton, S. R. Mielczarek, and D. C. Schubert, *J. Appl. Phys.* **33,** *No. 4, 1613–1614 (Apr. 1962).*
The electron optical schlieren method for study of gas behavior at very low pressures has been applied in stroboscopic fashion to produce photographs of chopped atomic beam pulses in flight. A photograph is shown of a cadmium atomic beam pulse moving at approximately 300 meters/sec. with maximum atomic density corresponding to about $2\cdot10^{-6}$ mm Hg equilibrium pressure. The potential usefulness of this technique for study of accommodation coefficients on aerodynamic surfaces is described briefly.

An electron resonance magnetometer for alternating magnetic fields, O. E. Spokas and M. Danos, *Rev. Sci. Instr.* **33,** *No. 6, 613–617 (June 1962).*
Alternating magnetic fields in the range of 2,800 gauss to 4,300 gauss are measured in terms of the frequency of the free electron spin resonance in 1:1-Diphenyl-2-picryl hydrazyl. The probe is constructed entirely of dielectric materials. An accuracy of 0.1 percent in the field determination was obtained.

Optical studies at high pressures using diamond anvils, C. E. Weir, A. Van Valkenburg, and E. Lippincott, *Book, Modern Very High Pressures Techniques, Ed., R. H. Wentorf, Jr., p. 51–69 (Butterworth & Co., London, England, 1962).*
A pressure cell capable of maintaining pressures up to 160,000 atmospheres has been constructed using a pair of type II diamonds for studies in the infrared, visible and ultraviolet spectrum. Temperature variations from 175° to −30 °C can be obtained with the cell. Major effects observed in the infrared spectrum of substances under pressure include shifts in absorption bands to both higher and lower frequencies, occurrence of new band as well as elimination of existing bands, the splitting of bands and changes in apparent band intensities. Examples of these effects using the infrared spectra of sodium nitrite, calcite, succinic acid, ice and ferrocene are given.

The molecular structure of chloroform, M. Jen and D. R. Lide, Jr., *J. Chem. Phys.* **36,** *No. 9, 2525 (May 1962).*
The structural parameters of the chloroform molecule have been previously calculated from microwave measurements on the $CHCl_3^{35}$, $CDCl_3^{35}$, $CHCl_3^{37}$, and $CHCl_2^{35}Cl^{37}$ species. The rather short CH distance which was reported (1.073A, as compared to 1.09–1.10A in CH_4, CHF_3 and the methyl halides) has prompted a re-examination of the chloroform spectrum. We have now measured the $C^{13}HCl_3^{35}$ species in natural abundance and have also carried out measurements on the other species under comparable conditions in order to obtain a self-consistent set of data for a structure determination by the substitution (r_s) method.

Collision-induced microwave absorption in compressed gases. II. Molecular electric quadrupole moments, G. Birnbaum and A. A. Maryott, *J. Chem. Phys.* **36,** *2032–2036 (Apr. 1962).*
A search for dielectric loss in the nondipolar gases, He, A, CH_4, SF_6, H_2, C_2H_6, N_2, and C_2H_4 was made at a frequency near 24 kMc and for densities not exceeding 100 amagat. For the first six gases, the loss factor was immeasurably small, less than 2×10^{-7}, at the maximum density. The loss observed in nitrogen and ethylene is attributed to transient dipoles induced by the molecular quadrupole fields during binary collisions. From the data on the quadrupolar gases, including previous results on CO_2, values of the quadrupolar moments (or upper limits where no loss was observed) are derived which are in reasonable agreement with other estimates.

Formation constant of the 1:1 pyridine-iodine complex, A. G. Maki and E. K. Plyler, *J. Phys. Chem.* **66,** *766–767 (1962).*
The equilibrium constant for PyI_2 in inert organic solvents has been measured using two different infrared bands, one at 601 cm^{-1} and the other at 184 cm^{-1}. The solvents n-heptane, CCl_4, and cyclohexane all gave approximately identical results. From intensity measurements of the infrared bands the best value for the constant was found to be 107 ± 25 1/mole at 26 °C. Consideration is given to the possible errors due to other pyridine-iodine complexes such as Py_2I_2. Evidence concerning the structure of this 1:2 pyridine-iodine complex is also presented.

Analytical Chemistry of Polymers, Parts II and III, Ed., G. M. Kline (*Vol. XII of High Polymers Series, Interscience Publishers, New York, N.Y., 1962.*)
These books have been planned and written by staff members of the National Bureau of Standards Polymers Division to survey measurement techniques for the determination of structure and composition of macromolecules and to summarize our present knowledge in this field. Modern instrumental methods of analysis are stressed; many of these techniques have been undergoing active development and perfection during the period in which these chapters have been written.
Each chapter in Part II presents the basic theory underlying the application of an instrumental method of analysis to the exploration of the structure of polymers. This is followed by descriptive information on available equipment and procedural details. Comprehensive data are presented on the characteristics of polymers as determined by the various analytical techniques. Finally, the authors review the application of this information to analytical problems and to investigations of polymerization processes, polymer structure, stability, and related research.
Identification of polymers by systematic procedures, color tests, and microscopic examination are covered comprehensively in the first three chapters of Part III. The two concluding chapters describe important developments in the application of radiochemical and end-group analysis to the unravelling of the complex composition of macromolecules. The subject matter of all chapters is fully tied to the published literature by extensive lists of references. These two volumes provide a broad review of developments in modern methods of polymer analysis, supplementing the information presented in Part I (published in 1959) on the control methods used in the analytical laboratories of materials manufacturers. The titles and authors of the chapters in Parts II and III are as follows:

Part II. Analysis of Molecular Structure and Chemical Groups. 619 pages.
- I. Molecular weights and sizes, S. G. Weissberg, S. Rothman, and M. Wales, p. 1–77.
- II. X-ray diffraction, A. S. Posner, p. 79–108.
- III. Optical methods, A. F. Forziati, p. 109–157.
- IV. Differential thermal analysis, H. E. Kissinger and S. B. Newman, p. 159–179.
- V. Pyrolysis, L. A. Wall, p. 181–248.
- VI. Mass spectrometry, L. A. Wall, p. 249–268.
- VII. Ultraviolet spectrophotometry, M. Tryon and E. Horowitz, p. 269–289.
- VIII. Infrared spectrophotometry, M. Tryon and E. Horowitz, p. 291–333.
- IX. Fluorescence, A. F. Forziati, p. 335–357.
- X. Chromatography, J. M. Cassel, p. 359–404.
- XI. Polarography, G. M. Brauer, p. 405–485.
- XII. Magnetic resonance spectroscopy, L. A. Wall and R. E. Florin, p. 487–559.

Author index. Subject index, p. 561–619.

Part III. Identification Procedures and Chemical Analysis. 566 pages.
- I. Systematic procedures, G. M. Brauer and E. Horowitz, p. 1–140.
- II. Color tests, G. M. Brauer and S. B. Newman, p. 141–259.
- III. Microscopy, S. B. Newman, p. 261–348.
- IV. Radiochemical analysis, R. E. Florin and L. A. Wall, p. 349–395.
- V. End-group analysis, M. Hellmann and L. A. Wall, p. 397–411.

General references. Pages 413–419.
Cumulative subject and author index. Pages 421–566.

Other NBS Publications

Journal of Research 66C (Eng. and Instr.) No. 4 (Oct.–Dec. 1962) 75 cents.
An ultra-high speed image dissecting camera for photographing strong shock waves. K. B. Earnshaw and C. M. Benedict.
Biprism method of determining the equivalent focal length of flat field lenses. W. R. Darling.
Effect of air drag on the motion of a filament struck transversely by a high-speed projectile. F. L. McCrackin.
A precision noise spectral density comparator. C. M. Allred.
Stresses in a plate uniformly compressed over portions of its two opposite edges. M. Chi and W. D. Kroll.
Studies of the stress-corrosions cracking of low-carbon steels. H. L. Logan.
A dual centrifuge for generating low-frequency sinusoidal accelerations. R. O. Smith, E. A. Willis, and J. S. Hilten.
Rotational micromanometers. K. Lofquist.
Study of gypsum plasters exposed to fire. J. V. Ryan.

Journal of Research 66D (Radio Prop.) No. 6 (Nov.–Dec. 1962) 70 cents.
RF impedance probe measurements of ionospheric electron densities. J. A. Kane, J. E. Jackson, and H. A. Whale.
Methods for applying numerical maps of ionospheric characteristics. W. B. Jones and R. M. Gallet.
Very-low-frequency radio propagation in the ionosphere. D. W. Swift.
Prolonged space-wave fadeouts in tropospheric propagation. A. P. Barsis and M. E. Johnson.
Range-error compensation for a troposphere with exponentially varying refractivity. J. J. Freeman.
On the geometrical optics of curved surfaces with periodic impedance properties. C. J. Marcinkowski and L. B. Felsen.
On the limitations of geometrical optics solutions for curved surfaces with variable impedance properties. C. J. Marcinkowski and L. B. Felsen.
Conversion of the amplitude-probability distribution function for atmospheric radio noise from one bandwidth to another. A. D. Spaulding, C. J. Roubique, and W. Q. Crichlow.
Some statistical properties of pulsed oblique HF ionospheric transmissions. M. Balser and W. B. Smith.
Induction in a small loop moving with a magnetostatic dipole toward a conducting half space. M. B. Kraichman.
Propagation of terrestrial radio waves of long wavelength—theory of zonal harmonics with improved summation techniques. J. R. Johler and L. A. Berry.
Terminal-zone corrections for a dipole driven by a two-wire line. K. Iizuka and R. W. P. King.
Pattern synthesis with a flush-mounted leaky-wave antenna on a conducting circular cylinder. A. Ishimaru and F. R. Beich.
Analysis of electric energy usage in Air Force houses equipped with air-to-air heat pumps, P. R. Achenbach, J. C. Davis, and W. T. Smith, NBS Mono. 51 (July 13, 1962) 30 cents.

Specifications, tolerances, and regulations for commercial weighing and measuring devices (corrected through 1961), NBS Handb. 44, 2d Ed. (1961) $1.00.

Index to the reports of the National Conference on Weights and Measures. From the first to the forty-fifth, 1905 to 1960. NBS Misc. Publ. 243 (June 28, 1962) 30 cents (Supersedes M203).

Quarterly radio noise data—December, January, February 1961–62, W. Q. Crichlow, R. T. Disney, and M. A. Jenkins, NBS Tech. Note 18–13 (PB151377–13) (1962) $1.75.

Characteristics of point-to-point tropospheric propagation and siting considerations, R. S. Kirby, P. L. Rice, and L. J. Maloney, NBS Tech. Note 95 (PB161596) (1961) $2.50.

Analysis of ionospheric vertical soundings for electron density profile data. III. Procedures for obtaining monthly summary virtual height curves for N(H) analysis (composite virtual height curves), J. W. Wright, NBS Tech. Note 146 (PB-161647) (1962) 75 cents.

Publications in Other Journals

Propagation of solar particles and the interplanetary magnetic field, C. S. Warwick, J. Geophys. Research **67,** No. 4, 1333–1346 (Apr. 1962).

Availability of machine-usable natural language material, M. E. Stevens, Proc. 3d Inst. on Information, Storage and Retrieval (American Univ., Washington, D.C.) **1,** 58–75 (Feb. 1961).

Physical measurements and experiment design, W. J. Youden, Le Plan d'Exper. Centre Natl. Recherche Sci. (Paris, France) **110,** 1–13 (Aug.–Sept. 1961).

A calculus for factorial arrangements, B. Kurkjian and M. Zelen, Annals of Math. Statistics **33,** 600–619 (June 1962).

Plastics, G. M. Kline, Encyclopedia Americana **XXII,** 221–229 (1962 Ed.).

Modular forms whose coefficients possess multiplicative properties (II), M. Newman, Ann. of Math. **75,** 242–250 (Mar. 1962).

A note on normal matrices, M. Marcus and N. Khan, Can. Math. Bull. **4,** 23–27 (1961).

A statistical comparison of the wearing characteristics of two types of dollar notes, E. B. Randall, Jr., and J. Mandel, Materials Research and Standards (ASTM Bull.) **2,** No. 1, 17–20 (Jan. 1962).

Study of the effect of large aperture on the performance of an Ebert spectrometer, L. R. Megill and L. Doppleman, J. Opt. Soc. Am. **52,** No. 3, 258–261 (Mar. 1962).

Prediction of pressure drop in two-phase single-component fluid flow, M. R. Hatch and R. B. Jacobs, A.I.Ch.E. Journal **8,** No. 1, 18–25 (Mar. 1962).

Potential heat: A method for measuring the heat release of materials in building fires, J. J. Loftus, D. Gross, and A. F. Robertson, Am. Soc. Testing Materials Proc. **61,** 1336–1348 (June 1961).

Comparison of standard and microtests for international rubber hardness, R. D. Stiehler and F. L. Roth, Materials Research and Standards (ASTM Bull.) **2,** No. 5, 388–391 (May 1962).

Comments on "Effects of ultrahigh pressures on glass", C. E. Weir and S. Spinner, J. Am. Ceramic Soc. **45,** No. 4, 196 (Apr. 1962).

The "vicious cycle" in secondary batteries—a mathematical approach, W. G. Eicke, Jr., J. Electrochem. Soc. **109,** No. 5, 364–368 (May 1962).

Communication between man and machine, S. N. Alexander and J. E. Karlin, Proc. IRE **50,** No. 5, 1124–1128 (May 1962).

The radio refractive index of air, B. R. Bean, Proc. IRE **50,** No. 3, 260–273 (Mar. 1962).

The reflection of logistics in electronic computer design, E. W. Cannon, Naval Research Logistics Quart. **7,** 365–371 (1960).

Variability of spectral tristimulus values, I. Nimeroff, J Opt. Soc. Am. **52,** No. 6, 685–691 (June 1962).

The propagation of electromagnetic waves along the earth's surface, J. R. Wait, Book, Electromagnetic Waves, Ed. by R. E. Langer, p. 243 (The University of Wisconsin Press, Madison, Wisc., 1962).

Emission flame photometry, M. Margoshes, Anal. Chem. **34,** No. 5, 221R–224R (Apr. 1962).

An auroral-zone electron precipitation event and its relationship to a magnetic bay, R. R. Brown and W. H. Campbell, J. Geophys. Research **67,** No. 4, 1357–1366 (Apr. 1962).

Tungsten helical-spring microbalance, S. L. Madorsky, Vacuum Microbalance Techniques **2,** 47–57 (Plenum Press, Inc., New York, N.Y., 1962).

Thermal explosives: adiabatic self-heating of explosive and propellants, D. Gross and A. B. Amster, Eighth Symp. (Intern.) on Combustion, p. 728–734 (The Williams and Wilkins Co., Baltimore, Md., 1962).

The evolution of concepts and languages of computing, R. D. Elbourn and W. H. Ware, Proc. IRE **50,** No. 5, 1059–1066 (May 1962).

National Bureau of Standards list of IGY flares with normalized values of importance and area, C. S. Warwick, IGY Solar Activity Report Series No. 17 (Intern. Geophys. Year, World Data Center A. Solar Activity, High Altitude Observatory, University of Colorado, Boulder, Colorado, May 1, 1962).

Extension of the Flory-Rehner theory of swelling to an anisotropic system, S. D. Bruck, J. Polymer Sci. **55,** 29–31 (Dec. 1961).

Polymer degradation (by heat, oxidation and radiation), in unsolved problems in polymer science, L. A. Wall, ASD Tech. Report 62–283, p. 32–36 (Mar. 1962).

Time and its inverse, J. M. Richardson, Intern. Sci. and Tech. **1,** No. 6, 54–61 (June 1962).

Effect of crystal growth on the comparative fixation of Sr^{89} and Ca^{45} by calcified tissues, R. C. Likins, A. S. Posner, B. Paretzkin, A. P. Frost, J. Biol. Chem. **236,** 2804–2806 Oct. 1961).

Infrasonic pressure waves associated with magnetic storms, P. Chrzanowski, J. M. Young, G. Greene, and K. T. Lemmon, J. Phys. Soc. Japan **17,** Suppl. A–II, 9–13 (1962).

Characterization of textile varns for use under ballistic impact conditions, J. C. Smith, Proc. Symp. Personnel Armor, U.S. Naval Research Laboratory **I, 1–21** (Oct. 4–5, 1961).

Introduction, H. S. Peiser, Book, Vacuum Microbalance Techniques, Ed., R. F. Walker, **2,** 1–5 (Plenum Press, Inc., New York, N.Y., 1962).

Charge-storage techniques for pulse-height analysis, L. Costrell and R. E. Brueckman, Nuclear Electronics (Intern. Atomic Energy Agency) **II,** 29–39 (1962).

Glass Dewars for optical and other studies at low temperatures, L. J. Schoen and H. P. Broida, Rev. Sci. Instr. **33,** No. 4, 470–473 (Apr. 1962).

The effect of geomagnetic activity on the F_2 region over central Africa, R. G. Rastogi, J. Geophys. Research **67,** No. 4, 1367–1374 (Apr. 1962).

Distillation analysis, R. T. Leslie and E. C. Kuehner, Anal. Chem. Suppl. 34, No. 5, 50R–56R (Apr. 1962).

Plastic standards in Government, F. W. Reinhart, Proc. Am. Standards Assoc. 12th Natl. Conf. Standards, p. 44–46 (Houston, Texas, Oct. 1961).

Anisotropies in angular distributions of molecular dissociation products, G. H. Dunn, Phys. Rev. **8,** 62–64 (Jan. 15, 1962).

Plastics, G. M. Kline, The Americana Annual, p. 603 (Americana Corp., Chicago, Ill., 1961).

Displacement and strain-energy distribution in a longitudinally vibrating cylindrical rod with a viscoelastic coating, P. Hertelendy, J. Appl. Mech. **29,** Series E, 47–52 (Mar. 1962).

Distribution of total service time for a fixed observation interval, W. S. Connor and N. C. Severo, J. Am. Stat. Assoc. **57,** 376–386 (June 1962).

Abstract shape recognition by machine, M. E. Stevens, Computers—Key to Total Systems Control, Proc. Eastern Joint Computer Conf. **20,** No. 1, 332–351 (Dec. 1961).

Catalytic effects of thermocouple materials, L. O. Olsen, SAE J. Paper No. 524G, **70,** No. 5, 94 (May 1962).

Determination of molecular weights and molecular weight distribution, D. McIntyre, ASD Tech. Rept. 62–283, p. 71–74 (Mar. 1962).

Characteristics of some air-turbine handpieces, D. F. Taylor, R. R. Perkins, and J. W. Kumpula, J. Am. Dental Assoc. **64,** No. 6, 794–805 (June 1962).

Tensile shear strength of adhesive bonded metals as a function of the rate of loading, D. A. George, H. R. Butzlaff, and J. Mandel, Symp. on Adhesion and Adhesives, Am. Soc. Testing Materials Spec. Tech. Publ. No. 271, 47–53 (1961).

Enviromental chemistry, F. W. Reinhart, Prevention of Deterioration Center Newsletter (Natl. Acad. Sci.-Natl. Research Council) **V**, No. 1, 1–2, 4 (Oct. 1961).

A study of solar activity associated with polar-cap absorption, C. S. Warwick and M. W. Haurwitz, J. Geophys. Research **67,** No. 4, 1317–1332 (Apr. 1962).

Stability of plastic impression trays, J. B. Woelfel and G. C. Paffenbarger, J. Am. Dental Assoc. **63,** No. 5, 705–706 (Nov. 1961).

Vacuum system for use with a microbalance, G. F. Rouse, Book, Vacuum Microbalance Techniques, Ed., R. F. Walker, **2,** 5969 (Plenum Press, Inc., New York, N.Y., 1962).

Departure from the steady state in two-intermediate enzyme reactions, H. Shin, Trans. Faraday Soc. **58,** No. 475, 1439–1450 (July 1962).

Calibration of vibration pickups at large amplitudes, E. Jones, S. Edelman, and K. S. Sizemore, J. Acoust, Soc. Am. (Errata) **34,** No. 3, 355 (Mar. 1962).

Pair production as an analyzer of circular polarization of gamma rays from neutral particle decays, H. Olsen and L. C. Maximon, Il Nuovo Cimento **24,** No. 1, 186–189 (Apr. 1962).

Emission flame photometry, M. Margoshes, Anal. Chem. Suppl. **34,** No. 5, 221R–224R (Apr. 1962).

Design requirements for mechanized systems in protective shelters, R. R. Achenbach, Heating, Piping and Air Conditioning **34,** No. 2, 73–79 (Feb. 1962).

Creep of pure-gum rubber vulcanizates from indentation-time measurements, L. A. Wood and F. L. Roth, Rubber Tech. Conf. (London, England, 1962).

The ideal Lovibond color system, D. B. Judd, G. J. Chamberlin, and G. W. Haupt, J. Opt. Soc. Am. **52,** No. 7, 813–819 (July 1962).

Single-trace sweep adapter for transistor-curve tracers, L. J. Swartzendruber, Rev. Sci. Instr. **33,** No. 5, 560–562 (Aug. 1961).

Proton magnetic resonance in clay minerals, R. L. Blaine, Highway Research Board Bull., No. 287, 44–55 (June 1962).

Spin-lattice relaxation in two rare earth double nitrates, R. P. Hudson and B. W. Mangum, Il Nuovo Cimento **23,** 1133–1135 (Mar. 1962).

Dimensional changes in fibrous macromolecules: The system alpha-keratin-lithium bromide, L. Mandelkern, J. C. Halpin, A. F. Diorio, and A. S. Posner, Am. Chem. Soc. **34,** No. 8, 1383–1391 (Apr. 1962).

Tchebycheff approximation by functions unisolvent of variable degree, J. R. Rice, Trans. Am. Math. Soc. **99,** 298–302 (1961).

Best approximations and interpolating functions, J. R. Rice, Trans. Am. Math. Soc. **101,** 477–498 (Dec. 1961).

The presence of singly-ionized gallium (Ga II) lines in stellar spectra, W. P. Bidelman and C. H. Corliss, Astrophys. J. **135,** No. 3, 968–969 (May 1962).

Theory and biomedical applications of the analog computers, H. L. Mason, Natl. Inst. of Health Workshop on Biomedical Computing, No. 1 (July 1961).

Universal-time control of the arctic and antarctic F region, R. A. Duncan, J. Geophys. Research **67,** 1823–1830 (May 1962).

Constitution diagram for 16% Cr-2% Ni stainless steel C. R. Johnson and S. J. Rosenberg, Trans. Quarterly Am. Soc. Metals **55,** No. 2, 277–286 (June 1962).

Effect of surface roughness on the oxidation rate of iron, A. G. Eubanks, D. G. Moore, and W. A. Pennington, J. Electrochem. Soc. **109,** No. 5, 382–389 (May 1962).

Evaluation of the nature of the surfaces of hard tooth tissues by a surface activity test, R. L. Bowen, Proc. Workshop on Adhesive Restorative Dental Materials (Indiana Univ., Bloomington, Indiana, Sept. 28–29, 1961).

Liquid drop collisions, O. G. Engel, Symp. Erosion and Cavitation, Am. Soc. Testing Materials Spec. Tech. Publ. No. 307, 3–16 (1961).

On the determination of disintegration rates by the coincidence method using high efficiency detectors, R. W. Hayward, Intern, J. Appl. Radiation and Isotopes **12,** 148–150 (Dec. 1961).

Mass spectrometry, R. M. Reese, Anal. Chem. **34,** No. 5, 243R–254R (Apr. 1962).

On the theory of diffraction grating interferometers, H. Mendlowitz and J. A. Simpson, J. Opt. Soc. Am. **52,** No. 5, 520–524 (May 1962).

Effect of oleophobic films on fatigue crack propagation, W. L. Holshouser and H. P. Utech, Am. Soc. Testing Materials Proc., **61,** 749 (1961).

Strange sounds in the atmosphere, Part II, R. K. Cook and J. M. Young, Sound—Its Uses and Control **1,** No. 3, 25–33 (May-June 1962).

Fifteen years ACM, F. L. Alt, Commun. Assoc. Computing Machinery **5,** No. 6, 300–307 (June 1962).

Scattered radiation from large cobalt-60 calibrating sources, L. Costrell, Health Phys. J. **8,** No. 3, 261–272 (June 1962).

Measurement characteristics of the farm milk tank, M. W. Jensen, J. Milk and Food Technol. **25,** No. 4, 112–115 (Apr. 1962).

The microwave Zeeman effect of free hydroxyl radicals: $^2\Pi_{1/2}$ levels, H. E. Radford, Phys. Rev. **126,** 1035 (1962).

Second breakdown in transistors, H. A. Schafft and J. C. French, IRE Trans. Electron Devices **ED–9,** No. 2, 129–136 (July 1962).

Effect of noncrystallizable components on the crystallization kinetics of polymers, F. Gornick and L. Mandelkern, J. Appl. Phys. **33,** No. 3, 907–913 (Mar. 1962).

Standards for plastics in the U.S.A., G. M. Kline, Proc. 13th Intern. Plastics Congress, p. 27–33 (Turin, Italy, Sept. 28–30, 1961).

Preservation of edge detail in metallography, W. P. Hayes, Jr., N. Tighe, and H. B. Kirkpatrick, Metal Progress **81,** No. 3, 112 (Mar. 1962).

Traces of products of angular momentum matrices, I. Cartesian basis, E. Ambler, J. C. Eisenstein, and J. F. Schooley, J. Math. Phys. **3,** No. 1, 118–130 (Jan.-Feb. 1962).

Measurement of linear photon polarization by pair production, L. C. Maximon and H. Olsen, Phys. Rev. **126,** No. 1, 310–319 (Apr. 1962).

Standards for vinyl chloride plastics, F. W. Reinhart, Proc. SPE Regional Tech. Conf. "Vinyl Plastics" (New York, N.Y., Nov. 15, 1961); SPE J. **18,** 308–311 (Mar. 1962).

Microsize magnetic field probes with axial symmetry, C. A. Shiffman, Rev. Sci. Instr. **33,** No. 2, 206–207 (Feb. 1962).

Radiation hazards in realistic perspective, L. S. Taylor, Phys. Today **15,** 32–38 (June 1962).

Stress-strain relationships in yarns subjected to rapid impact loading. 9. Effect of yarn structure, J. C. Smith, J. M. Blandford, P. J. Shouse, and K. M. Towne, Textile Research J. **32,** 472–480 (June 1962).

Device for chemically thinning crystals for transmission electron microscopy, H. B. Kirkpatrick and S. Amelinckx, Rev. Sci. Instr. **33,** No. 4, 488–489 (Apr. 1962).

Signs of nuclear resonance coupling constants in saturated aliphatic systems, H. Finegold, Proc. Chem. Soc. (London, England) No. 6 (June 1962).

Stress corrosion of high strength cast aluminum alloys, F. M. Reinhart and W. F. Gerhold, Corrosion **18,** No. 4, 158 (Apr. 1962).

Fluorescence in comets as a Markov process, T. Carrington, Astrophys. J. **135,** No. 3, 883–891 (May 1962).

Digital pattern recognition by moments, F. L. Alt, J. Assoc. Computing Mach. **9,** No. 2, 240–258 (Apr. 1962).

The nuclear photoeffect in holmium and erbium, E. G. Fuller and E. Hayward, Nuclear Phys. **30,** 613–635 (1962).

Phase-modulated calibrator for testing phase meters, M. C. Thompson, Jr., Rev. Sci. Instr. **33,** 563–564 (May 1962).

**Publications for which a price is indicated (except for Technical Notes) are available only from the Superintendent of Documents, U.S. Government Printing Office, Washington 25, D.C. (foreign postage, one-fourth additional). Technical Notes are available only from the Office of Technical Services, U.S. Department of Commerce, Washington 25, D.C. (order by PB number). Reprints from outside journals and the NBS Journal of Research may often be obtained directly from the authors.*

UNIVERSITY MICROFILMS
313 NORTH FIRST STREET
ANN ARBOR, MICHIGAN
SJR-A-OCT

UNITED STATES
GOVERNMENT PRINTING OFFICE
DIVISION OF PUBLIC DOCUMENTS
WASHINGTON 25, D.C.

OFFICIAL BUSINESS

PENALTY FOR PRIVATE USE TO AVOID PAYMENT OF POSTAGE, $300 (GPO)

JOURNAL OF RESEARCH of the National Bureau of Standards Vol. 66A, No. 6 November-December 1962
A. Physics and Chemistry

Contents

Page

Heat of formation of nitronium perchlorate. Alexis A. Gilliland. 447

Phase equilibrium relations in the binary system bismuth sesquioxide-niobium pentoxide. R. S. Roth and J. L. Waring. 451

Elastic constants of rutile (TiO_2). J. B. Wachtman, Jr., W. E. Tefft, and D. G. Lam, Jr. 465

Reaction of hardened portland cement paste with carbon dioxide. Charles M. Hunt and Lewis A. Tomes. 473

Titanium standards for hydrogen content. J. T. Sterling, F. J. Palumbo, and L. L. Wyman. 483

Ultraviolet stability of crosslinked polycaprolactam systems. Stephen D. Bruck. 489

Spectral-line intensities and *gf*-values in the first spectrum of copper. Charles H. Corliss. 497

Batch adsorption from solution. William V. Loebenstein. 503

Separation of hafnium from zirconium and their determination: separation by anion-exchange. Lawrence A. Machlan and John L. Hague. 517

Publications of the National Bureau of Standards. 521

Index to volume 66A. Physics and Chemistry, January to December 1962. 529

For sale by the Superintendent of Documents, U.S. Government Printing Office, Washington 25, D.C. Price 70 cents (single copy). Subscription price: $4 a year; 75 cents additional for foreign mailing.

UNITED STATES GOVERNMENT PRINTING OFFICE, WASHINGTON : 1962